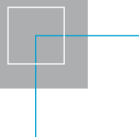# The wind-wave climate of the Pacific Ocean.

Mark Hemer, Jack Katzfey and Claire Hotan
Final Report
30 September 2011

Report for the Pacific Adaptation Strategy Assistance Program
Department of Climate Change and Energy Efficiency

www.cawcr.gov.au

Enquiries should be addressed to:
Mark Hemer
Email. Mark.Hemer@csiro.au

Distribution list

DCCEE   1

Copyright and Disclaimer

Important Disclaimer

Contents

EXECUTIVE SUMMARY

Surface wind-waves are a key driver of coastal zone processes in the Pacific Island Countries and Territories (PICTs), and their climatological variability must be considered within any comprehensive assessment of potential climate change driven impacts on the coastal zone. These wave driven processes can impact on many aspects of the PICT coastal environment, including: coastal flooding during storm wave events; coastal erosion, both during episodic storm events and due to long term changes in integrated wave climate; characterisation of reef morphology and marine habitat/species distribution; flushing and circulation of lagoons; and transport and energy solutions.

> **Pacific Island Countries and Territories (PICTs) are arguably more vulnerable to variability and change in the surface wind-wave climate than sea-level rise.**
>
> **Future coastal vulnerability assessments for the region must consider potential changes in wave properties, together with the influence of mean sea-level rise and changes to other sea-level extremes.**

In order to support such assessments, this project had two objectives:

1. Describe the current wave climate on the basis of existing information, including understanding the dominant modes of seasonal and inter-annual variability in the Pacific wave climate, and identifying gaps in current knowledge which require future attention.

2. Carry out a preliminary assessment of potential changes in Pacific basin wave climate under future climate scenarios.

The literature describing the current knowledge of the Pacific basin wave climate has been reviewed, with focus on the region of the PICTs, including Hawaii. Throughout this region, a multi-modal wave spectrum is observed, with contributions from locally trade wind generated seas, swell waves generated in both the northern and southern hemisphere extratropical storm belts, and episodic tropical storm (cyclone) events (See Figure ES1). The relative fraction of each of these components depends on location. Islands located on or north of the equator have wave fields dominated by sea generated by north-easterly trade winds and the northern Pacific generated swell, although Islands located further eastwards (e.g., Hawaii) also experience southerly ocean swell. Islands located south of the equator have wave fields dominated by sea generated by south-easterly trade winds. Southern Pacific generated swell is also a major contributor to the wave climate at those islands which are not sheltered by other islands. For example, Samoa, French Polynesia and Fiji both experience southern ocean swell.

Available long-term wave data for the Pacific region has been compiled, including available in-situ wave buoy records, model hindcast and reanalyses products, and satellite altimeter derived records. We have assessed these datasets to determine their ability to describe the observed wave climate in the region.

Figure ES1: The wind-wave climate in the region of the PICTs has several contributing components (multi-modal). To understand climatological variability of wave climate in the region, the response of each of these contributions must be understood.
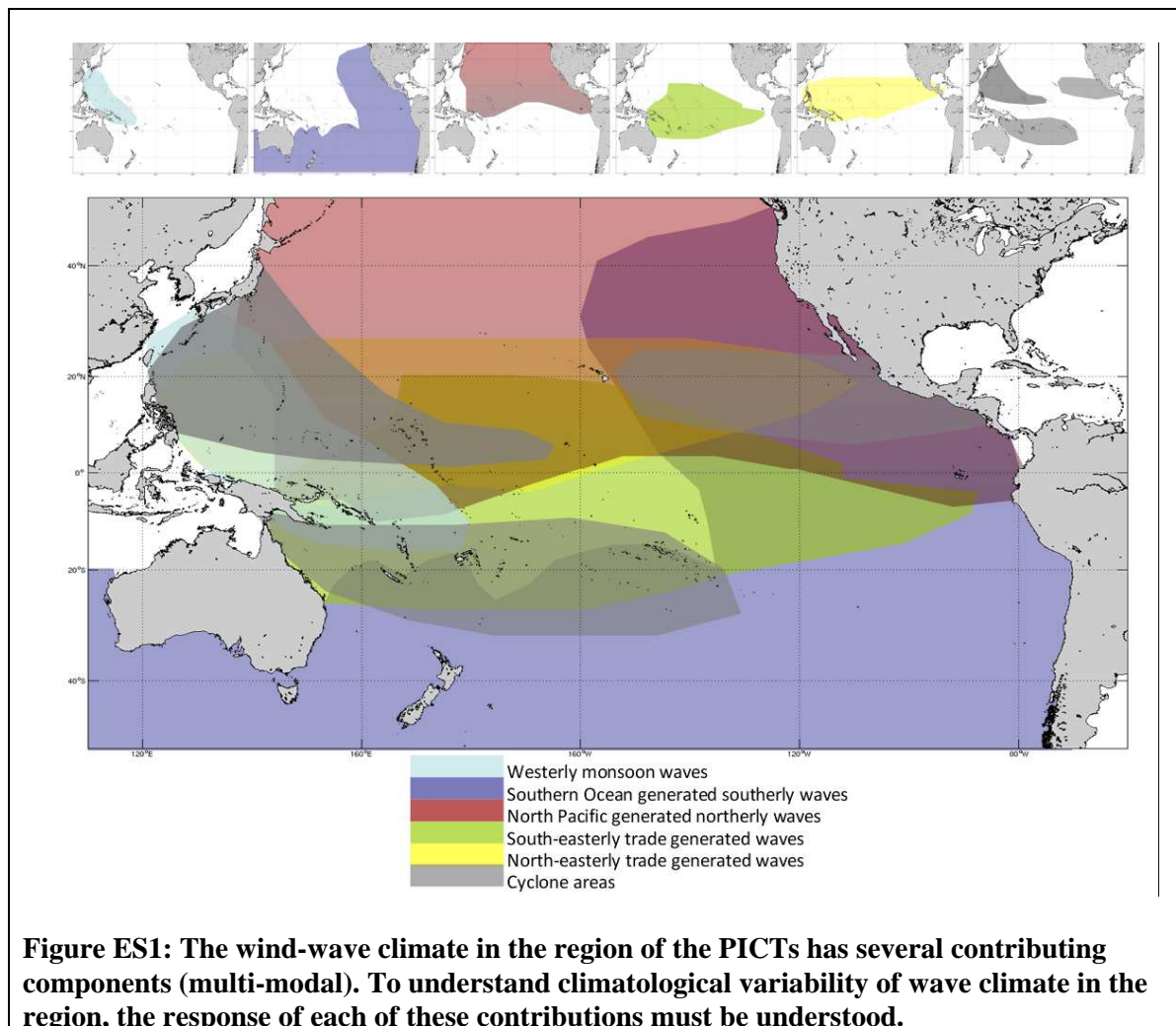
The in-situ collected wave buoy data held by SOPAC is a valuable dataset describing the wave field at selected locations within the PICTs. However, these data are limited to few locations, and have a maximum record length of 5 years. Consequently the data contain little information to identify the key modes of inter-annual (and decadal) wave climate variability. Only a small collection of these records contain directional information

Longer term in-situ buoy records are available from within the Pacific basin, collected as part of the United States National Oceanographic and Atmospheric Administration National Buoy Data Centre (NOAA NBDC). These data provide longer records from which inter-annual variability of wave climate can be determined, which has been the focus of several North American research projects in recent years, but are limited to few locations directly applicable to PICTs.

Satellite altimeters provide a long-term (1985 to present, with 2-3 yr gap) spatially uniform record of significant wave height across the globe. These data enable understanding of seasonal and inter-annual variability of wave heights in the region, but have no application for understanding the directional, multi-modal aspects of the Pacific wave climate. The long repeat

sampling interval of a point on the ocean surface by altimeter also limits the use of this data to describe the wave climate in near-shore environments, particularly without directional data.

Available observational data (in-situ buoys and satellite altimeter) have limited application for establishing climatological variability of wave climate in the region

Satellite derived synthetic aperture radar (SAR) data, made recently available via the GlobWave project, provides an additional wind-wave datastream which resolves spectral wave properties globally over an extended period. Developing capability to exploit these data for the Pacific region should be investigated.

Attribution of coastal impacts to sea-level rise vs wave climate variability change is not possible given lack of wind-wave observations and sparse shoreline position records.

Investment in a long-term wave observation programme (in-situ buoy network, or other wave measuring equipment) would increase the adaptive capacity of the region to deal with coastal hazards, by:
- **Increasing the understanding of relationships between climate variability and the multi-modal wave climate,**
- **Provide ground truth validation for SAR data in the region,**
- **Contribute a database to which coastal shoreline response studies can measure change**
- **Support coastal hazard monitoring, and**
- **Increase forecasting capabilities.**

Analysis of the latest wave reanalysis from the European Centre for Medium Range Weather Forecasting (ECMWF), ERA-Interim, has shown this dataset describes the buoy and altimeter observed Pacific wave climate with high skill. ERA-Interim provides a 1989-2009 record of 6-hourly values of integrated wave parameters (significant wave height, mean wave period and mean wave direction). Spectral wave data are available from ERA-Interim at cost from ECMWF, but we have not assessed these for this project. Despite these data describing the broad scale wave climate of the region well, the archived data are limiting for a number of reasons: archives of integrated wave parameters reduces the ability to describe the multi-modal characteristics of the wave field in the region; 6-hourly temporal resolution limits representation of peaks in wave conditions for coastal studies; and the relatively coarse spatial resolution (1.5°) has limited application for coastal studies and study of cyclone events.

Analysis of the ERA-Interim dataset indicates that each of the contributing components of the Pacific wave climate vary seasonally. The North Pacific generated northerly swell waves peak in the boreal winter, and lead to greater influence of this component of the wave field on most of the Northern Pacific during this period of the year. The Southern Ocean generated southerly swell are more consistent than the Northerly swell, but seasonal variability shows maximum energy observed during the austral winter when the southern extra-tropical storm belt moves northwards. The contribution of trade wind generated waves typically peaks during the respective winter (boreal winter for the northern hemisphere north-easterly trades and the austral winter for the southern hemisphere south-easterly trades). In the western Pacific, the seasonal variability in the position of the monsoon trough (over ~20°S in February to over ~40°N in August) further influences the wave climate in this region, and the occurrence of

tropical storm (cyclone) events. Due to the resolution of available data products, cyclone generated wave systems are poorly represented in this study.

Limited application of observation data increases dependence on available wave model products. Archives available from these wave models also limit application for wave climate studies in the region.

The European Centre for Medium Range Weather Forecasting (ECMWF) ERA-interim wave reanalysis is able to resolve seasonal and inter-annual variability of wave climate in the region, observed by the available observations.

A high-quality multi-decadal wave hindcast for the Pacific region, which archives high temporal resolution (hourly) spectral wave data, is required. This hindcast must be capable of providing spectral wave boundary conditions for nested, high spatial resolution models for Country/Island scale studies, to support coastal and nearshore coastal hazard assessments.

Developing regional/in-country capability to carry out high resolution national or island scale wave studies, with forcing taken from hindcast, should be prioritised.

A strong correlation between the significant wave height and the Southern Oscillation Index (SOI), and both directional components of the wave energy flux and the SOI shows that the El Niño-Southern Oscillation (ENSO) variability has a strong influence on the wave climate of the Pacific. The eastward shift in tropical storm (cyclone) activity during El Niño years leads to increases in wave height over large portions of the equatorial Pacific. Associated directional changes correlated with the SOI are also observed. A strong correlation between the observed wave climate variability and the Southern Annular Mode (SAM) is also observed. The SAM is a measure of north-south pressure gradient between the mid and high southern latitudes. High positive values of the SAM represent a stronger pressure gradient across these latitudes, and are associated with intensified Southern Ocean storm activity. During positive phases of the SAM, a wave height increase and greater southerly component is observed over large regions of the Pacific Ocean. Relationships to other indices (Arctic Oscillation, Indian Ocean Dipole, Pacific-North American Index, and the North Atlantic Oscillation) were investigated. While significant relationships were observed between the regional wave climate variability and these other indices, these were not as strong as to the SOI and SAM. These established relationships provide useful measures by which to estimate potential future impacts of inter-annual wave climate variability on PICTs coastal and nearshore infrastructure and ecosystems.

The length of wind-wave record in the Pacific is relatively short (approximately 25 years). While trends are observed in wave properties over this period of time, these are strongly biased by the magnitude of inter-annual variability in the record, particularly associated with the ENSO cycle.

Inter-annual variability of wave heights and directions correlate strongly to El Niño – Southern Oscillation (ENSO) in the equatorial Pacific Ocean.

El Niño events are associated with increased wave heights and anticlockwise rotation of wave direction (a greater southerly component to the south-easterly annual mean wave directions) in the eastern equatorial Pacific.

Wave climate variability in the region also corresponds with the Southern Annular Mode Index (SAM). Positive anomalies of SAM are associated with increased swell wave heights and more southerly swell direction in the region.

Projecting future change in Pacific wave climate is strongly dependent on skill of climate models to represent ENSO. Guilyardi et al (2009) showed most (but not all) IPCC AR4 climate models are qualitatively consistent in their projections of mean changes over the tropical Pacific (warming SST and general weakening of the Walker Circulation). However, these models are inconsistent with respect to their projections of change in ENSO variability (some models show increasing ENSO variability, others exhibit no change, others show a decrease).

Wave climate projection for the Pacific Ocean will benefit from future improvements in ENSO model skill.

An objective of the study has been to assess the ability of a dynamical wave modelling approach to project potential changes in wave climate under future warmer climate scenarios. We assessed the wave model skill to describe the present wave climate (using ERA-Interim as a control) when forced directly with climate model derived surface winds. The climate model winds used to force the wave model were taken from the dynamical downscaling 60km resolution climate model runs carried out for the Pacific Climate Change Science Programme, using CSIRO's cubic conformal atmospheric model (CCAM). CCAM Surface winds were used to force a 1° global implementation of the WaveWatch III 3rd Generation spectral wave model, for a present 30-yr time-slice period (1979 to 2009). A two-member ensemble, using CCAM downscaled CSIRO Mk3.5 and CCAM downscaled ECHAM5 outputs for the SRES A2 climate scenario, was carried out to provide limited quantification of the magnitude of uncertainty within the dynamical wave projections. While the climate model derived wave field and ERA-Interim exhibit similar characteristics, an assessment of the climate and variability bias between the two wave fields indicates that the wave model forced directly with climate model derived surface winds has poor skill in describing the wave climate in some regions (e.g., notable differences in dominant wave direction are observed compared to ERA-Interim in the region of French Polynesia).

Climate model surface winds have been adjusted for both climate and variability bias following the method described by Hemer et al. (2011b). When forced with the bias adjusted climate model winds, the wave model shows marginal improvement of the mean wave climate, through removing spatial variability of bias, when compared to ERA-Interim wave data. However, a spatially consistent negative bias of approximately 0.25m (Bias-Adjusted CCAM forced run underestimating wave heights) throughout the Pacific basin. No improvement to variability bias is achieved when forcing the model with bias-adjusted winds.

A preliminary assessment of the climate change signal in the Pacific wave climate was carried out. The global 1° WaveWatch III wave model was forced with CCAM surface winds for a future 30-yr time slice (2070-2099). A two-member ensemble, using the same CCAM outputs, was generated to provide limited quantification of the uncertainty surrounding project changes. When forced directly with climate model winds, the wave model (which exhibits variable skill in representing the current wave climate) shows an increased contribution of swell waves generated at the higher latitudes, particularly from the Southern Ocean, and reduced influence of the north-easterly trade wind generated waves. These influences are particularly noted as an increase in wave heights and period, with accompanying changes in wave direction in the eastern Pacific region. Throughout the western Pacific in the ocean surrounding the PICTs, changes in wave height, period and direction are projected to occur, as a decrease in wave heights and periods during the austral summer and an increase in wave heights and periods during the austral winter. These changes, accompanied with projected changes in wave direction should be considered within the context of long-term coastal response to physical drivers of change.

When forced with bias-adjusted climate model surface winds, the projected changes in wave climate are consistent with those observed from the model when forced with un-adjusted winds. Robust projected changes in the annual mean significant wave height (Hs) are greatest in the north-west equatorial Pacific (the Federated States of Micronesia), where a projected 10% decrease in Hs is observed in both ensembles. This projected decrease is greatest during the northern winter months (Dec-Feb). During the austral winter, 5-10% increase in seasonal mean Hs is projected in the south-equatorial Pacific, reaching a peak in the Cook Islands, but extending eastwards to Fiji, consistent with increasing south-easterly trade winds observed in the CCAM dataset. The projected changes are relatively small over the period between the 1979-2009 and 2070-2099 time-slices, and qualitatively consistent with prior studies, based on statistical (Wang and Swail, 2006) and other dynamical (Mori et al., 2010) projections. On the basis of linear interpolation, projected conditions for a mid-century (2030-2050) time-slice are small, and expected to be within range of current inter-annual variability.

The wave climate projections presented in this report require several qualifiers. The focus of analysis has been on representation of the mean and seasonal cycle of the mean wave fields. Potential changes in extreme wave climate, rather than the changes to the mean wave fields, are likely to have greater impacts. However extremes are poorly represented in the available historical data, and this is beyond the scope of the present wave climate model skill, and a focus for future activities. The dynamically downscaled climate model (CCAM) outputs on which these projections depend are broadly consistent with projections taken from the CMIP3 GCMs, but some differences in the projected conditions occur. The GCM's on which the projections in this study are based (ECHAM5 and CSIRO Mk3.5) do not provide the best representation of the current climate in the Pacific region, although they are not significant outliers (Guilyardi et al., 2009), and also only represent a very limited subset of the total range of projected climate conditions within the CMIP3 ensemble. However, GCM SST biases were corrected before being used by CCAM, and performance of the GCM does not directly relate to accuracy of the CCAM simulations. This adjustment also leads to a much reduced range of variability within the CCAM derived ensemble than the corresponding GCM derived ensemble. While the CCAM runs tend to better represent the position of the South Pacific Convergence Zone, other climatic features (e.g., those associated with atmosphere-ocean feedbacks, such as monsoon processes) are less well represented in the CCAM models than the GCMs. As a

consequence, the confidence in projected wave climate conditions in the present study is low, but provides a valuable framework on which to build for future studies.

> **Dynamical wave climate projections carried out within this study suggest changes in wave climate are anticipated over the 21st Century under increasing greenhouse gas scenarios. Best estimates of projected changes in wave conditions over the next Century include:**
> - **Austral winter mean significant wave height is projected to increase in the eastern equatorial Pacific by approximately 0.2m (~5-10%).**
> - **Annual mean wave period increases in the eastern Pacific from approximately 8 to 9s.**
> - **Wave directions in the equatorial Pacific display an increasingly greater southerly component over the 21st Century.**
>
> **Dynamical wave climate projections were carried out for only a very limited set of climate models. Thus, projected changes in wave conditions from this study have poor (unquantified) values of uncertainty.**
>
> **Increased effort is required to develop a larger ensemble of wave climate projections for the PICTs, using the framework established in this project. These efforts, carried out on global scales, will contribute to an international community ensemble of wave projections which will ultimately enable a more complete distribution of potential changes (range of uncertainties) in wave properties to be determined.**
>
> **A distribution of projected change in wave properties will more adequately support future coastal impacts of climate change assessments.**

Recommendations

The observational wave record in the region of PICTs is limited to a comprehensive, relatively short term, study in the late 1980s and early 1990s. These data provide valuable understanding of seasonal variability of wave properties in the region, however have limited application for understanding climatological variability in wave climate. A long-term observation wave programme would provide information for ongoing coastal hazard assessments aiming to understand island shoreline response to climatological variability and change. Considerable capability in wave measurements was developed in the region during the previous study. Whether this capability remains in the region is unknown, however building on this prior program and the archived datasets would be invaluable. This would involve ongoing operation of wave measuring buoys, similar to the Australian Government Agency for International Development (AusAID) funded South Pacific Sea Level Monitoring Program, at locations of previous deployments.

Available wave model products archive only select integrated wave parameters (significant wave height, mean wave period and mean wave direction). These archives are insufficient to describe the multi-modal characteristics of the Pacific wave climate. We propose a high-quality multi-decadal hindcast be carried out, which represents the Pacific wave climate, and archives high temporal resolution (e.g., hourly) characteristics of multiple sea states (height, period and direction of local wind sea, and primary and secondary modes of swell), and spectral data at appropriate locations.

The proposed hindcast must span all of the Pacific Ocean (ultimately global), and computing and storage limitations restrict this hindcast to relatively coarse resolution (~0.5-1°). For the PICT region, nested high resolution wave models should be applied to provide high spatial resolution information in coastal and nearshore regions to support coastal hazard assessments.

Regional capability to carry out high resolution, national or island scale wave studies should be developed. The proposed hindcast should aim to provide boundary conditions for these nested studies, which may be used by regional organisations to develop in-house modelling capability, so that local challenges and studies of interest can be addressed. Collaboration with SOPAC-SPC is underway to support this recommendation.

When forced directly with climate model winds, the wave climate is not well represented by the wave model. This leads to low confidence in the projected changes in wave climate. To overcome deficiencies in the climate model winds, adjustment of climate and variability bias of the surface winds is made, following the method outlined by Hemer et al. (2011a). When forced with bias adjusted climate model winds, marginal improvement in the modelled wave climate is achieved. Development of improved wind bias adjustment schemes is required to support wave climate projection studies. Ultimately, climate model improvement to provide robust surface wind fields is required. The skill of the wave model, when forced with climate model winds, to represent inter-annual and decadal variability was not assessed, and requires attention in future studies.

A range of wave climate projections is observed within the ensemble used within this study. Although this ensemble is too small to adequately quantify the range of values within the projected conditions, it does suggest large uncertainty exists within the wave climate projections once multiple levels of uncertainty are considered. Sources of uncertainty include emission scenarios (un-tested in this study, as only one emission scenario – SRES A2 – was investigated), model uncertainty (different global climate model forcing which is tested here), downscaling approaches (here a single regional climate model is used) and wave modelling approaches (a dynamical approach is taken for this study – a statistical approach may further increase uncertainty). The sources of uncertainty must be understood when projecting climate variables. However, with respect to wave climate projections, a quantitative assessment of each of these multiple levels of uncertainty is a considerable task for a single research group. Consequently, isolated studies generating projections of wave climate should contribute to an international community ensemble of wave projections, following method outlined by Hemer et al (2010a), to allow quantification of the multiple levels of wave projection uncertainty.

1.   INTRODUCTION

The Earth's climate is dynamic and varies naturally over a range of time-scales - seasonal, inter-annual, decadal, centennial, and longer. These variations and trends drive a number of physical processes which can impact on the coastal environment. Sea-level rise, a symptom of warming oceans and melting terrestrial ice, is one process which has received considerable attention over the past decade or more. These climate variations also drive changes in the atmospheric circulation, and consequently the surface winds. Surface wind waves (and storm surges) are generated by the action of wind on the sea surface, and as a result properties of wind-waves will vary in response to the climatological variations in the surface atmospheric circulation. While the potential impacts of variability of wave climate can be large, until recently they have been largely ignored. The Intergovernmental Panel for Climate Change (IPCC) fourth assessment report (AR4) noted that coastal impacts of climate change assessments focussed on sea-level rise, and suggested this be broadened to consider a larger number of coastal processes subject to climate variability and change (Nicholls et al., 2007). Surface waves were identified as one of eight key drivers in the coastal zone requiring increased attention.

Once waves have been generated by a forcing wind, they will continue to travel away from the area of generation as swell. The observed wave field at any point therefore reflects both the locally generated waves (the wind sea) and waves which may have been generated several hundreds, or even thousands, of kilometres away and travelled to that location (as swell). Thus, variability of the wind-wave climate at any location is not only a property of the local wind field, but the integrated variability of the wind field across large areas of the ocean over which the waves have been generated.

Surface waves are an important consideration for a range of processes in the Pacific region. A directional wave climatology, or an understanding of the distribution of wave height and direction, and its variability over time, is an important first step in the study of a number of key threats to coastal areas in Pacific Island Countries and Territories (PICTs) which are subject to wave climate variability and change. These threats are outlined in the following sections.

Coastal flooding.

High coastal water levels are comprised of several components: mean sea-level, astronomical tides, the inverse barometer (IB) effect (e.g., water level is depressed by high atmospheric pressure, and higher beneath a centre of low pressure), wind-driven storm surge (when surface winds push the water towards the coast and hence water level piles up), wave setup (the increase in still water level landward of the breaking point of waves) and wave run-up (the size of the last push of individual waves onto land). In many areas of the global ocean, high coastal water levels are dominated by the wind-driven surge and the IB effect, and the wave driven component is relatively small. This is due to most of the world's continents having a broad continental shelf, over which wave energy dissipates, but more importantly allows a larger distance over which the wind-driven surge can increase in magnitude. In the Pacific Island Countries and Territories however, the continental shelf is typically narrow, and the dominant contributor to high coastal water levels (and hence coastal flooding events) is wave setup and runup. Figure 1.1 displays a schematic of the different contributions to high water levels, and

the relative magnitudes of different components in steep slope scenarios (e.g., PICTs) and shallow slope scenarios (e.g., Australia). The magnitude of wave setup increases with breaking wave height, and during high wave events it can be large. In PICTs, waves often break on the reef, driving a wave setup and increase in still water level everywhere landward of the reef. In December 2008, over 50000 people were displaced in the central west Pacific (Papua New Guinea, Solomon Islands, Federated States of Micronesia, Marshall Islands and Kiribati) during an extreme swell event, generated by an extratropical storm in the NW Pacific. The storm persisted over several days with winds in excess of 20m/s. A preliminary analysis of this event, by Jens Kruger of the South Pacific Applied Geoscience and Technology Division shows that while the significant wave height of this event was not very large (~2.8m), it was the considerably long swell period (mean wave period 14.6s, an approximately 20-yr return period event) which lead to the flooding event (Kruger, 2009). A wind-wave driven coastal flooding event was also observed on the southern Fiji coast in May 2011 (ABC News, 2011). In addition to the immediate consequences of coastal inundation, long term effects of these flooding events includes the contamination of freshwater lenses and swamp taro pits on the islands through the intrusion of salt water, impacting human health.

An understanding of the variability of intense storms which can drive increased extreme wave events, and consequent coastal flooding is required in order to aid PICTs to develop coastal hazard assessments to allow incorporation into adaptation plans and development policies.

Coastal erosion

Surface waves are a dominant driver of coastal sediment budgets, through the transportation of sediment across-shore and along-shore. A slight shift in wave conditions can therefore influence shoreline position, via erosion and deposition, or island progradation and extension. For example, for straight sandy coastlines, longshore transport reaches a maximum when waves approach the coast at an angle of approximately 45°. i.e., according to the CERC formula (Komar, 1971):

$$Q_S = K_S H_b^{5/2} \cos(\theta_b - \theta) \sin(\theta_b - \theta)$$

Where Q_S is the longshore sediment transport, K_S is an empirical constant which is a function of water density and local sediment properties, H_b is the breaking wave height, θ_b is the breaking wave angle, and θ is the angle of the shore normal, such that $(\theta_b - \theta)$ is the wave angle with respect to the coast. The shoreline position responds to convergence/divergence of the longshore transport as accretion/erosion, respectively. (e.g., Slott et al., 2006)

$$Dn / dt = (-1/D) \, dQ_S / dx,$$

Where n is shoreline position, D is the local closure depth, and x is the longshore axis.

If the angle of approach of waves changes by just a few degrees, the longshore transport of sediment can therefore change significantly. Under the effects of such changes, regions of transport convergence/divergence will shift along the coast, altering the equilibrium state of the shoreline leading to changes in shoreline position (erosion or accretion).
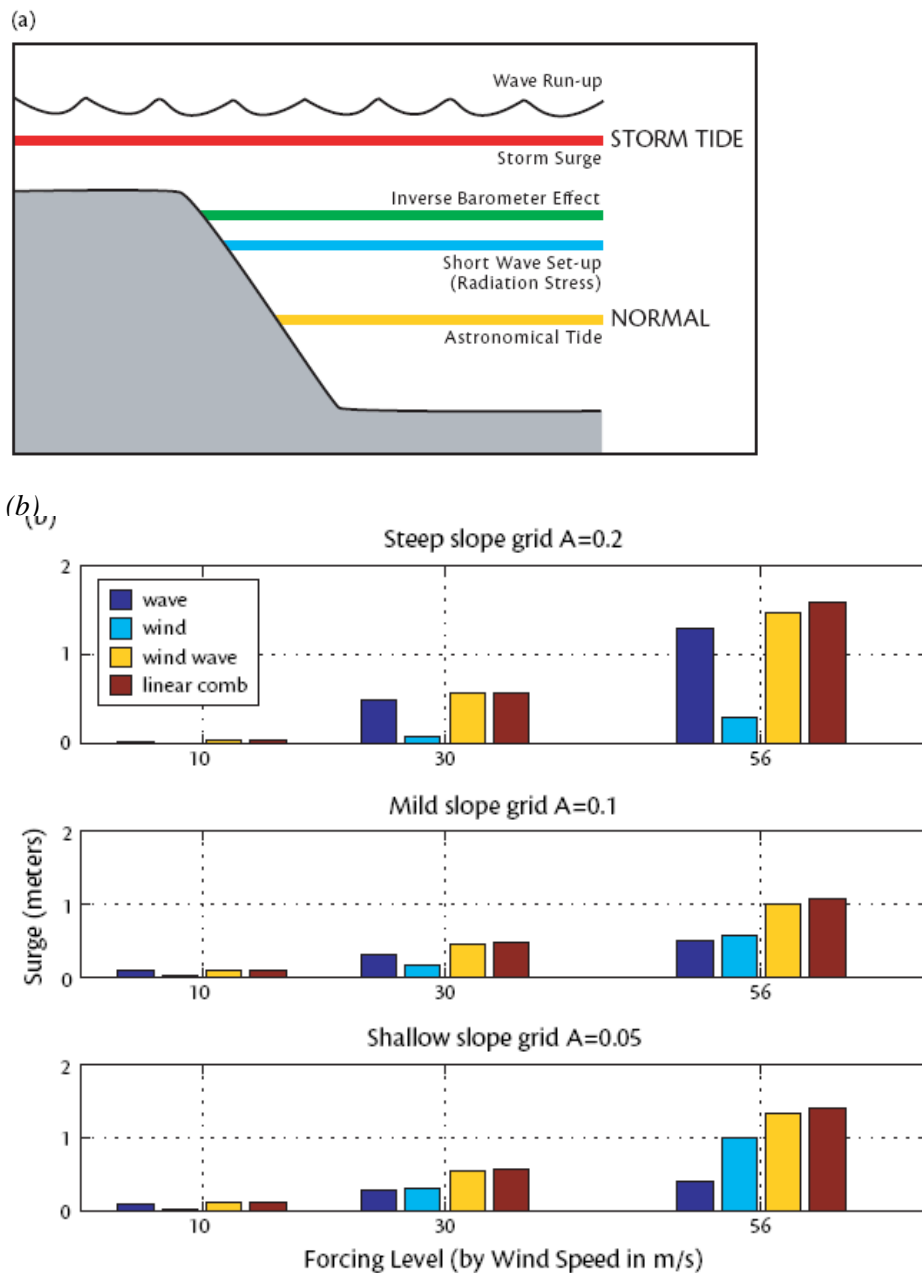
(a)

(b)

Figure 1.1. (a) Schematic showing the different contributions of water-level changes that the make up the total rise in water elevation. (b) Storm surge simulations, including the wave effect, due to radiation stress for steep (top), mild (centre) and shallow (bottom) bottom slopes defined by A, and for wind speeds covering gale (17.5 m/s), tropical storm (26 m/s) and hurricane (33 m/s) force. The simulations show that for steep slopes (top panel), the wave-induced water level rise (dark blue) dominates the wind-driven storm surge effect (light blue). On the contrary, for gentle slopes (bottom), the wind-induced storm surge (light blue) causes the largest water level rise rather than the waves. The yellow boxes represent the results of total storm surge when the wind-driven and wave induced water levels are added nonlinearly within the model., while the brown boxes shows the linear combination of these. Figure taken from Graber et al. (2006).

The impacts of changes in shoreline position in response to variability of wave conditions, considered in the context of increasing coastal population, require understanding to support production of appropriate planning and development zones for PICTs.

Reef morphology and marine habitats/species distribution.

Marine and coastal habitats can be characterised by the frequency with which they are disturbed (e.g., Hall, 1994), and hence wave driven disturbances are a characterising feature of the marine environment. Wave climate characteristics are an important factor for many geological and ecological processes. Waves affect the structural complexity of reef morphology and associated coral species distribution (Storlazzi et al., 2001). They influence the extent and form of seagrass and mangrove habitats, and consequently affect opportunities for shelter, breeding and feeding for fish and other sessile fauna that sustain coastal fisheries (Grech and Coles, 2010). The full extent of the role of waves in the near-shore and coastal ecosystems is still poorly understood, and an area of active research.

Understanding variability and changes in wave climate in nearshore regions of the PICTs is required to enable adaptation plans to support marine and coastal livelihoods in the region.

Lagoonal circulation and water quality

For many reef-lagoon systems in the PICTs, the dominant circulation patterns are driven primarily by breaking waves at the reef edge which generates a wave setup within the surf zone. Depending on the morphology of the reef and lagoon, a difference in water level may be established between the reef crest and the back reef, which can drive strong cross-reef flows (commonly termed wave pump). This flow may then drive the dominant lagoonal circulation which impacts a number of other key processes within these systems (e.g., sediment transport, biogeochemical cycling and spatial ecology; Lowe et al. 2009).

The magnitude of wave pump is dependent on reef morphology, and the size of the wave setup, and hence the magnitude of the breaking waves. Variability and change in wave conditions, and hence wave pumping across reefs, will lead to variations in the strong coupling between the surface waves and lagoon water flow, particularly when considered within the context of changes in mean sea level. These changes will impact on lagoon flushing times, and consequently lagoon health.

Transport and energy solutions

Under adverse wave conditions, transport between islands within PICTs can be affected as vessels are unable to travel. The loss of days at sea, or the inability to leave port due to bad weather may considerably influence transport of goods to some communities.

Many PICTs rely on expensive diesel generated power for electricity. One option available to these communities is to extract energy from the waves, using wave energy devices which are costs-competitive with diesel generation. Understanding the magnitude of the wave energy resource, and its variability, is important information in establishing the potential for wave energy development in PICTs.

Project Aims

With the key influences of the wind-wave climate on PICTs introduced above, this project set out to achieve two aims:

1. To use existing data and knowledge of waves in the Pacific region to characterise the historical wave climate. The objective here is to understand large scale changes, including seasonal variability, historical inter-annual variability and potential trends, and identify the key modes of variability of observed changes. This broad scale information is considered critical understanding for anticipated future studies (beyond the scope of the current project), which will assess the downscaled influences of the observed variability at the scale of individual PICTs. This objective also aims to assess gaps in current knowledge and provide recommendations to address these.

2. To carry out a preliminary assessment of potential changes in Pacific basin wave climate under future climate scenarios. In order to develop suitable coastal adaptation strategies to climate change, PICTs require current best estimates of how wave climate is projected to change in future scenarios (in addition to other processes in the coastal zone, e.g., sea-level rise). Wave climate projections are currently at a very preliminary stage, lagging several years (or even decades) behind the developments of other climate variables. Consequently, the focus of this component of the project is on understanding the broad-scale changes to the Pacific wave climate, and on method development under a limited subset of climate scenarios. These projections will have high (or unquantifiable) uncertainty, but the methods developed will be refined in proposed ongoing activities (outside scope of current project) to quantify the associated uncertainty and downscale this understanding to the scale of individual PICTs.

It is important to note that the scale of interest for this study is broad scale, in understanding the key large scale climatological drivers of the Pacific wave climate, with focus on the region of the PICTs. Local scale effects are beyond the scope of the current project. Our study has limited the spatial extent of the Pacific to 110°E to 300°E and 50°S to 50°N, however the study has focussed on the region covered by the 22 Pacific Island Countries and Territories, plus the Hawaiian Islands. This region is consistent with the membership of the Pacific community.

2.   EXISTING KNOWLEDGE

An aim of the present pilot wave study of the Pacific basin was to identify current knowledge on the wave climate of the region, in order to identify gaps in knowledge to be addressed in future studies. Several studies of the wave climate have been carried out previously, and a brief summary of these is given here.

In the late 1980's into the early 1990's, the Norwegian Government supported a multi-year wave data collection program by the SOPAC Secretariat with the specific objective of assisting island member countries to gather and assess wave and weather data to identify sites with wave energy resource potential. Data collection commenced in 1987, and was completed in 1993. A number of reports were completed documenting the wave climate of several member countries of the Secretariat (e.g., Barstow and Patiale, 1992, Barstow and Haug, 1994a,b,c,d,e,f) and two further reports on the wave climate of the South-West Pacific more generally, building on the knowledge from the in-situ observational campaign in combination with the limited altimeter database of the time and the best available global wave model at the time (Barstow and Haug, 1994g and Barstow and Falnes 1996). This is a critically important dataset for understanding the wave climate of the region. The limitations of this dataset are the site specific nature of the measurements, and the limited length of dataset. The longest of the in-situ records, off the coast of the Kingdom of Tonga, spans a period of 5 years, however most of these records are limited to 3 years or less. This provided a valuable dataset in understanding the seasonal variability of the regional wave climate, but limited use for understanding the inter-annual climate variability. Barstow and Falnes (1996) supplemented the observational data with available satellite altimeter data at the time (1986-1989 GEOSAT mission), which resolved some of the spatial variability of wave heights in the region. These studies also aimed to supplement the in-situ buoy data with available wave model data from the UK Met Office, to extend the spatial representation of other wave variables not measured by the altimeter (wave period and direction). However, it was concluded that the modelled wave directions were not entirely satisfactory due to systematic underestimation of swell in the model. The studies noted the critical importance of wave direction data for the estimation of coastal wave climates.

These studies made some comparisons of the effect of the El Niño/Southern Oscillation phenomenon on ocean wave heights, but recognised the limited period of study could not be considered representative of observed variability. These authors suggest that the increased frequency of westerly winds in the low latitudes during El Niño conditions lead to decreased wave heights, and hence lower wave power levels on the eastern coasts of the islands. These authors also considered the contention of higher southerly swell in El Niño years in the South Pacific caused by more frequent southerly gales in the mid-latitudes. The investigators noted the need to extend the study investigating long term variability of ocean waves in the South Pacific when more satellite and wave model data were available.

Barstow and Haug (1994g) found open ocean annual average wave heights to vary from a little under 2 m to the west of the Kiribati group at the equator and to the west of the Vanuatu group in the Coral Sea, to close to 3 m at 30°S south of the Southern Cook Islands. They found that seasonal variability was relatively modest, particularly in the low latitudes. At the southern most locations, there was a tendency for waves to be larger during the austral winter, and at the

northern most locations, there was a tendency for wave heights to be larger during the austral summer. Wave conditions were mainly characterised by trade wind driven seas and long distance swells from both the Northern and Southern Pacific storm belts. In the buoy records at Funafuti, Efate and Rarotonga, both southerly and northerly swells were present. Northerly swells occur predominantly during the northern hemisphere winter (October to March) whereas southerly swells occurred at any time of the year, but were more energetic during the southern hemisphere winter. At Tongatapu, Western Samoa and Kadavu only southerly swells were observed. In addition to the seasonal influence of the northern hemisphere swells on northerly exposed shores, the strongest seasonality was observed close to the coast due to the fact that over much of the area wind seas have a relatively large seasonal shift in direction, typically from south-easterly during the austral winter to north-easterly during the austral summer. Tropical cyclones were described as being most frequent in the west of the region (Vanuatu group) and south of 10°S, occurring most frequently in December to March.

The wave climate in Micronesia, in particular around Guam, is relatively well studied due the presence of the US Military in the region. The Pacific region integrated climatology information products (Marra et al., 2008) summarise climatology impacting the Pacific region. The offshore wave climate in this region is dominated by the north-easterly trade winds and northerly swell from extratropical storm systems, both more frequent during the boreal winter (McGehee and Boc, 1997). As the trade winds have a long fetch into this region (from Hawaii to Micronesia), periods of enhanced trade winds will generate a large wind sea of order 3-4 m wave height from the north-east. Swell generated by northern Pacific extratropical storms is also most common in winter, when the strongest storms develop in the mid-latitudes of the North Pacific Ocean. While most of the swell from these systems is directed further eastwards (towards Hawaii), some of this moderate to long period (10-18 s) swell enters Micronesia, and aside from tropical cyclone generated waves, are the cause of largest wave events in the region, impacting on the north facing shores of the islands. The severe inundation event recorded through Micronesia and southward to the northern coastline of Papua New Guinea in December 2008 was attributed to a northerly swell event (Kruger, 2009). Blocking by Papua New Guinea and other south-west Pacific islands shelter Micronesia from swell generated in the South Pacific.

The trade wind sea and northerly swell dominate a strong seasonal cycle in the western North Pacific, with higher mean wave heights recorded during these winter months. However, large waves can be experienced at any time of year. During summer months, the monsoon trough is a dominant feature of the western North Pacific. The monsoon trough is an east-west oriented trough of low pressure, with easterly winds observed to the north and (south) westerly winds observed to the south. The monsoon trough forms at low latitudes (south of 10°N) and drifts slowly north-west. As one monsoon trough leaves the region, another forms to replace it, and the cycle repeats. During summer, the trough often extends into Micronesia, and the south westerly winds south of the trough can generate large waves over the long fetch available. The western shores of the islands are exposed to these waves. ENSO is known to have a strong influence on the behaviour of the monsoon trough in this region. During strong La Niña (positive SOI), the trough is weakened and restricted to the far west. Consequently the associated south-westerly waves are not experienced. During El Niño years however, the trough extends further eastwards than normal, and is established earlier than normal. This has the effect of increasing fetch of the south-westerly waves during this period, but also, monsoon depressions developing in the trough are the initial phase of the majority of western north

Pacific tropical cyclones. During El Niño, cyclone frequency increases significantly in Guam, and in eastern Micronesia, cyclones are almost exclusively experienced during El Niño. Sasaki et al. (2005) reported a recent increase in summertime extreme wave heights in the western North Pacific, associated with a recent (up to 2004) increase in total duration of intense tropical cyclones in the region.

The wave climate in the central North Pacific is well studied, owing to the amount of research carried out on the Hawaiin wave climate and the presence of National Oceanic and Atmospheric Administration (NOAA) National Data Buoy Center (NDBC) buoys in the region. The average directional wave spectrum in Hawaiian waters is bimodal, dominated by the north Pacific and trade wind swell regimes (Aucan 2006). Also observed, but not with the same magnitude or frequency as these wave regimes, are southerly swell and subtropical cyclone (Kona storm) generated wave events. The north Pacific swell is generated by the northern hemisphere extratropical storm systems that track predominantly eastwards from origins in the northwest Pacific. These north-north-westerly swells reach their peak during the northern hemisphere winter when the storm belt intensifies and shifts southwards. Consequently these swells have a strong seasonal signal, with winter mean significant wave heights of over 3 m, and a summer mean significant wave height less than 2 m. Vitousek and Fletcher (2008) report an annual recurring maximum significant wave height of 7.7 m, with peak periods of 14-18 s.

Trade wind swell is relatively persistant on the Hawaiian coast from the north-east throughout the year. These winds generate fetch limited swell with average wave heights of approximately 2m and peak periods of approximately 9 s, ,which are felt on the north-east facing coasts of the Hawaiian islands. Trade wind swell has been observed to exceed 5 m in height, and have long periods (in excess of 15 s).

Snodgrass et al. (1966) showed that swell generated in the southern Pacific Ocean in the southern hemisphere extratropical storm belt can propagate to Hawaii with little attenuation of energy outside the storm generated region. This southerly swell is observed at Hawaii predominantly during the Northern Hemisphere summer (southern hemisphere winter months), when the southern storm belt is more intense and further northwards. These swell have an annual mean significant wave height of 2.5 – 3m and peak periods of 14-22 s – slightly longer than the north Pacific swell observed in the region (Vitousek and Fletcher, 2008).

Subtropical cyclones (kona storms) occur more locally to Hawaii, and generate south-westerly waves of significant wave heights of 3-4 m and periods of 8-10 s (and bring clouds and rain to the islands). Rooney and Fletcher (2005) reported the extensive damage Kona storm waves can cause to the islands during the 20-30 year negative Pacific Decadal Oscillation (PDO) cycle, while Positive (warm) PDO, and El Niño phases tended to suppress Kona storm activity.

Hemer et al. (2010) assessed the inter-annual variability of the southern hemisphere directional wave climate as recorded in a 15 year satellite altimeter record, and the 45 year European Centre for Medium Range Weather Forecasting (ECMWF) ERA-40 waves reanalysis. They found that the primary mode of variability of wave climate, extending from the Southern Ocean northwards into the eastern equatorial Pacific, was significantly correlated to the Southern Annular Mode (SAM) Index – particularly during the austral winter. During positive SAM, the extratropical storm belt intensifies and shifts southwards. The response observed in the wave climate to this signal was an increase in significant wave height both in the region of generation

in the Southern Ocean, but also in the eastern equatorial Pacific region where these waves are observed as swell. Also observed correlated with this signal was an anticlockwise rotation of wave direction in the region of southern ocean generated swell. During the austral summer, this principal mode of variability was observed to significantly correlate to the Southern Oscillation Index (SOI). Negative anomalies of the SOI (El Niño events) were associated with increased wave heights over large regions of the south-west Pacific Ocean. Also correlated with the SOI was a rotation in the direction of the trade wind generated waves. During negative anomalies of the SOI (El Niño), the increased frequency of westerly winds resulted in a clockwise rotation of the south-easterly trade winds in the latitudes north of 10°S to become more south-south-easterly when averaged over the year.

Young et al. (2011) assessed the 25-yr (1985-2009) significant wave height record obtained from satellite altimeters for trends. They found no statistically significant trend in the mean monthly values, but for the upper tail of the wave distribution, a clear, statistically significant trend of increasing wave height at high latitudes was observed, but more neutral conditions were found in the equatorial regions.

To summarise, a clear picture of the Pacific wave climate has emerged from previous studies. In the equatorial bands (between 30°S to 30°N), a multi-modal wave spectrum is observed almost everywhere. The dominant modes of this spectrum are dependent on where in the Pacific Ocean the waves are observed. In the northern sector of the equatorial Pacific Ocean, the two dominant modes are the swell generated by the northern extratropical storms and the north-easterly trade winds, but the influence of southern swell are still observed. In the southern sector of the equatorial Pacific Ocean, the south-easterly trade wind generated waves tend to dominate, and the presence of southerly or northerly swell depends on the local geography and whether these wave regimes have been sheltered by up-wind-wave islands or land masses. Tropical cyclones are important in generating large wave events, particularly in the western equatorial Pacific.

3.   AVAILABLE DATA

In the region of Pacific Island Countries and Territories, long-term in-situ wave data are sparse. Thus, knowledge of the historical wave climate must be determined from satellite data, or wave modelling studies (hindcasts and/or reanalyses – i.e., a model simulation constrained by observations). One of the key tasks for the present project was to compile existing wave datasets for the Pacific region, to both assess the variability and change in the historical record, and determine data gaps in the region which may be addressed in future research activities. Several datasets are available to describe the current wave climate of the Pacific Ocean basin, however these all have particular properties which limit their usefulness, whether due to spatial resolution, or data archive limitations, or other. A brief summary of the datasets used in this study is given below.

3.1   United States Army Corps of Engineers (USACE) Wave Information Study (WIS)

The Wave Information Studies (WIS) is a US Army Corps of Engineers (USACE) sponsored project that generates consistent, hourly, long-term (20+ years) wave climatologies along all US coastlines, including the Pacific Ocean. The WIS have developed a 20 year wave hindcast for the Pacific Ocean Basin. The wave hindcast predicts past wave conditions using the WaveWatch III numerical spectral wave model, forced using value-added 3-hourly wind fields (which combine ground and satellite wind observations with modelled wind fields). WaveWatch III was developed at the National Oceanic and Atmospheric Administration (NOAA) / National Centers for Environmental Prediction (NCEP), where it has been used operationally since 2000. It is a 3rd generation wave model, meaning that non-linear wave-wave interactions (which act to distribute energy amongst different wave frequencies) are included in the model dynamics, and that there are no restrictions placed on the shape of the evolving wave spectrum. The wave model is applied at 0.5° spatial resolution covering 64°S-64°N, 110°E-60°W. The spectral resolution covers 25 logarithmically spaced frequency bins from 0.03 to 0.4Hz, and a directional resolution of 15°. Further details of the model implementation are described by Hanson et al. (2010).

At the time of gathering data for this study, the USACE WIS had identified a persistent positive bias in hindcast wave height relative to buoy data, and consequently removed access to the hindcast data for 3rd Parties (Robert Jensen, USACE, Pers. Comm.). The USACE were very willing to supply their data for the study at a later date once confidence in results was obtained. However, this dataset was unfortunately not available for this study.

3.2   ECMWF ERA-40

The European Centre for Medium-Range Weather Forecasts (ECMWF) completed the ERA-40 re-analysis of global meteorological variables, including surface waves, using ECMWF's Integrated forecasting system, a coupled atmosphere-wave model that uses variational data assimilation (Uppala et al., 2005). The period of the re-analysis is from September 1957 to August 2002 (45 years), and includes ocean surface wind waves on a 1.5° x 1.5° latitude-

longitude grid covering the whole globe, generated using ECMWF's coupled WAM wave model (Komen *et al*., 1994). WAM is also a 3rd Generation wave model, similar to WaveWatch III. A subset of the re-analysis output on a 2.5° x 2.5° latitude-longitude grid at 6-hourly intervals is freely available to the research community from ECMWF (ECMWF, 2006). The complete dataset at full model resolution is available but is not a free service. Sterl and Caires (2005) carried out an extensive assessment of the quality of the significant wave height (H_S) and mean wave period (Tm) produced from the re-analysis, comparing the data against 20 American National Data Buoy Centre (NDBC-NOAA) wave-rider buoys, and "along-track quality" checked deep-water altimeter measurements of H_S from GEOSAT, TOPEX, ERS-1 and ERS-2. Sterl and Caires (2005) used these data to build the Web-based KNMI/ERA-40 wave atlas describing the global wave climate. The ERA-40 data has received considerable attention in describing the global wave climate (see Sterl and Caires, 2005). These studies indicate considerable negative bias in global wave heights, particularly related to large wave events. Caires and Sterl (2005) produced a statistically corrected version of this wave height dataset (C-ERA40), which has also received considerable prior attention. No further analysis of this dataset has been carried out in this study, as ECMWF now advocate the use of their revised reanalysis product - ERA-Interim (see below).

3.3   ERA-Interim

ERA-Interim is a reanalysis similar to ERA-40, described above, where the ECMWF integrated forecasting system, including a coupled atmosphere-wave model using variational data assimilation, is used to describe the state of the atmosphere, land and ocean-wave conditions. ERA-Interim was intended as an interim reanalysis in preparation for the next generation extended reanalysis (ERA-clim) which will replace ERA-40. Most importantly for the purposes of this study, ERA-Interim data is available at a higher spatial resolution (1.5° globally) than ERA-40. Unfortunately, ERA-Interim spans a shorter 20-yr data period (1989-2010), and is a limitation of this dataset in describing the magnitude of inter-annual variability of climate properties. Recent news (April 2011) is that ECMWF intend to extend the ERA-Interim dataset back to 1979, so that a 30-yr reanalysis will be available (J. Bidlot, ECMWF, Pers. Comm).

ERA-Interim surface wave data which are freely available to the research community include 6-hourly values of integrated significant wave height (Hs), mean wave period (Tz) and mean wave direction (Dm). These data provide a very useful dataset which is both consistent in time and space for assessing variability in the mean wave climate in the Pacific Ocean basin. However, the available wave parameters are not sufficient to distinguish between locally generated wind sea or swell generated by storms elsewhere and propagated to the site. Given the Pacific wave climate is characterised by its bimodal wave spectrum, with locally generated short-period easterly wind-seas generated locally by the trade winds, and long-period swell generated by storms at mid to high latitudes in the extratropical storm belt, which are typically observed as having a westerly direction in the region. Additionally, the 6-hourly temporal resolution of these data are relatively coarse, and peaks in wave conditions which occur during storm wave events may be smoothed over this period. Finally, the 1.5° spatial resolution is coarse, and this influences two aspects of the wave climate: 1. the coarse model resolution results in reduced intensity of intense storm systems (e.g., tropical cylones), and waves resulting from these type of events are likely to be significantly underestimated; and 2. the

resolution is coarse with respect to individual PICTs, and so only the broad scale wave properties in the region may be determined. With these limitations in mind, ERA-Interim was chosen as one of the key datasets for analysis in this study.

3.4 Satellite Altimeter record (Swinburne University)

Satellite altimeters provide an alternative to visual or in-situ measurements of ocean wave height. Since the launch of GEOSAT in 1985, there exists an almost continuous record of measures from seven altimeter missions (a gap exist in 1990-1991). Zieger et al. (2009) carried out systematic calibrations of significant wave height (and wind speed) and cross-platform validations of all altimeter missions over the full 23-yr altimeter record, against 12 in-situ buoy records. They provide a consistent data set over this extended period. Young et al. (2011) used this dataset to investigate trends in the mean, 90th and 99th percentiles of wind speeds and wave heights for 2° x 2° regions covering the globe. These authors have made this data available for this study, to investigate the seasonal and inter-annual variability. While Young et al. (2011) use the full altimeter record from 1985 to 2009 (using GEOSAT data from 1985 to 1989), we have discarded the GEOSAT data for this study. We do this for two reasons: to maintain a continuous record full year records from Jan. 1992 to Dec. 2009, and due to inconsistent values being identified in the 1985-1989 GEOSAT period data.

These data include monthly values of mean, 90th and 99th percentile significant wave height (and 10-m wind speed) on a 2° global grid. These provide a very useful observational dataset to assess the seasonal and inter-annual variability of the Pacific Ocean wave climate. However, it also has several limitations. Wind-sea and swell can not be distinguished, assessment of storm wave conditions are limited to statistics of the monthly 90th and 99th percentiles within a 2° grid cell, limiting the ability to assess frequency of storm wave events. Also, it should be noted that altimeters typically have a long interval between sampling the same point on the ocean surface (of 10 days at least). This leads to large wave events potentially being un-sampled if they occur in between these samples. The merging of data into 2 degree bin aims to remove the effects of this sampling characteristic, so that all events are sampled. Sampling data into 2 degree bins limits the spatial resolution of these data, so that like the reanalysis data, only broad scale wave properties can be obtained from the data, limiting application in assessing the effect of waves coming ashore. With these limitations in mind, the altimeter dataset was chosen as one of the key datasets for analysis in this study.

3.5 In-situ Buoy Data

Most properties measured by buoys in the marine environment (e.g., wind speed, direction, air temp, water temp etc) are direct measurements, in that they do not typically require complicated data processing, or supplemented data from other sensors. In contrast, waves are an indirect measurement, in that wave data are derived from motion of the buoy and require extensive processing and analysis. From the motion of the buoy, a corrected wave spectrum is determined, for some buoys, directional wave spectrum may be determined. From this spectrum, integrated wave parameters such as significant wave height, mean and peak wave period and direction (if available) can be determined at the location of the buoy. For this study,

it is only the integrated wave parameters which have been considered and were available. Analysis of peak wave period indicates what the frequency of the most energetic waves in the spectrum are, and can be used to determine whether the spectrum is dominated by wind sea (e.g., Tp<8s) or swell (Tp>8s).

The U.S. National Data Buoy Centre (NDBC) of the National Weather Service, a part of NOAA, operates a large number of wave measuring buoys in areas of interest to the United States. These include buoys of interest to this study, along the U.S. Pacific coast, and in the region of the Hawaiian Islands. The NDBC first deployed a wave measuring buoy in 1973, and these data are provided in real-time, and in delayed mode to the archives for a variety of users.

In 1987, a wave power collection program was started in the South Pacific, financed by the Royal Norwegian Ministry for Development Cooperation , NORAD, providing support to the South Pacific Applied Geoscience Commission (SOPAC). The operation of these buoys was initially carried out by the Norwegian Hydrotechnical Laboratory (NHL), and in 1990 was taken over by the Oceanographic Company of Norway A/S, OCEANOR. Buoys were deployed in Tongatapu, Kingdom of Tonga (April 1987 to July 1992), at Eua, Kingdom of Tonga (June 1992 to September 1992), Rarotonga, Cook Islands (July 1987 to January 1991), Western Samoa (September 1989 to July 1992, and directional from March 1993 to June 1993), Tonga (in December 1989), off Funafuti, Tuvalu (May 1990 to April 1992), and Efate Island, Vanuatu (November 1990 to February 1992, and directional from November 1992 to February 1993). These data are critically important for characterising the wave climate of the Pacific region, but are limiting in that they span only a short period of time. The use of these data is limited to being used to determine how well other datasets represent the observed wave climate of the region.

3.6   NCEP Climate Forecast System Reanalysis

The US National Center for Environmental Prediction Climate Forecast System Reanalysis (CFSR) is a global high resolution coupled atmosphere-ocean-land surface-sea ice system aimed to provide the best estimate of the state of these coupled domains over the 31-yr period from 1979 to 2009. CFSR derived surface (10m) winds and mean sea level pressure (MSLP) fields are available at hourly temporal resolution and a horizontal resolution of 0.5° longitude x 0.5° latitude. These data were used to as a benchmark for comparison for surface wind/MSLP fields presented in this study.

4. DATA PROCESSING METHODS

The focus of this study is the seasonal and inter-annual variability of wave climate in the Pacific region. To address these aims, we have processed the available datasets to describe monthly statistics. Monthly statistics determined include the monthly mean significant wave height, and the Xth percentile of significant wave height in each month, for X = 90, 95 and 99, to focus on the upper tail of the wave height distribution. Monthly statistics of significant wave height are determined for all available datasets. For example, for the ERA-Interim reanalysis dataset, the processed dataset contains 252 monthly values (21 years) for each model grid cell.

Monthly wave period and direction data are determined for each of the reanalysis data, the project specific datasets (climate model forced wave model runs), and buoy data where these parameters are defined. For monthly mean data, the corresponding monthly mean of the integrated wave parameters is determined. For high percentile data (e.g., the 99th percentile), we limit the data to focus on the upper tail of the distribution only. For example, the monthly 99th percentile of wave direction is defined here as the mean wave direction of all occurrences where the significant wave height exceeds the 99th percentile of Hs. This definition is used for all percentiles, and the same approach is taken for mean wave period.

The model, reanalysis, and Swinburne altimeter datasets are pre-processed datasets, and required no further quality control for this project. The buoy data required some quality control checks, including removal of non-physical values, and where values were inconsistent with preceding points. The data were of high quality and this procedure removed only few points. The buoy data had variable temporal resolution. To ensure consistency with reanalysis and model data, buoy data are linearly interpolated onto the 6-hourly data before computing monthly statistics.

5. ASSESSMENT OF THE PRESENT WAVE CLIMATE

Surface ocean waves are generated by wind. If a wind blows over an initially calm surface, the water surface will be disturbed, and ripples in the surface appear, with wavelengths on the scale of centimetres. As the wind continues to blow, the wavelength, period (the time taken for two consecutive wave crests to pass a point) and height of the waves increases. In deep water, waves at the sea surface are determined by the wind speed, the duration that the wind has been blowing, and the fetch over which the wind has blown. When the duration and fetch are sufficiently large, a sea-state referred to as a fully developed sea is reached, and waves can grow no larger (as the wave speed and wind speed are similar). The duration and fetch is governed by the characteristics of storms and other weather systems which vary in space and time, and by the geometry of a particular ocean or sea. The sea-state rarely becomes fully developed. When the wind direction and/or wind speed change (as the storm passes), a new wind-sea field develops corresponding to the new wind field. The old waves still exist, but are decoupled from the wind forcing, and are referred to as swell. Swell can propagate over large distances with only little damping. Consequently, at any location there are often several wave systems which exist simultaneously. Each system can be characterised by different wave periods, directions and heights. At a point, they may be represented by a wave spectrum – wave energy as a function of wave period and direction. Few wave spectra data are available for the Pacific region, and is a notable shortcoming of the datasets available for this study. Refer recommendations for further details. In this study, we are forced to characterise the wave field by the mean integrated wave field, including significant wave height (roughly corresponding to the 1/3rd largest waves in a wave field), the mean wave period (the average of all wave periods), and the mean wave direction (the average of all wave directions). In some instances, some inferences may be made on the properties of sea and swell, but no definitive results are presented.

The good comparison between ERA-Interim (EI) data and observations from altimeter and buoy data shown in Appendix A provide confidence in the use of Era-Interim to describe the wave climate of the Pacific region. We acknowledge the lack of observational wave period and direction data in the region casts greater uncertainty on the skill of EI to represent these variables, the EI provides a useful dataset to describe the directional wave climate. Firstly, we further summarise the Pacific wave heights.

5.1.1 Significant Wave Height

Monthly mean wave heights, derived from altimeter data, are used to calculate the mean annual cycle. Figure 5.1 shows the mean annual cycle for the Pacific basin. Figure 5.2 maps the sample standard deviation (an estimate of the inter-annual variability of significant wave height). Inter-annual variability is largest in the northern extratropical storm belt during the northern winter months (Nov-Feb). High inter-annual variability is also observed in the southern extratropical storm belt during the austral winter months (May to Oct), near to the edge of the domain of interest, at approximately 50°S. If the sample standard deviation is normalised by the mean wave height, other regions with strong inter-annual variability are resolved (Figure 5.3). Despite the spatial resolution of the Era-Interim reanalysis being too coarse to adequately resolve tropical cyclones and typhoons, normalising the standard deviation

by the mean wave height resolves strong inter-annual variability associated with tropical storms systems. Notably, variability is in excess of 20% of the mean in the western equatorial Pacific: In the Philippine and East China Seas during the Pacific typhoon season (June-Oct); and in the Coral and Arafura Seas during the Australian cyclone season (Dec-Apr). The variability of the southern tropical storms appears not as strong as the northern tropical storms, but tends to extend further east across the Pacific. In February, the variability is greater than 12% of the mean as far east as approximately 220°E in the southern extra-tropical Pacific. In the northern equatorial Pacific in August, the variability is greater than 12% of the mean to approximately 180°E. The variability associated with the northern extra-tropical storm belt remains a region of high inter-annual variability during the northern winter months (variability approximately 15-20% of the mean), particularly towards the USA coast. The eastern equatorial Pacific Ocean has relatively low variability (less than 5% of the mean) throughout the year. This large scale behaviour in inter-annual variability becomes more pronounced when the inter-annual variability of monthly 90th and 99th percentiles is determined (not shown). While variability is expected at the scale of individual storms, the high level of inter-annual variability in monthly statistics suggests other coherent patterns influencing the Pacific wave climate.

To investigate the potential influence of other coherent patterns, we have removed the mean annual cycle from the monthly mean significant wave heights (*Hsm*) to generate a monthly anomaly (*Hsm_anom*). Similarly, we remove the mean annual cycle of *Hsm90* from the monthly 90th percentile values of significant wave height to generate a monthly 90th percentile anomaly (*Hsm90_anom*), and similarly again for the 99th percentile. For each of these 3 datasets, we then run a 12-month running mean to remove the noise in each anomaly time-series at each grid point. This processing is repeated for each of our wave height datasets. The period of coverage differs for each set, spanning 1989-2009 using ERA-interim derived data, 1993-2008 for the Altimeter derived data, and 1979-2009 using the NCFSR forced hind-cast.

For each dataset, we regress the gridded values of the significant wave height anomaly against time (to determine presence of significant trends in record). The Era-Interim data exhibit significant trends in the Pacific basin over the 20-yr period, however these are unsupported by buoy data. The trends over this 20-yr period are too short to represent long term change in wave conditions, and any apparent trends are subject to the strong inter-annual variation in wave climate in the region.

We have also experimented with regression of the de-trended significant wave height anomalies with a number of climatological indices, including the Southern Oscillation Index (SOI), the Southern Annular Mode Index (SAMI), the Pacific/North American index (PNA), the Indian Ocean Dipole (IOD), the Arctic Oscillation (AO) and the North Atlantic Oscillation (NAO). These climate indices were obtained from the United States National Oceanic and Atmospheric Administration Climate Prediction Center (NOAA CPC, 2011).

Significant correlation is observed between wave height variability and the Southern Oscillation index throughout the Pacific basin. This is observed as a strong negative correlation in the western equatorial Pacific and a band of negative correlations across the basin to the north-east in the Northern Hemisphere, and to the south-east in the southern hemisphere. Strong negative correlation between the Hs anomalies and the SOI are observed over the PICTs. Positive correlations are observed over the eastern Pacific adjacent to the South American continent, and in the Tasman and Coral Seas adjacent to the east Australian continent. These

results are consistent with the ENSO cycle observed in the Pacific basin. The positive correlation on Australia's east coast reflects the stronger influence of tropical storm and cyclone systems in the coral sea during positive SOI anomalies (La Niña). During negative SOI anomalies (El Niño), higher sea-surface temperatures shift eastwards into the central Pacific Ocean, and consequently the frequency of tropical storm and cyclone systems increases in the central Pacific during these events. The observed negative correlation (i.e., wave height increase during negative SOI anomalies) is consistent with this broader understanding. We have looked at the average wave height when the SOI is less than its 20th percentile values (to represent negative anomalies or El Niño events). Over this period, we see that the mean wave heights are approximately 10cm higher than the long term average. The significant positive correlation in the eastern tropical Pacific indicates that the slackening of the trade winds in this region during El Niño events (negative SOI anomalies) results in reduced wave heights in this region during these periods. The mean wave height when the SOI is less than its 20th percentile value is approximately 5cm less than the long term mean (Figure 5.5).

Correlation to the Indian Ocean Dipole displays a very similar spatial structure to the correlation to the SOI (Not Shown). The regions of negative correlation to the SOI correspond to the regions of positive correlation to the IOD, however the correlations to IOD (CC~0.35 in western equatorial Pacific) are not as strong as the correlations to the IOD (CC~0.7). It is accepted that positive phases of the IOD co-occur with El Niño (Luo et al., 2010), and this observed response corresponds to this relationship.
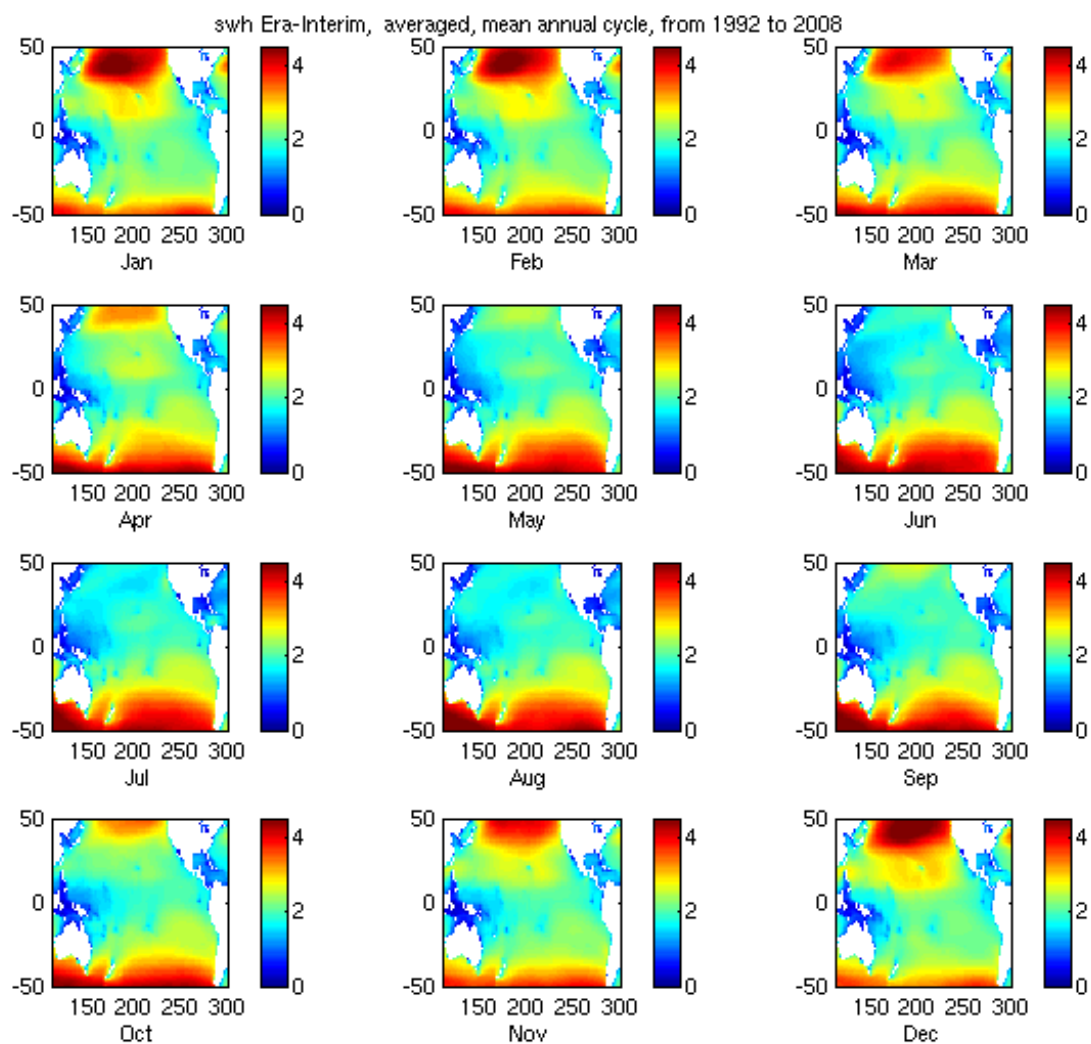
Figure 5.1: Mean annual cycle of Hsm derived from the ERA-Interim reanalysis.
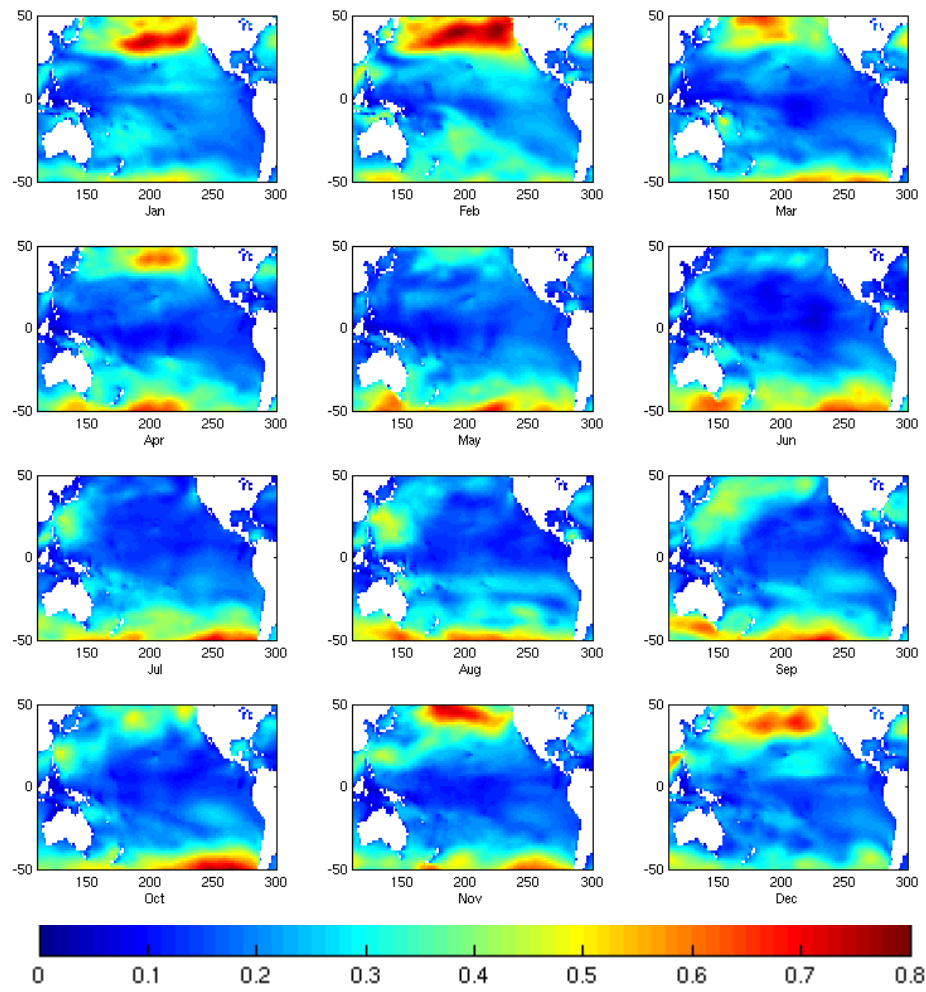
Figure 5.2: Inter-annual variability (sample standard deviation) of monthly mean wave heights in the Pacific basin (Jan 1989 to Dec 2009), derived from ERA-Interim data. Units in metres.
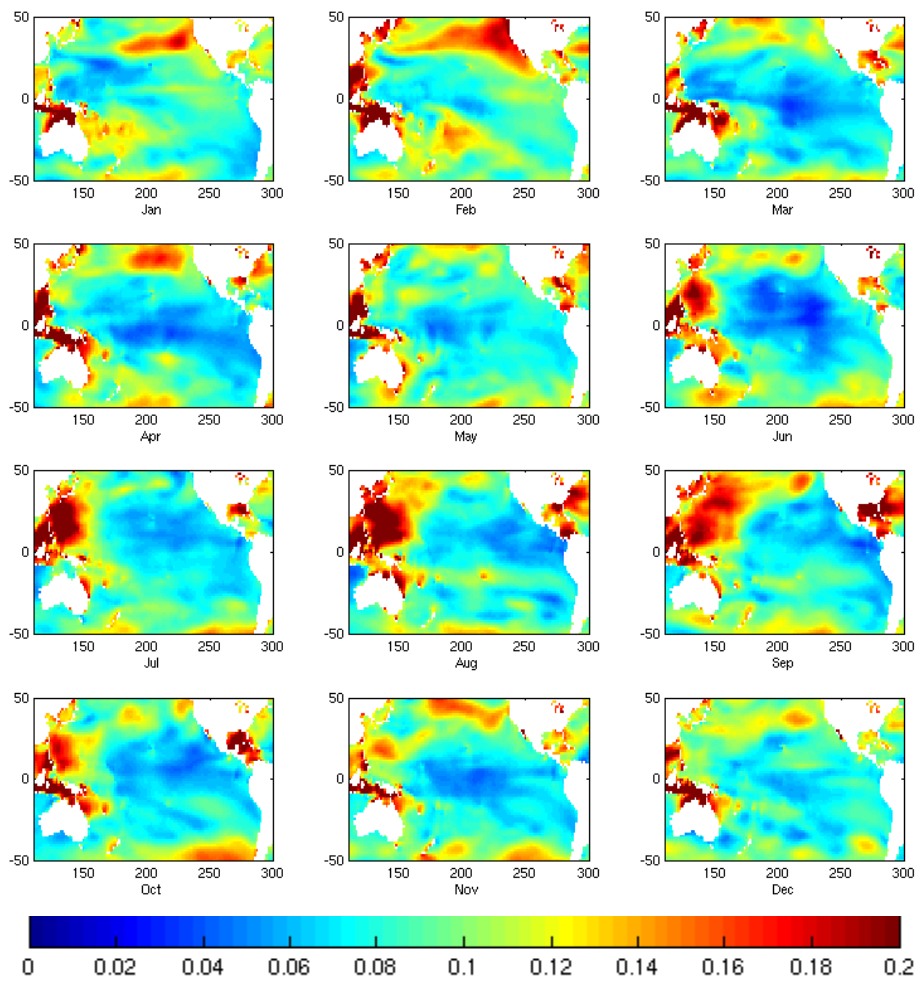
Figure 5.3: Inter-annual variability (sample standard deviation) of monthly mean wave heights normalised by the monthly mean wave height in the Pacific basin (Jan 1989 to Dec 2009), derived from ERA-Interim reanalysis. Dimensionless.

Significant positive correlation between *hsm_anom* and the SAMI is observed (Figure 5.4b). This positive correlation is strongest in the Southern Ocean and tends towards the eastern Pacific in the equatorial and northern latitudes, associated with the propagation of the swell signal throughout the Pacific Ocean. A positive SAM anomaly (SAM > 80th percentile of SAM) leads to increases in wave height (of order 30-40 cm) in the Southern Ocean, the influence of this signal on the eastern equatorial Pacific is of order 5-10cm (Figure 5.6). A 5-10cm increase in wave height associated with positive anomalies of the SAM is similarly observed in the Tasman Sea extending north-eastwards and is likely to influence the coasts of New Caledonia and potentially Vanuatu, Fiji Tonga. However, a shadow zone of less correlation to the SAM is observed to the north-east of New Zealand, and this effect, and sheltering of other islands within the PICTs will reduce influence of the increase in southern ocean swell on large areas of the PICTs.

Significant correlation is also observed against the other climate indices (not shown), however their structure is much less complex. Significant correlation between the AO and wave heights in the North Pacific is observed, and this influences extends towards the eastern Pacific to the

a)
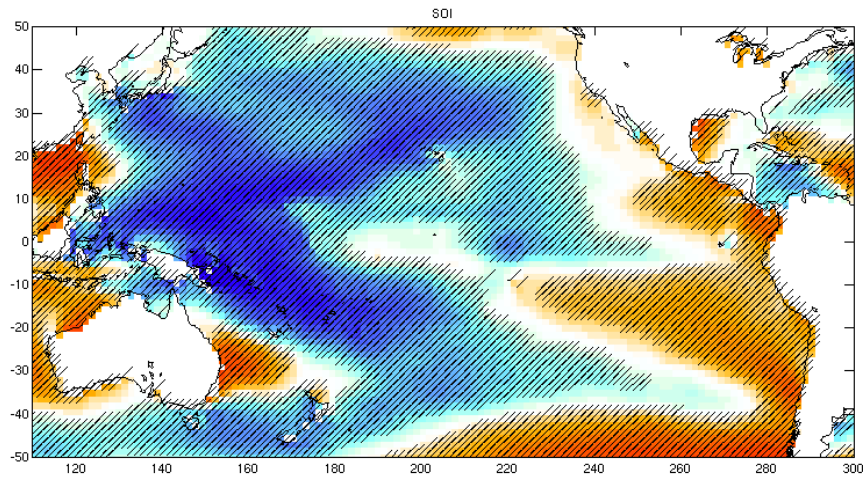
b)
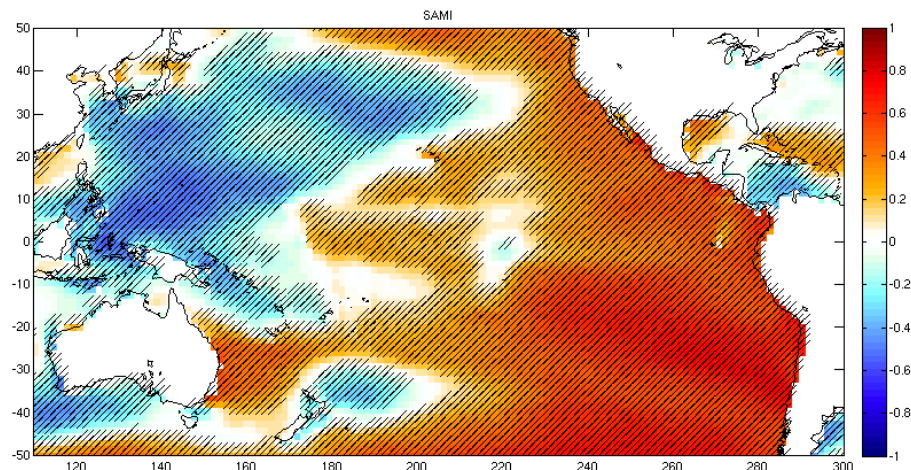
Figure 5.4. Correlation between monthly mean significant wave height anomalies (after annual cycle is removed) and a) the Southern Oscillation Index, and b) the Southern Annular Mode Index. Hashing indicates significant correlation at the 95% confidence level.

equator. Averaging wave heights over the period when the AO is less than its 20th percentile (negative anomalies), indicates a 5-10cm increase in North Pacific wave heights over the long term mean. Positive anomalies of the AO do not necessarily correspond with wave height decreases in the region. Correlations between wave height anomalies and the PNA (positive correlation) and NAO (negative correlation) are relatively uniform across most of the Pacific, however the magnitude of influence is relatively small. During the period when these indices are greater than their respective 80th percentile, the change in mean wave heights is less than 5cm with respect to the long term mean. Analysis of Hs_m99 and Hs_m90 (not shown) display similar correlation patterns to the analysis of Hs_m shown above. This result is somewhat surprising as one would expect the mean wave climate to display correlations trade wind influences, and the extreme wave climate to display correlation with cyclone events. The result here suggests that the coarse resolution of the reanalysis product does not resolve the large wave events adequately. Understanding how wave generation events (typically a storm component of the wave record, but in equatorial regions this may also correspond to trade wind generated systems) vary in response to climatological forcings is therefore critical to

understanding the full wave record, and attention should focus on this component of the wave record (at these broad scales).

5.1.2   Directional wave climate

The above section contains information regarding the properties of wave heights in the Pacific. In this section, we concentrate on summarising the directional wave climate using the energy flux vector, E_F, derived from the archived Era Interim (EI) data. The wave energy flux is a vector with magnitude being a function of the wave height squared and the wave period, and direction is given by the direction the waves are travelling. According to Holthuijsen (2007):

$$E_F = EC_G = \rho\, g\, H_S^2\, C_G/16 \quad (1)$$

Where E is the wave energy density, C_G is the group wave speed (Holthuijsen, 2007), g is the gravitational acceleration and ρ is water density. The magnitude (from equation 1) and direction (given by the ERA-interimmean wave direction) of energy flux are converted to eastward and northward components of wave energy flux, E_{Fu} and E_{Fv}, respectively. This follows the same approach outlined by Hemer et al. (2010).

Monthly mean wave energy flux magnitudes, directions and vector components were determined from the 20 year record of 6-hourly wave height, period and direction data. From these, the mean annual cycle and seasonal and annual mean wave energy flux were determined for each of the 20 years. Similar to the wave height statistics, monthly high percentile statistics were also determined (the 90th, 95th and 99th percentiles of wave energy flux), where the given Xth percentile is that of the flux magnitudes during each month, and the corresponding direction is taken as the corresponding percentile direction defined in the previous section. The map of mean wave energy flux (Figure 5.7) shows a distribution of magnitude similar to that of wave heights, shown in the previous section. The magnitude of wave energy flux is largest in the higher latitudes, with magnitudes of approximately 70 kW/m at 50°S and 50°N. The wave energy flux decreases in magnitude towards the equator, with a mean deep water wave energy flux at the equator of approximately 20kW. Also observed in the map of mean wave energy flux is the mean direction. We observe wave energy direction to largely correspond to the known mean surface atmospheric circulation, with westerly fluxes observed at the high latitudes. In the mid-latitudes, these directions have a strong equatorward component, and near the equator, convergence is observed (roughly in the location of the intertropical convergence
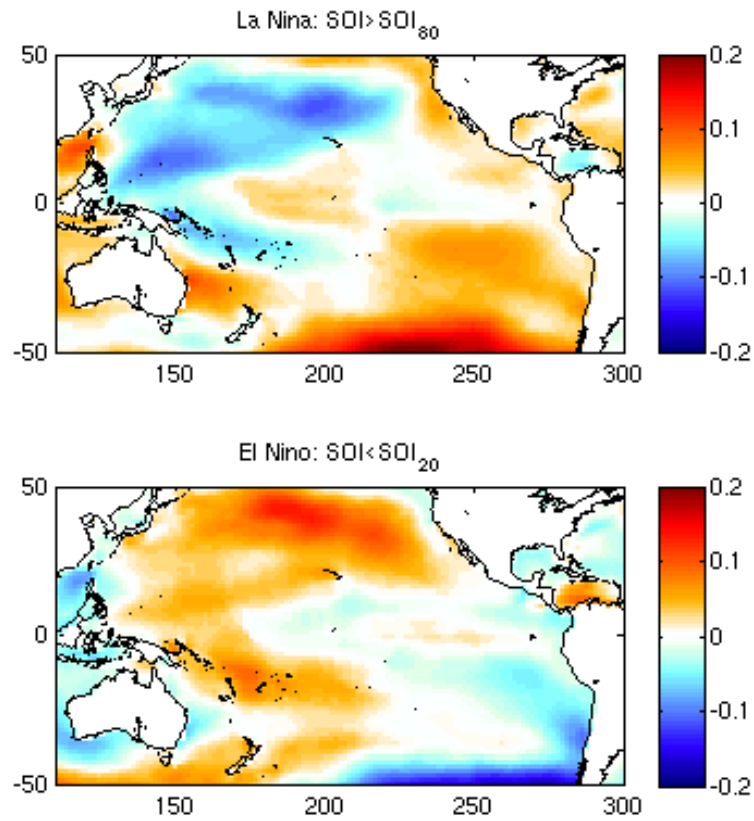
Figure 5.5. Top. Mean significant wave height anomaly for period when southern oscillation index is greater than its 80th percentile. i.e., approximately La Niña conditions. Bottom. Mean significant wave height anomaly for period when southern oscillation index is less than its 20th percentile. i.e., approximately El Niño conditions.
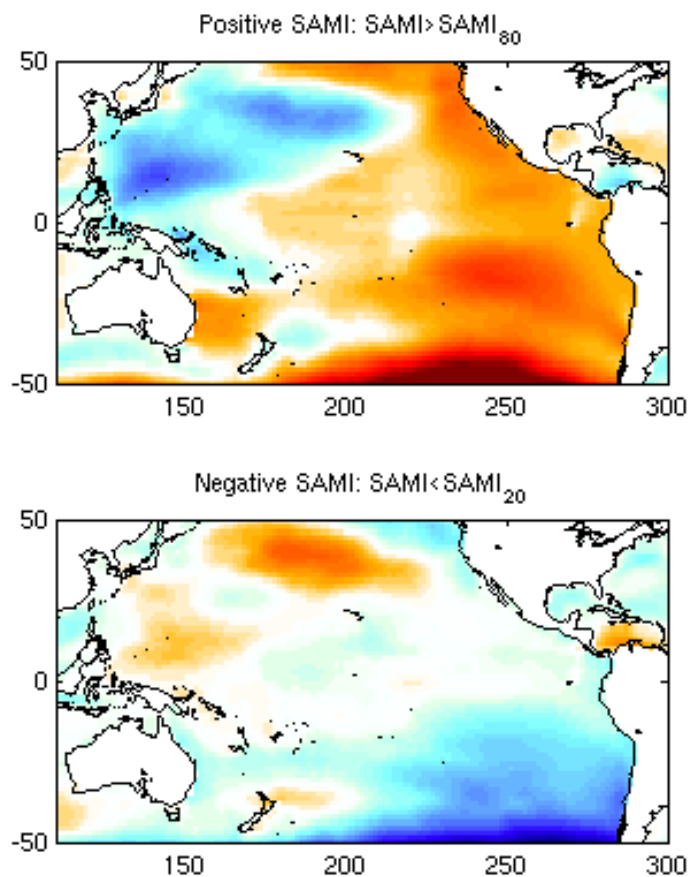
Figure 5.6. Top. Mean significant wave height anomaly for period when southern annular mode index is greater than its 80th percentile. i.e., intensified southern ocean storm conditions. Bottom. Mean significant wave height anomaly for period when southern oscillation index is less than its 20th percentile.

zone). In the western equatorial Pacific, these fluxes predominantly align with the easterly trade winds. However, further eastwards, the wave energy fluxes are typically aligned equatorward, illustrating the strong influence of the swell generated at high latitudes on the mean wave energy flux in this region.

The seasonal variability of the wave energy flux magnitude closely follows that for the wave height. Figure 5.8 shows the mean annual cycle of the zonal mean wave energy flux magnitude across longitudes 110 – 300°E. Here, we see the strong seasonality in the magnitude at the high latitudes, with highest zonal mean energy fluxes of approximately 90 kW/m at 50°S during the austral winter months. The North Pacific also shows a strong seasonal variability, with zonal mean wave energy fluxes ranging between approximately 70kW/m in December to approximately 15kW/m in July at 50°N. The equatorial wave energy flux magnitudes remain relatively steady throughout the year with mean zonal mean magnitudes of around 25 kW/m. In contrast, the equatorial region displays some of the strongest seasonal variability of wave energy flux direction (Figure 5.9). Between latitudes 12°S to 5°N, a seasonal reversal of zonal mean wave energy flux direction is observed, associated with the seasonal reversal of Monsoon (Dec-Mar) and Trade wind seasons (April-November). Consequently, despite wave energy flux

magnitudes being relatively uniform offshore, this strong seasonal variability of direction will result in strong seasonal variability of nearshore wave energy flux at any point in the region. In the southern Pacific, the seasonal variability of wave direction is relatively small (Figure 5.9). The wave direction is predominantly south-westerly, with a slightly greater westerly component during the austral winter months when the southern extra-tropical storm belt extends further northwards. The northern Pacific exhibits greater seasonal variability in the mid-latitudes than the southern Pacific. During the boreal winter months, the zonal mean wave direction is predominantly north-westerly. During the boreal summer months however, the zonal mean wave energy fluxes have a southerly component owing to the greater influence from the southern ocean and south-Pacific trade wind generated swell.

A similar analysis as presented for wave heights was carried out for the monthly wave energy flux statistics. For each of the eastward and northward directional components of wave energy flux, the mean annual cycle was removed from the monthly time-series, producing a 252 month anomaly time-series of each directional component from the ERA-Interim data. These monthly wave energy flux anomaly time-series were then regressed against time, and several climate indices, for each directional component separately, to establish the directional response of the flux. This analysis was carried out for each of the monthly mean, and the monthly 90th, 95th and 99th percentiles of wave energy flux directional components. The patterns observed were relatively consistent between the different monthly statistics, and here we present results of the monthly mean fluxes only.

For the eastwards energy flux (Figure 5.10a) significant negative trends in the equatorial Pacific are observed over the 1989 to 2009 record. In this region, the mean fluxes are easterly, and so this negative trend corresponds to increasing magnitude of these fluxes. These trends are inconsistent with trends in wave height observed from the altimeter record over a similar period, as reported by Young et al. (2011). For the northwards component of energy flux (Figure 5.10b), significant positive trends are observed in the southern mid-latitudes. This region is characterised by southwesterly wave energy fluxes, and so this postive trend in the northward component (and no or little trend in the eastwards component) suggests a slight strengthening and anticlockwise rotation of the flux direction to have a greater southerly component. The trends in both components are strongly biased by the short temporal record over which this analysis is carried out and the strong inter-annual variability in the region, and are not considered representative of a long term change in wave conditions of the region.

Given this strong variability, understanding the main modes of variability of the directional wave climate is required. To investigate the influence of larger coherent patterns on the directional wave climate, we have regressed the monthly anomaly of each directional component against the same 6 climate indices as were outlined for the Hs analysis. This was done for the monthly mean directional components, and the monthly high percentiles. The derived patterns were similar from each of these datasets, and only the regression results with respect to the monthly mean anomalies are shown here.

Figure 5.11 displays significant correlation between monthly anomalies and the SOI throughout the Pacific Ocean. Strongest correlations are observed in the western equatorial Pacific. To the north of the South Pacific convergence zone, the eastward component of energy flux displays strong negative correlation to the SOI and the northward component displays positive correlation to the SOI. This suggests that a negative anomaly in SOI (El Niño) correlates with

positive anomalies in the easterly (negative eastward) fluxes in this region – essentially a weakening of the trade wind driven easterly wave energy flux in the region.

South of the South Pacific convergence, and nearer to the Australian continent, a positive correlation between the monthly eastward flux anomalies and the SOI is observed (Figure 5.11). This is accompanied by negative correlation between the monthly northward flux and SOI in this region. Mean fluxes in this region are south-easterly. A negative anomaly in SOI (El Niño) correlates to an anticlockwise rotation of the wave energy flux vector, with a greater westerly component during El Niño years in this region, but no significant change in magnitude. These inter-annual directional changes in wave direction are potentially important to several aspects of coastal wave climate which require further attention.

Figure 5.11 (2nd row) shows correlation between the monthly anomalies of energy flux components and the southern annular mode index. Significant correlations are observed over large areas of the Pacific Ocean, particularly in the South and East. These regions correspond to the southern extratropical storm belt and the associated active wave generation there, and with regions where waves generated in the storm belt have propagated to as swell. The storm belt generated waves have a strong south-westerly directional component in the Southern Pacific. We see significant positive correlation between both energy flux directional components and the SAM exists over most of the south-east Pacific, extending well into the Northern Hemisphere. This indicates a positive anomaly of the SAMI (consistent with a southern intensification of the storm belt) corresponds with an increase in magnitude, and anticlockwise rotation of the wave energy flux to have a greater southerly component, consistent with the results of Hemer et al. (2010). A distinct shadow zone is observed behind New Zealand, with negative correlation between energy flux and the SAMI is observed. In this region, which includes Tonga, Niue and Fiji, a positive anomaly in the SAMI will lead to a decrease in wave energy flux brought about by the sheltering of available swell wave energy from the Southern storm belt.

The Pacific-North American Index also shows significant correlations between both directional components of the wave energy flux and the PNA index (Figure 5.12, middle row). This correlation indicates significant increase in the north-westerly wave energy fluxes of the North Pacific associated with positive anomalies of the PNA.

Another climate index which displays significant correlation to the monthly energy flux directional component anomalies is the Indian Ocean Dipole (Figure 5.12, bottom row). Significant positive correlations are observed between the IOD and the northward energy flux over much of the western Pacific. The eastwards flux displays positive correlation to the IOD north of the intertropical convergence zone, and negative correlations south of it. These relationships indicate a positive anomaly of the IOD is correlated with a clockwise rotation of energy flux in the western Pacific. It is accepted that positive phases of the IOD co-occur with El Niño (Luo et al., 2010), however, the spatial structure of correlation of the wave climate and IOD is considerably different to the SOI correlations.
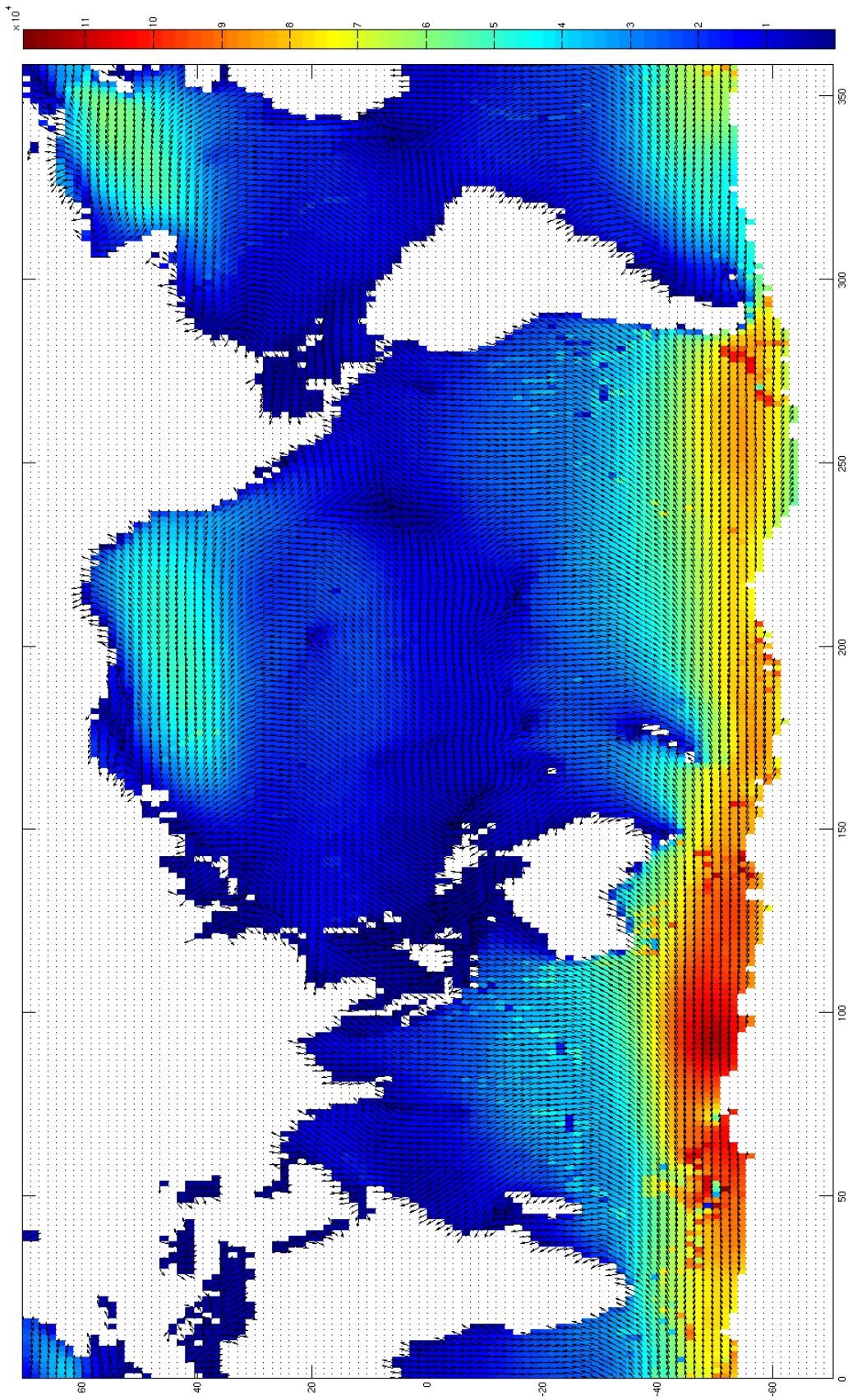
Figure 5.7: Mean energy flux (Units W/m)
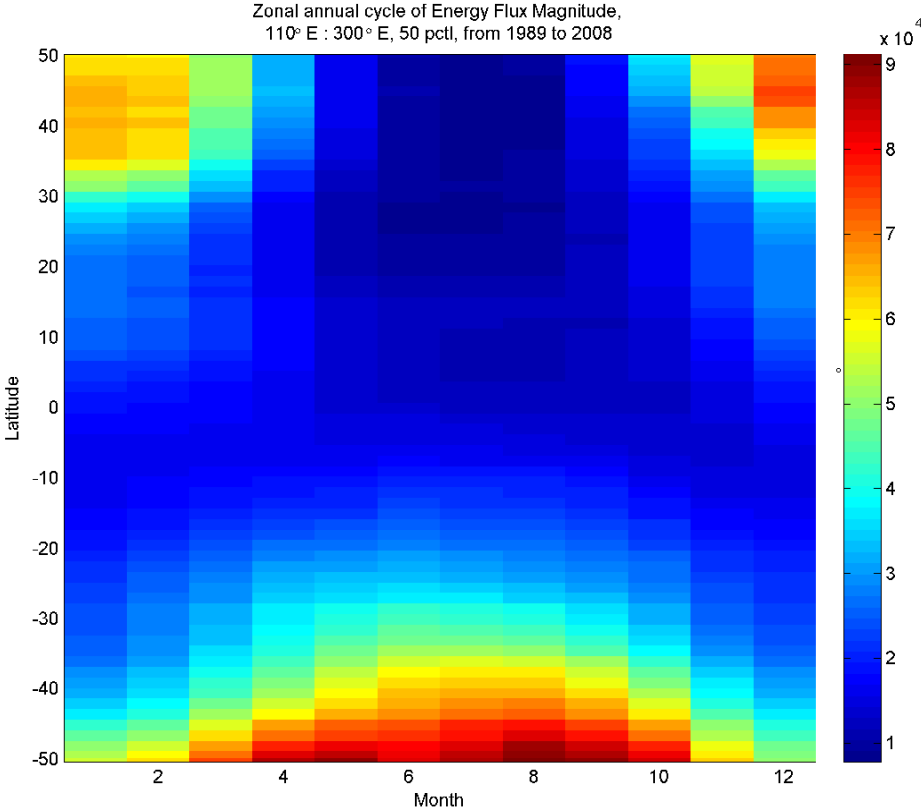
Figure 5.8: Mean annual cycle of zonal mean (110-300°E) wave energy flux magnitude. Units W/m.
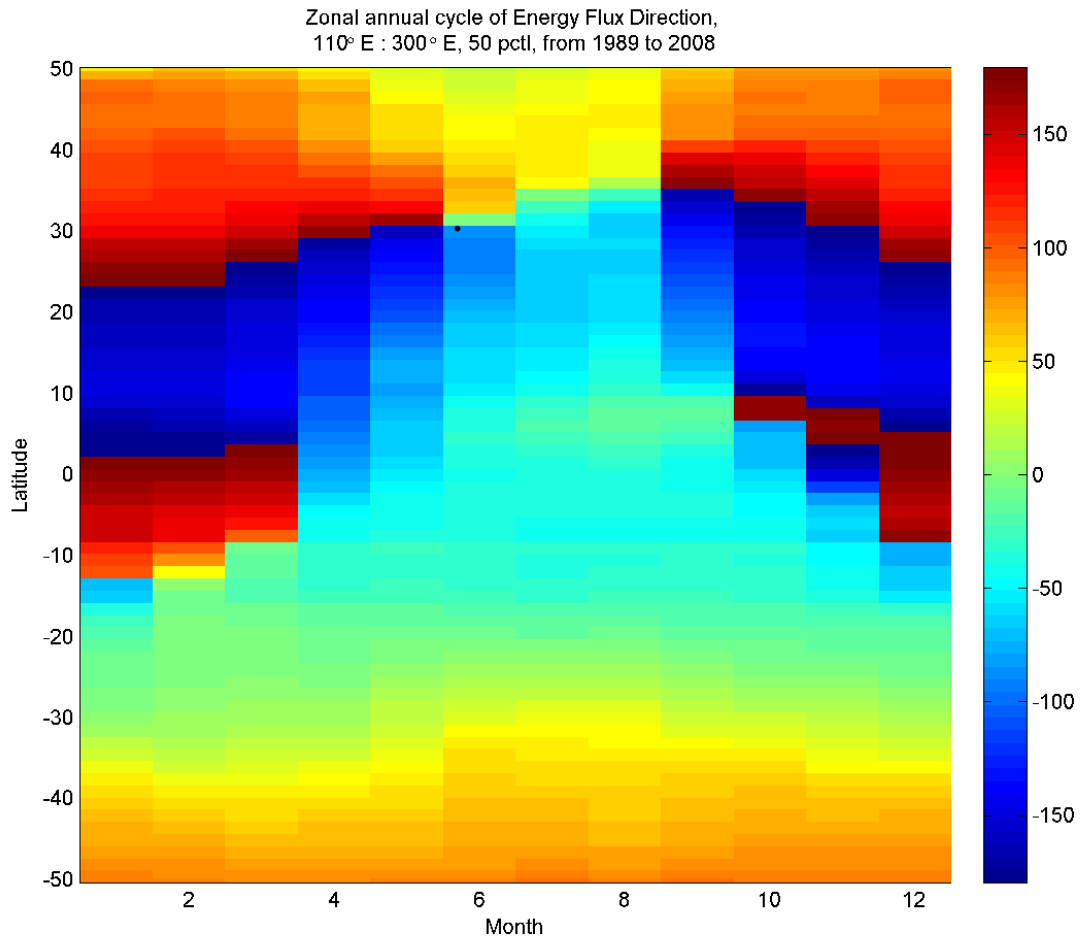
Figure 5.9: Mean annual cycle of zonal mean (110-300°E) wave energy flux direction. Units °N.

a)

b)
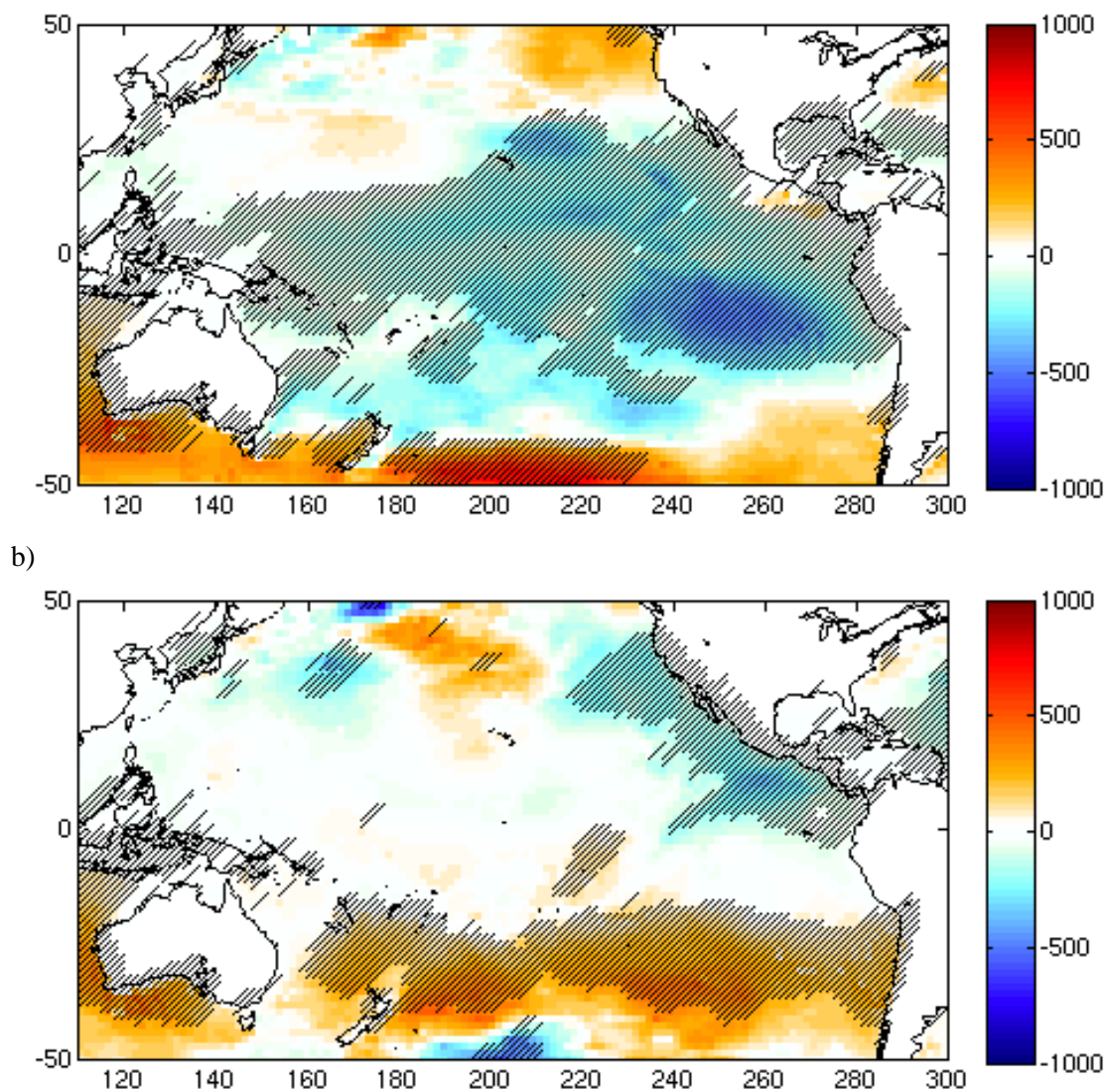
Figure 5.10: Regression statistics of (top) eastwards component of ERA-Interim derived energy flux vs time (1989-2009) and (bottom) northwards component of energy flux against time. Units W/m/yr. Hashed shading indicates trend is significant. Hashed shading indicates significant trend at the 95% confidence level.

R: Eastwards Component of E_F · R: Northwards Component of E_F
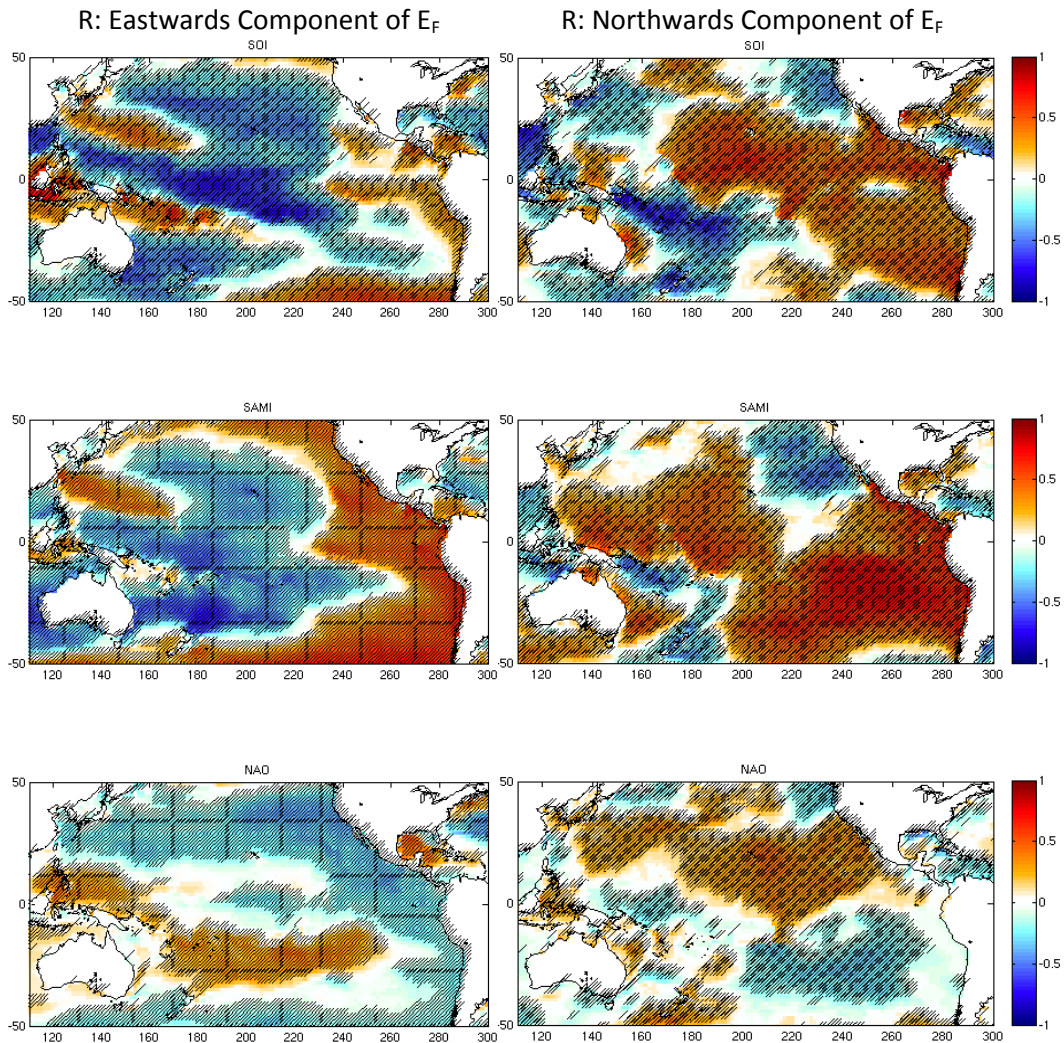
Figure 5.11: Correlation coefficient, R, of (left) eastwards component of wave energy flux anomaly against specified climate index, and of (right) northwards component of wave energy flux against specified climate index. Dimensionless. Top are correlation to SOI. Middle are correlation to the SAMI, and the bottom are correlation to the NAO. Hashed shading indicates significant correlation at the 95% confidence level. Note for example, El Nino (negative anomaly of SOI) is associated with a weakening of the trade winds in the western equatorial Pacific. This feature is seen here as a negative correlation, implying a positive anomaly (weakening) of the negative zonal flux.
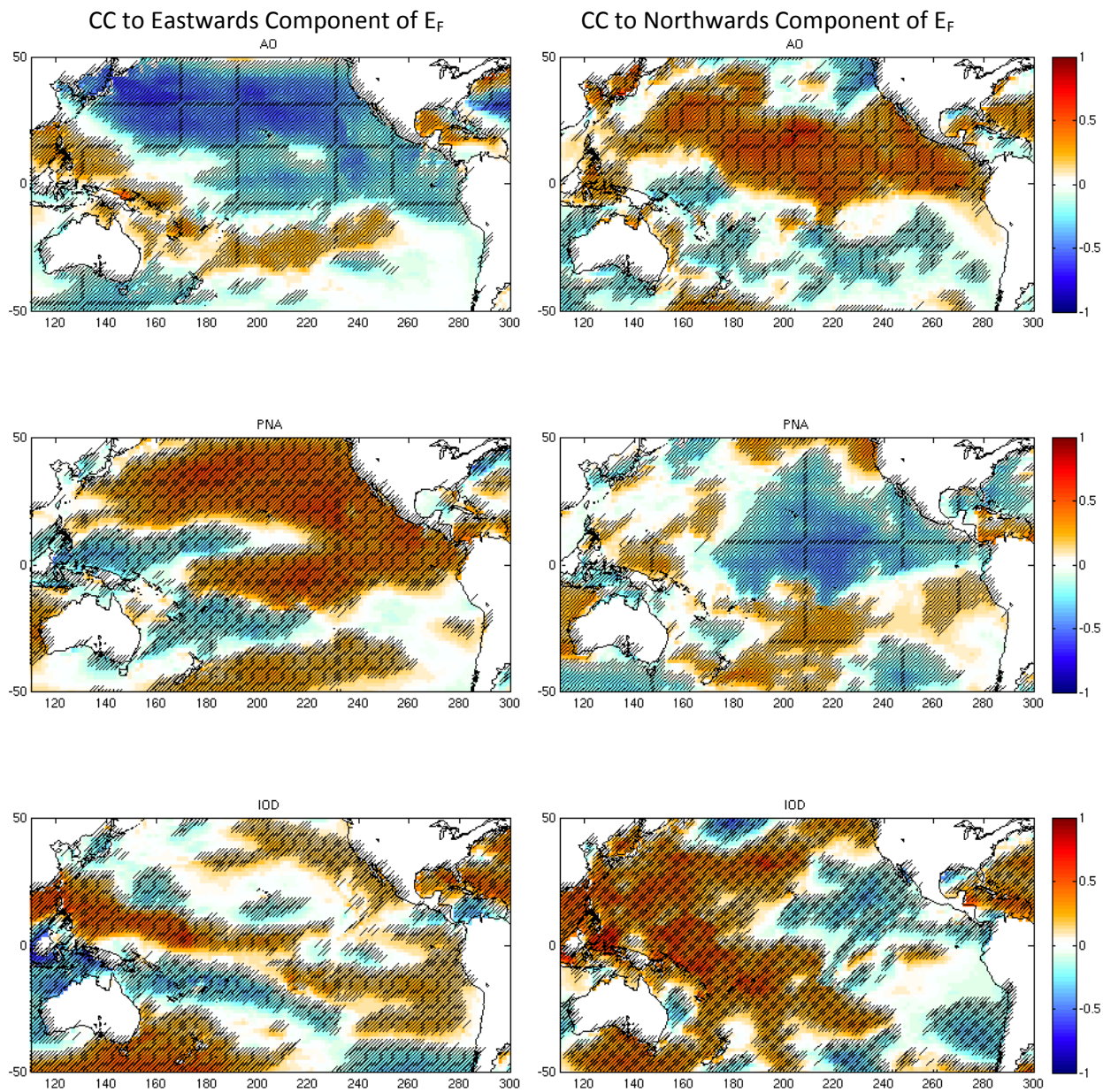
Figure 5.12: As for Figure 5.11, except top plots display correlation to AO. Middle display correlation to the PNA, and the bottom display correlation to the IOD. Hashed shading indicates significant correlation at the 95% confidence level.

5.1.3   Site records

For five locations chosen to represent broad regions of the Pacific wave climate, 6 hourly data from the ERA-Interim record are used directly to assess the extreme wave climate, and bivariate characteristics of the wave climate. The locations are:

1. Central Pacific (Hawaii) – Longitude 198°E, Latitude 24°N

2. South-west Pacific (Vanuatu-Fiji) – Longitude 173°E, Latitude 20°S

3. Equatorial Pacific (Kiribati-Tuvalu) – Longitude 180°E, Latitude 3°S

4. South Pacific (French Polynesia) – Longitude 225°E, Latitude 23°S

5. Western North Pacific (Micronesia – Guam) – Longitude 150°E, Latitude 12°N

At each of these point locations, the 21 year record is used to construct a wave rose for each of four seasons (Dec-Feb, Mar-May, Jun-Aug, and Sep-Nov) displaying the seasonal variability of wave height, period and direction.

At these 5 sites, data is broken into 12 directional segments of 30° span each [0° to 30°, 30° - 60°,…]. The annual maximum significant wave height is recorded in each directional segment. In each directional segment, a generalized extreme value distribution is fit to the 21 annual maxima values using a maximum likelihood method. Annual, 10 year and 100 year return period significant wave heights were then determined for each directional segment. The 100-yr return period significant wave heights are presented here as a commonly used engineering criteria. It should be noted that these values are derived from only 20-yrs of data, and that extreme statistics beyond 40-yr return period are unreliable. This analysis provides assessment of which directional segment extreme waves are likely to come from.

Hawaii

During the northern Pacific winter (Dec-Feb), the Hawaiian wave climate (Figure 5.13) is dominated by large (>3m), long-period (11-13s) north-westerly swell, generated in the northern extratropical storm belt. Throughout the rest of the year, the wave climate is dominated by east-north-easterly trade wind generated wind seas of smaller magnitude (1.5-3m) and shorter period (7-11s). This direction is most easterly during the boreal summer months (Jun-Aug), when waves are smallest and of shortest period. During the boreal summer (austral winter), a larger (but still small) component of southerly waves are observed, corresponding to swell generated in the Southern Pacific Ocean.

Figure 5.18 indicates that the highest annual and 10-yr return period wave heights are directed from the north-west, associated with the north-westerly swell events (315°N). The annual (10-yr) return wave height is approximately 4.5 m (6.0m), which is considerably less than the buoy derived values from Vitousik and Fletcher, 2008. The highest 100-yr return period wave heights (in excess of 8 m) are observed to come from either the north-east, or slightly south of east. These events correspond with rare wave generation events in this sector, associated with tropical storm (central Pacific hurricane) systems. Given the poor representation of hurricane systems in the ERA-Interim model, these events may be underestimated.

South-West Pacific (Vanuatu-Fiji)

The south west Pacific wave climate is dominated by the south-easterly trade winds (Figure 5.14). These waves are consistent, with offshore south-easterly waves of heights exceeding 4m observed throughout the year. During the austral winter (Jun-Aug), a slight increase in wave activity from the south is observed, with a larger component of swell from the southern storm belt, represented by the increased component of long period waves from the south. Highest annual and 10-yr return period wave heights are received from across the whole south-east sector, of magnitudes of approximately 3 and 4.5 m respectively (Figure 5.18). The largest 100-yr return period wave heights are observed to come from the north-east (approx. 10m). These events are likely associated with Pacific cyclone events, and are likely underestimated given the poor representation of cyclone systems by the ERA-Interim model.

Equatorial Pacific (Kiribati – Tuvalu)

The wave climate nearer to the equator on the northern side of the Pacific Islands shows a larger directional variability that on the southern side of the Islands (Figure 5.15). During the austral summer, the wave climate is dominated by the north-easterly trade wind generated waves. The more northerly of these waves have a longer period (>11s), and likely correspond to swell generated in the North Pacific. During the austral winter (Jun-Aug), the south-easterly trade winds dominate, with shorter 7-9s waves less than 2 m in height dominating the wave climate. At this site, the directional extremes analysis indicates that extreme wave heights are greater from the westerly direction (Figure 5.18). Wave events are rare from this direction, and these statistics have high uncertainty, associated with cyclone systems which are poorly sampled in the available 20-yr record.

South Pacific (French Polynesia)

The wave climate of this region is dominated by swell generated in the southern storm belt and propagated to the region (Figure 5.16). South-westerly waves dominate year round, with mean periods of between 9-13 s. The magnitude varies from approximately 2m in the austral summer to over 3m in the austral winter. During the austral summer, a greater component of trade wind generated westerly waves, of relatively short period, is observed. The directional extremes analysis indicates that annual, 10-yr and 100-yr return period waves are relatively consistent across the whole southerly sector, with magnitudes of approximately 3.3 m, 4.5m and 5.5m respectively (Figure 5.18).

Western North Pacific (Micronesia-Guam)

The wave climate at this location is dominated by waves from the north-easterly sector year round (Figure 5.17). These waves are larger (approx 2-3m), longer (<11s) and have a greater northerly component during the boreal winter (Dec-Feb). During the boreal summer (Jun-Aug), the wave climate is dominated by smaller waves (<2m) of shorter period (<9s) from the east. Annual return and 10-yr return period wave heights of approx 3m and 4m respectively are obtained from any directional sector (Figure 5.18). However, maximum 100-yr return period wave heights of over 10-m are observed to originate from the south-east (135°N), most likely associated with typhoons.

a)
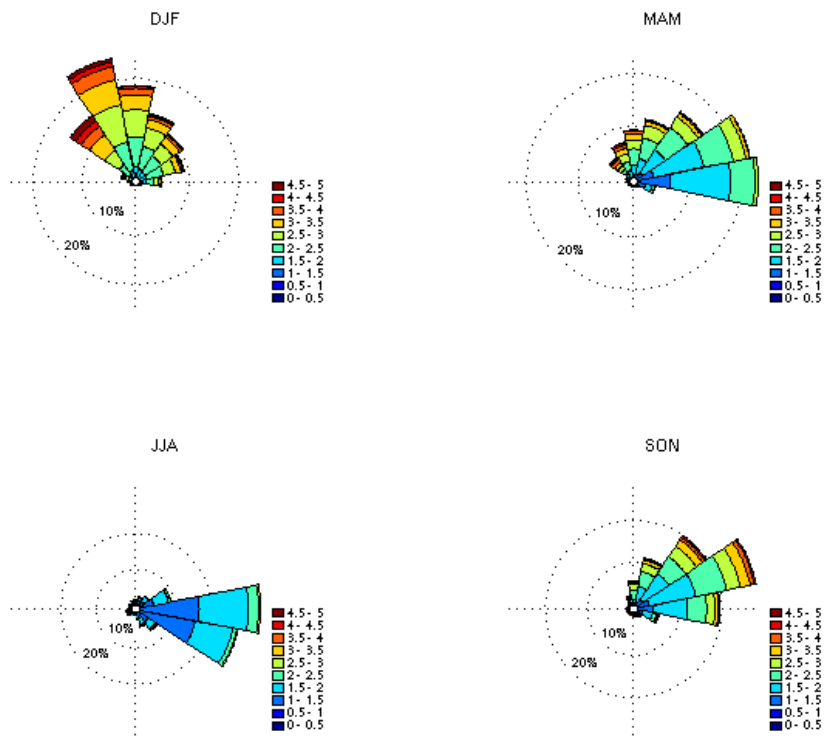
b)
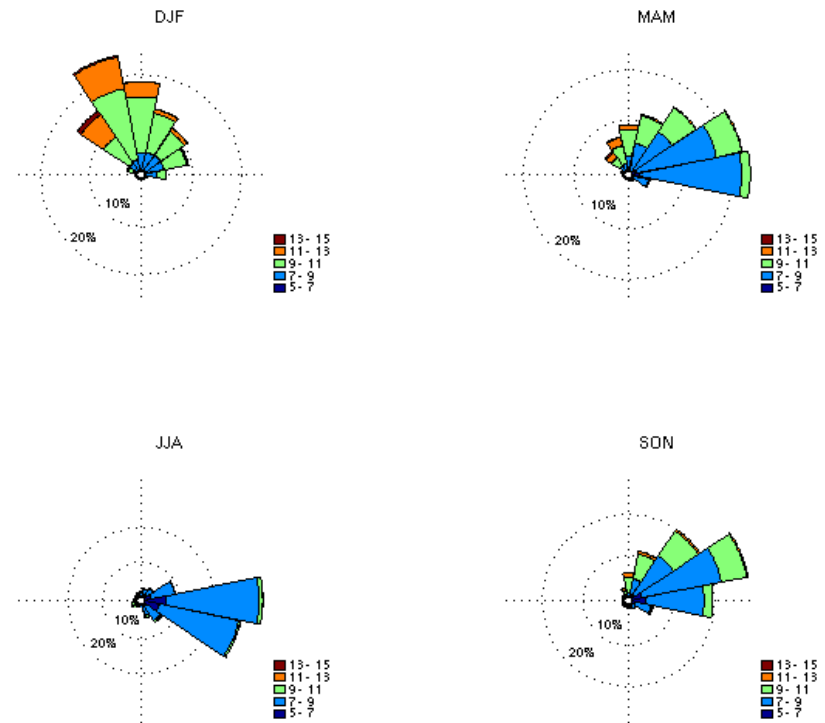
Figure 5.13: Wave roses for Hawaii indicating a) mean wave direction and significant wave height; b) mean wave direction and mean wave period.
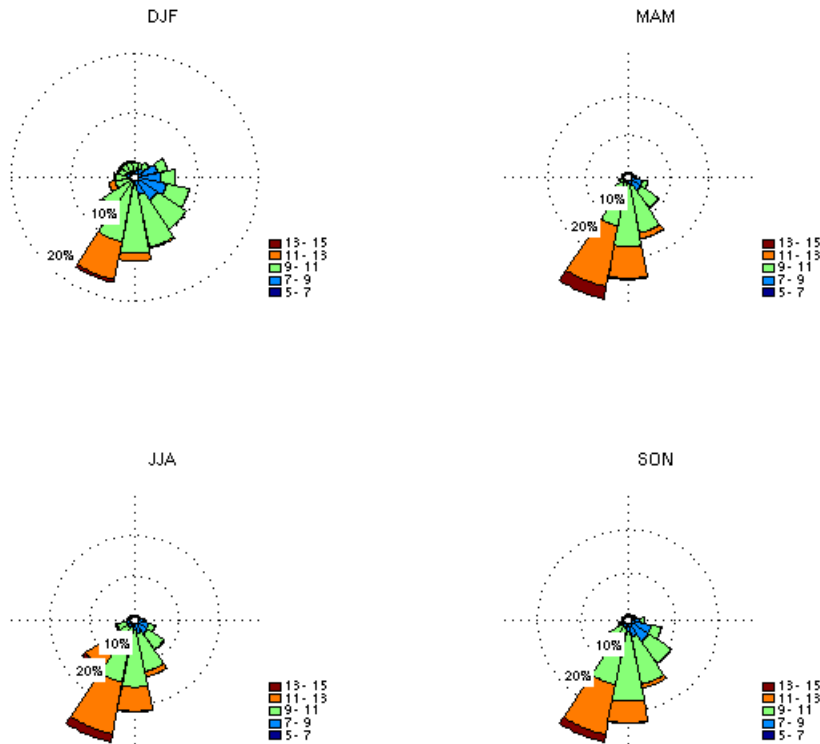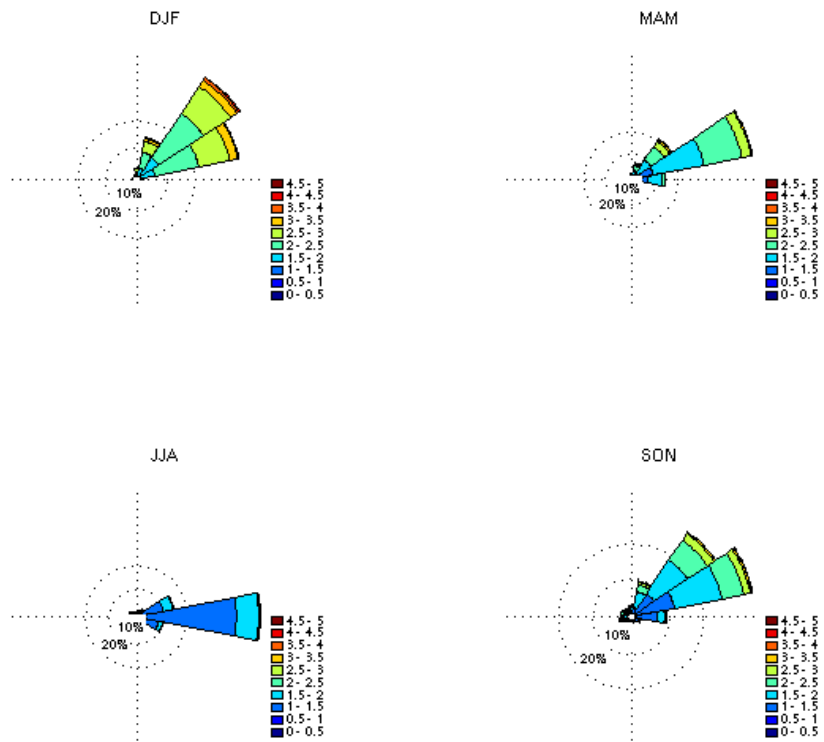
a)
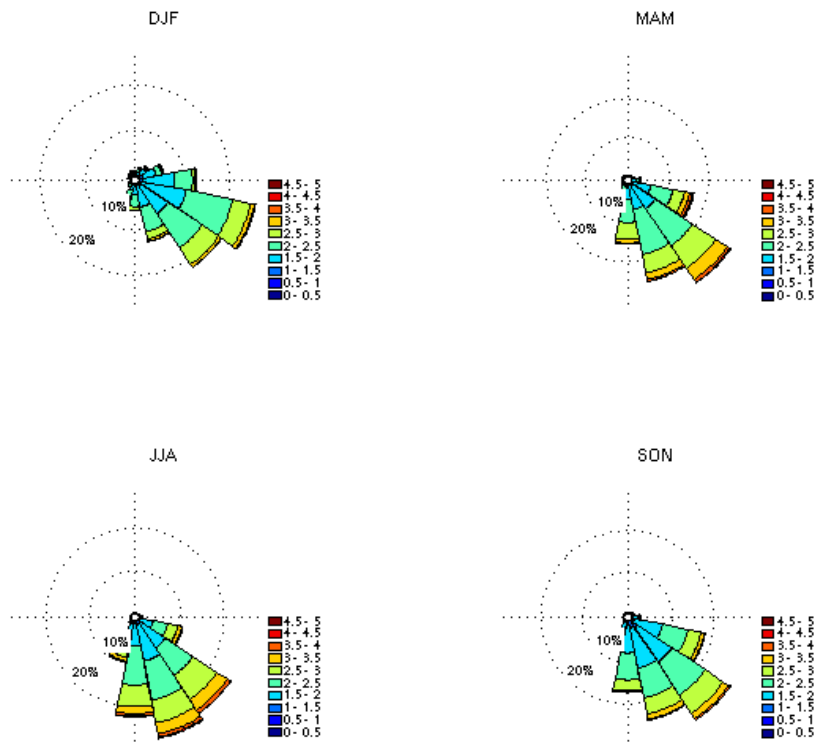
b)
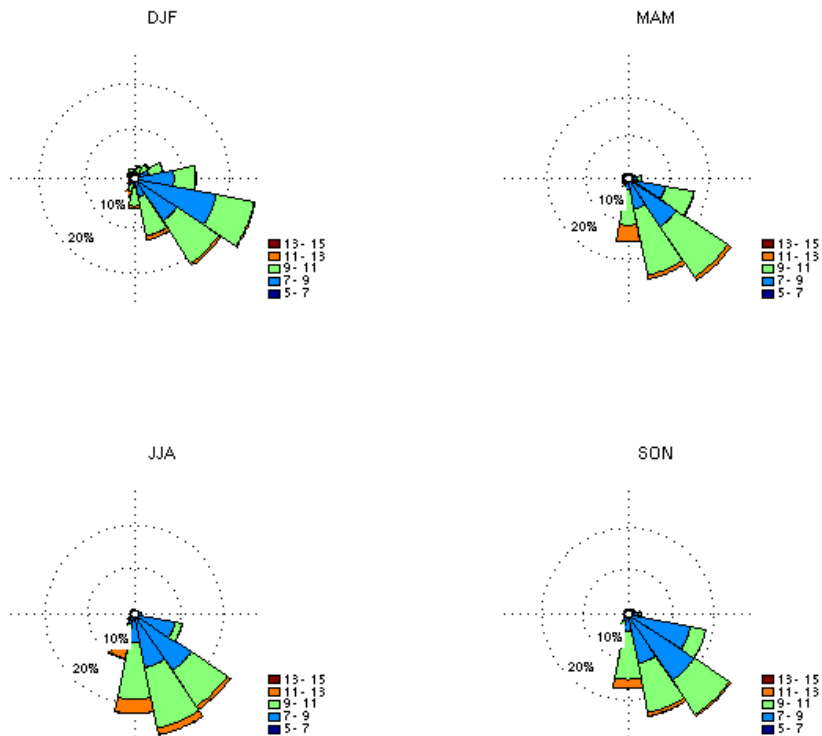
Figure 5.14: Wave roses for South-West Pacific indicating a) mean wave direction and significant wave height; b) mean wave direction and mean wave period.
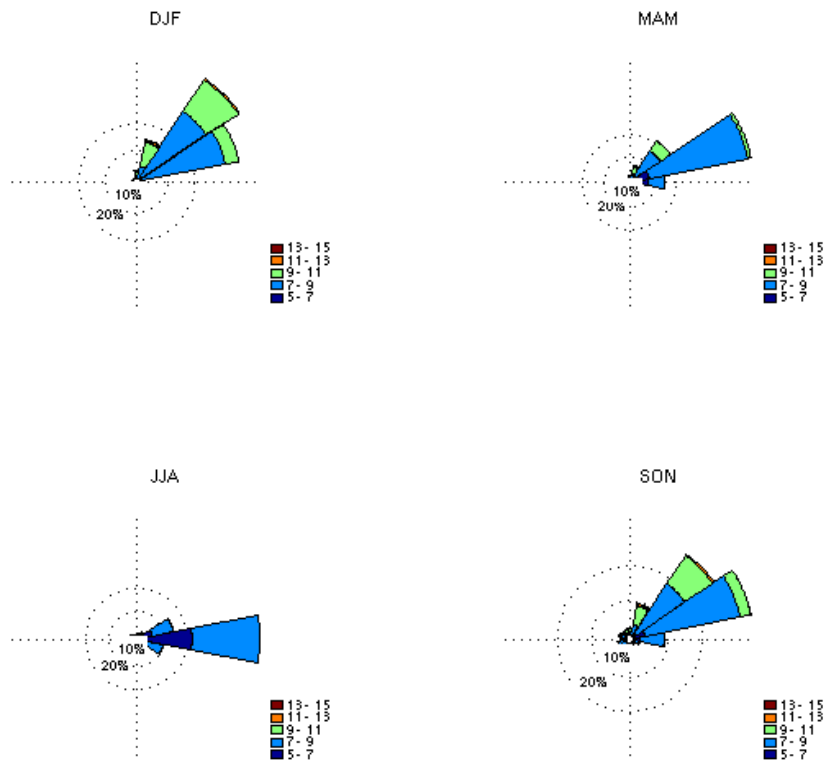
a)
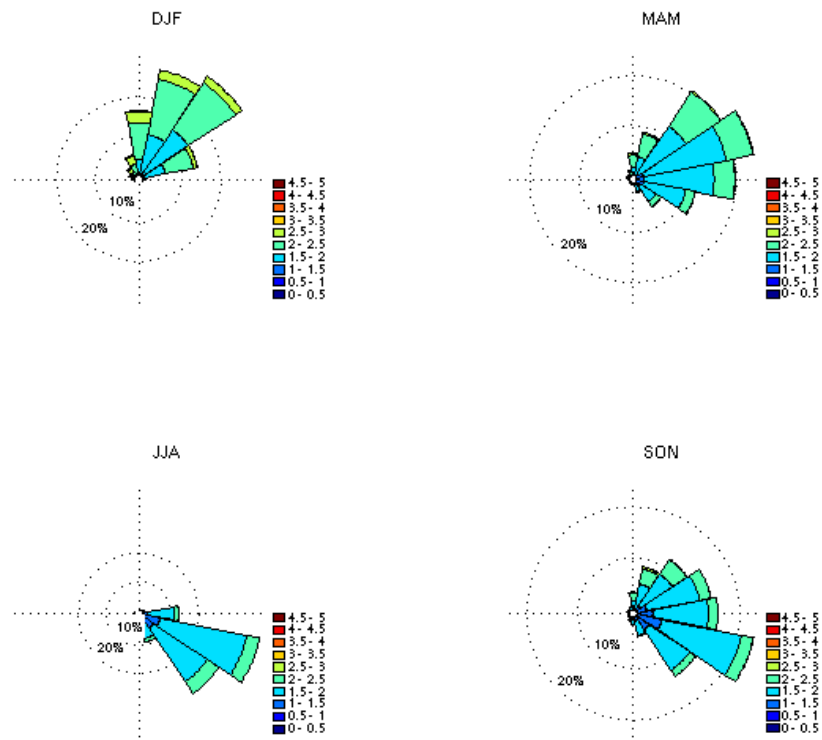
b)
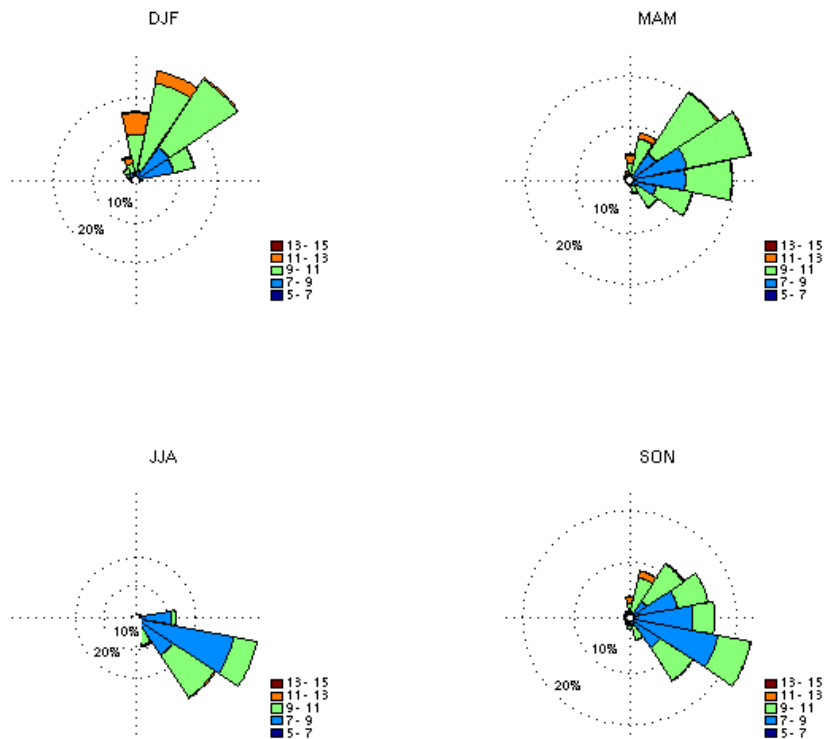
Figure 5.15: Wave roses for Equatorial Pacific indicating a) mean wave direction and significant wave height; b) mean wave direction and mean wave period.

a)
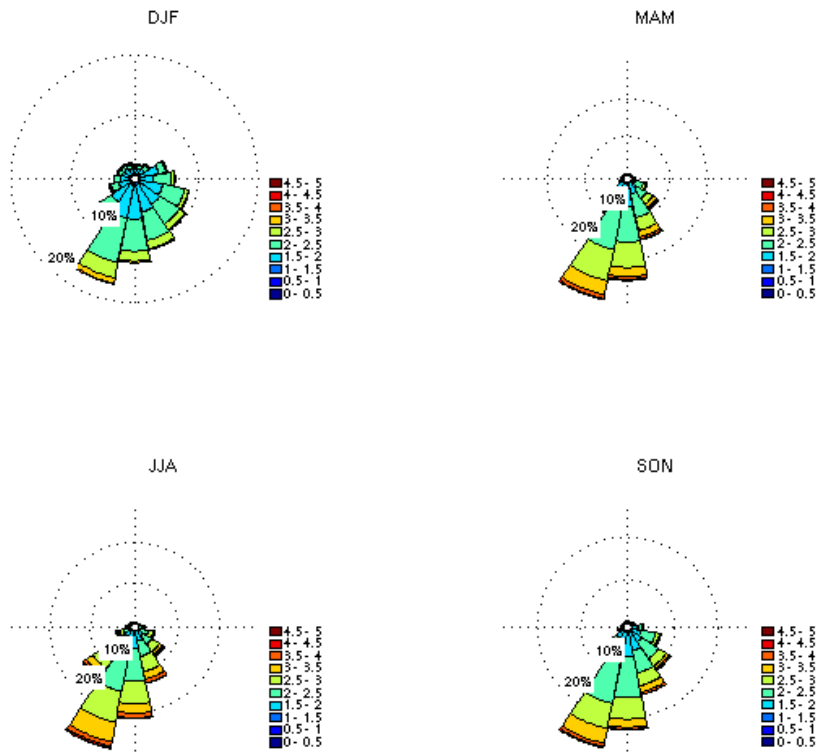
b)

Figure 5.16: Wave roses for South Pacific indicating a) mean wave direction and significant wave height; b) mean wave direction and mean wave period.

a)

b)

Figure 5.17: Wave roses for Western North Pacific indicating a) mean wave direction and significant wave height; b) mean wave direction and mean wave period.
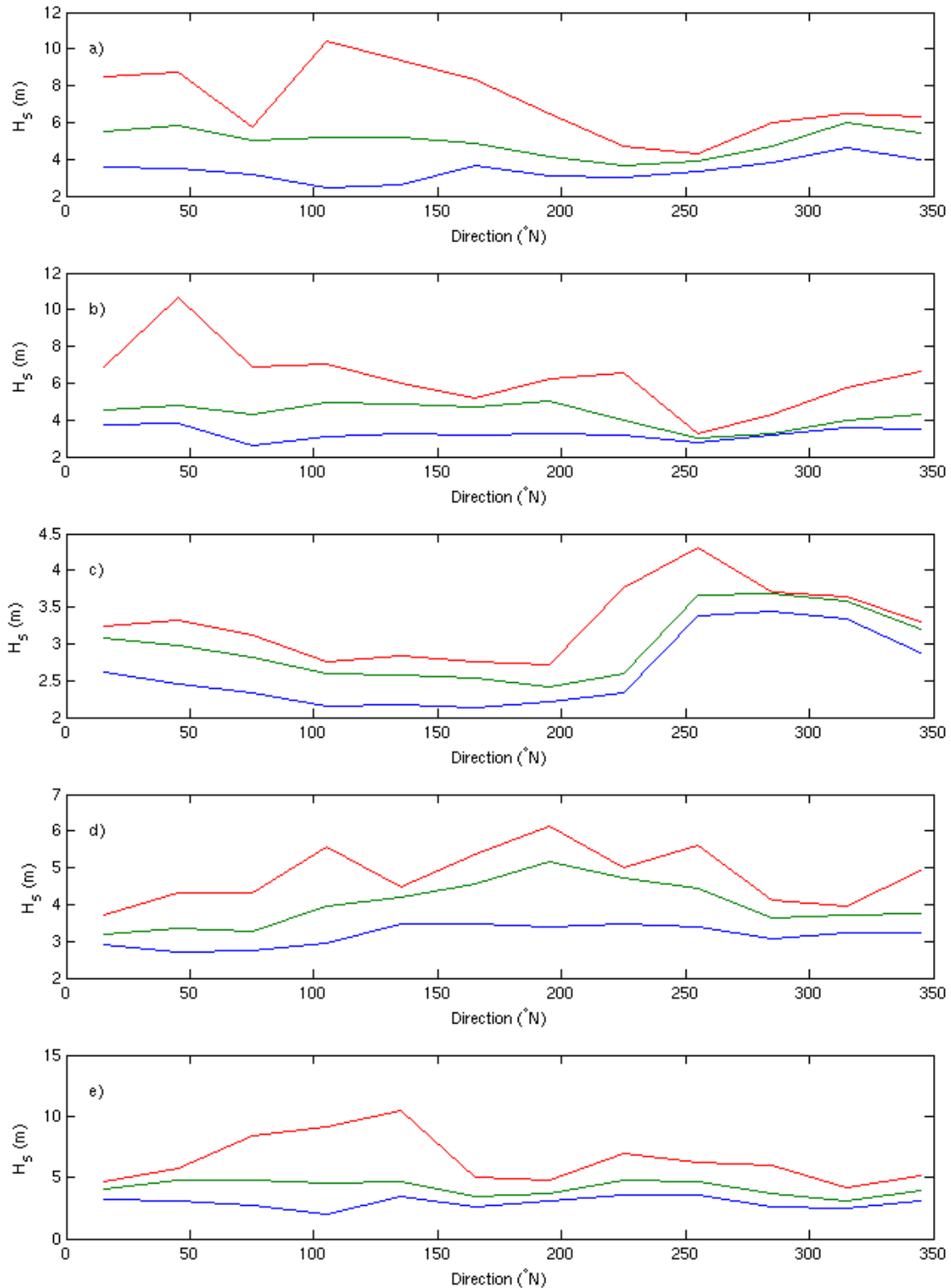
Figure 5.18: Return period significant wave heights by direction for 5 sites. a) Hawaii; b) South Pacific (Vanuatu-Fiji); c) Equatorial Pacific (Kiribati-Tuvalu); d) South Pacific (French Polynesia); e) Western North Pacific (Guam- Micronesia). The blue line represents the annual return significant wave height for each directional segment, the green line is the 10-yr return value, and the red line is the 100-yr return value.

6.   PRELIMINARY WAVE CLIMATE PROJECTIONS FOR THE PACIFIC REGION

Wave models require suitable surface winds as forcing, and it is important that the regional atmospheric circulation is well represented in the forcing model. In this study, we have made use of the dynamically downscaled climate model results generated in the Pacific Climate Change Science Programme (PCCSP). In PCCSP, the Conformal Cubic Atmospheric Model (CCAM; McGregor and Dix, 2008) is applied with a global resolution of approximately 60 km to dynamically downscale six GCMs using bias-adjusted sea-surface temperatures (SSTs) and sea-ice as forcing (i.e., no atmospheric forcings; Katzfey et al., 2009).

Projections of future climate change include a range of uncertainties that must be considered in climate impacts research. An ensemble modelling approach is required to quantify uncertainty. An ensemble of different climate models (multi-model ensemble) will provide an estimate of the impact of different model structure on uncertainty. A perturbed physics ensemble (in which model parameterisations are systematically varied within plausible parameter ranges) and an intra-model ensemble (initialisation of the model is altered) both provide estimates of climate uncertainty within a single model. Uncertainty due to climate change is investigated using a range of emission scenarios which influence future atmospheric composition. The Coupled Model Intercomparison Project (CMIP) (Meehl et al., 2007) assembles a large number of runs from global climate models which provide projections of future climate on a global scale. While these models provide relatively consistent projections of global mean parameters, large differences may occur between models at the regional scale, a contributing factor of which is the spatial resolution of the models are often unable to resolve the regional flow patterns adequately.

This study presents results from an ensemble of two 60km CCAM runs, in which two GCM's (CSIRO Mk3.5 and ECHAM5) were dynamically downscaled. The 2-member ensemble was considered in order to explore the uncertainty associated with multi-model ensembles but we note that this is too limited an ensemble to provide an adequate estimate of the uncertainty within the total sample space. This ensemble was limited to two members due to the computing effort required to generate wave fields for the study, and after Hemer et al. (2011b) showed that the CCAM downscaling significantly reduced the ensemble range within the surface wind fields. Hemer et al. (2011b) indicated that the multi-model uncertainty within the wave climate projections was a minor source of uncertainty relative to the need for bias adjustment of forcing winds. No perturbed physics or intra-model ensembles are included within the run-set. We have taken the near-surface marine wind fields at 10-m height, archived at 3-hourly intervals, from two 30 year time-slices (1979-2009 and 2070-2099) to represent the present and future respective wind climatologies. These wind fields were interpolated onto a global, regular 1.0° (~60-km) latitude-longitude grid, to force a global 1° resolution implementation of the WaveWatchIII (v3.14) spectral wave model, parameterised using "BAJ" source terms (Bidlot et al., 2005; Tolman, 2009). The next section explores how well the CCAM C160 runs represent the surface atmospheric circulation (10-m winds and mean sea level pressure) and the climate change signal of these properties. The following section assesses the skill of the wave model to produce a representative wave climate when forced with these climate model winds and preliminary projections of changes to wave climate under a future emission scenario.

6.1 An assessment of the PCCSP CCAM surface winds

6.1.1 Evaluation of Currrent Climate CCAM 60 km simulations

In this section, the CCAM 60 km downscaled simulations are evaluated against the NCEP CFS dataset for mean sea level pressure and 10 m wind speed. Figure 6.1 shows the main regions of higher wind speed. In the Northern Hemisphere, the highest wind speeds are in the North Pacific and North Atlantic in DJF, and still strong in MAM and SON. The trade winds are also evident all year around 15ºN in the Pacific. In the Southern Ocean, strong westerly winds are evident around 50ºS throughout the year, with the strongest winds in JJA south of the Indian Ocean. The trades around 25ºS are evident for most seasons but are also strongest in JJA.
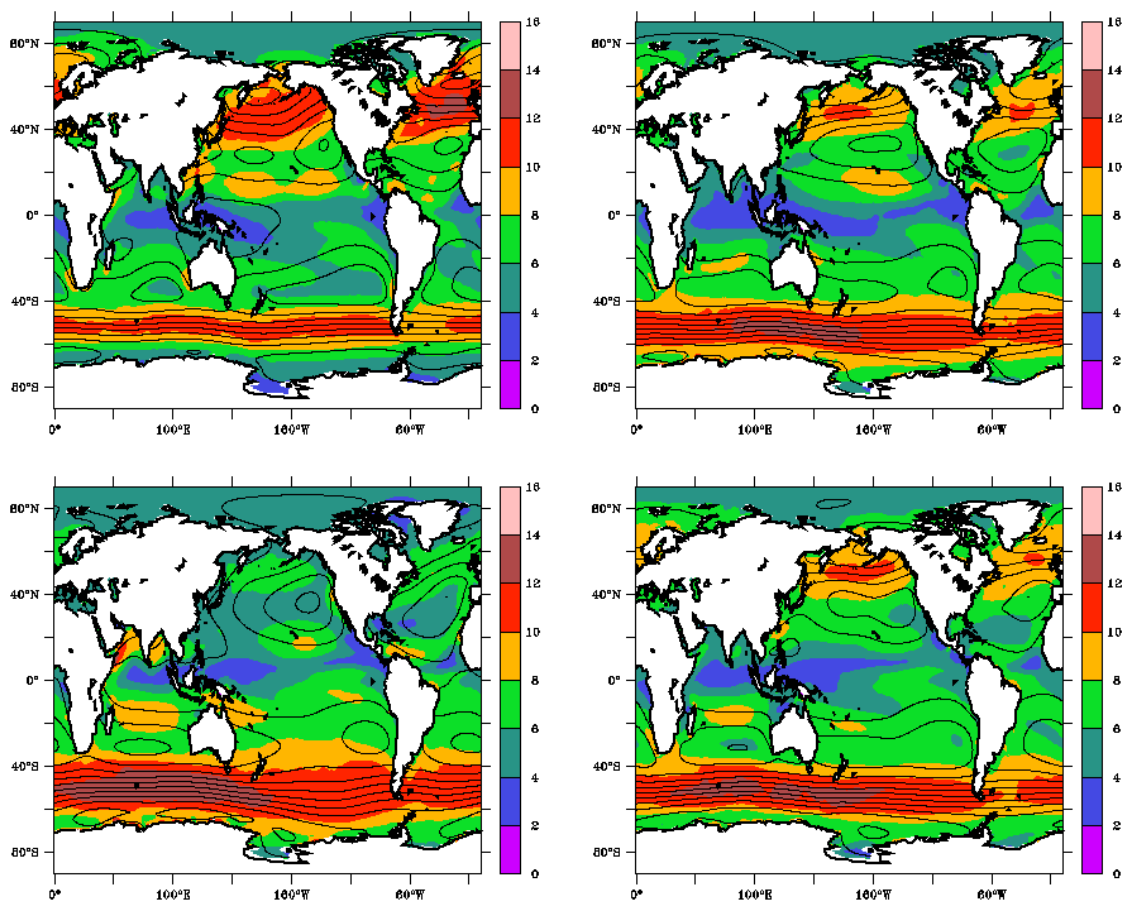
Figure 6.1: Mean sea level pressure (contours) and 10 m wind speed in the CCAM 60 km downscaled simulation using the CSIRO Mk3.5 sea surface temperatures for DJF (top left), MAM (top right), JJA (bottom left) and SON (bottom right). Means are for the period 1980-1999.

The biases of the CCAM 60 km CSIRO Mk3.5 simulation of mean sea level pressure compared against the NCEP CFS analyses (Figure 6.2) has pressures that are too low over the Arctic region and too high over the northern subtropical latitudes, around 40ºN. As a result, the wind speeds in the northern North Pacific are too strong (not shown). In the Southern Ocean, the model generally predicts highs that are too strong around 40ºS and pressures that are slightly too low near Antarctica, which also leads to too strong zonal winds (not shown). Having a pattern of flow that is too strong and too zonal is typical of most global models. The cause is under investigation.

The results for the CCAM 60 km ECHAM5 simulation for the current climate are very similar to the previous results and are not shown. The similarity is a result of the bias-corrected sea surface temperatures, which forces the climatological temperatures for the current climate to be like the observed and like each other, with the resulting circulations also very similar.
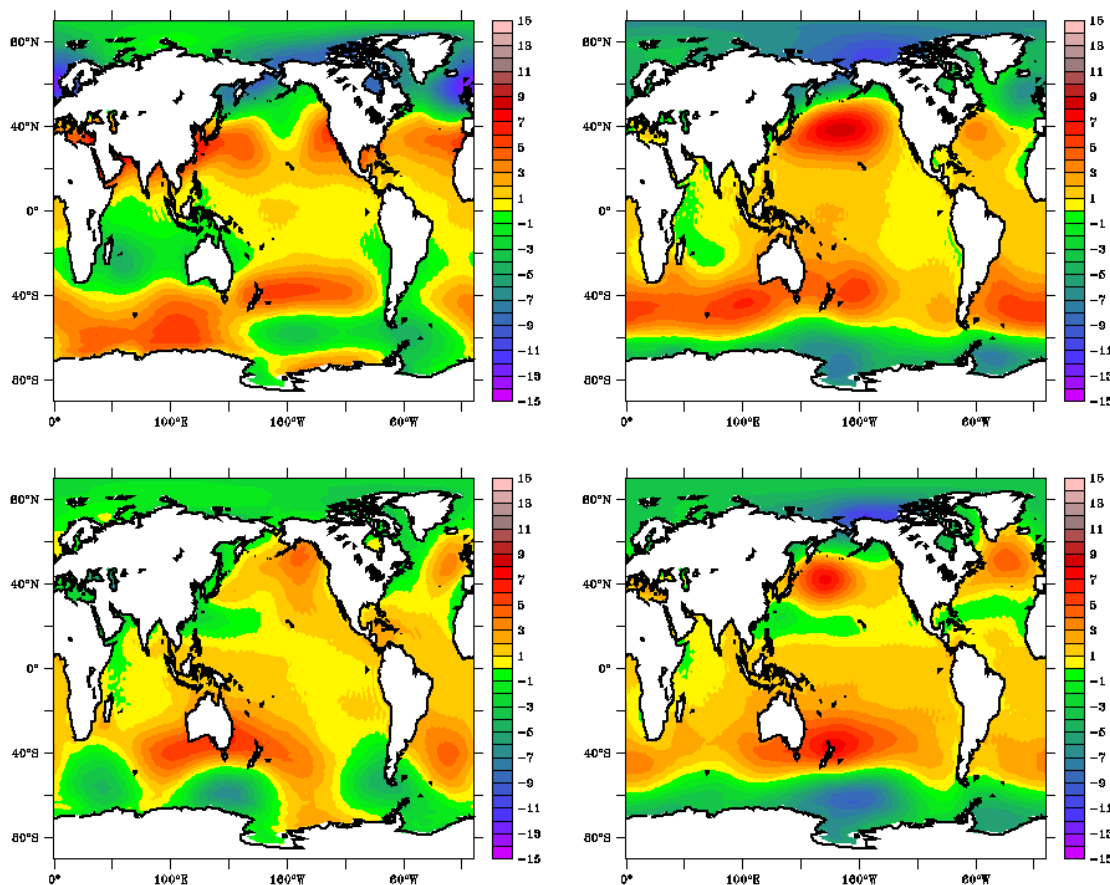
Figure 6.2: Bias of mean sea level pressure for the 1980-1999 period for the CCAM 60 km CSIRO Mk3.5 simulation compared against the NCEP CFS analyses for DJF (top left), MAM (top right), JJA (bottom left) and SON (bottom right).

Comparing surface wind speed, U10, between the CCAM downscaled simulations and the NCEP CFSR (Figure 6.3), it is seen that the CCAM model qualitatively reproduces the observed wind field structure, but some large quantitative biases are observed. The strongest bias is observed in the Pacific sector of the Southern Ocean, with positive (CCAM overestimating) biases of nearly 2 m/s in annual mean surface wind speed in this region. In the low and equatorial latitudes, a negative bias is observed in the region of the intertropical convergence zone (CCAM winds underestimated), but a slight positive bias in the region of the tropical easterlies. A negative bias is then observed in the region of both the northern and southern subtropical ridge (STR). This banding suggests the position of the STR is misrepresented in the CCAM model (a poleward bias). The seasonal bias of U10 (Figure 6.4, 6.5 and 6.6) show that this structure is largely consistent throughout the year, although positive biases are greater during respective hemispheric winters (stronger in south during austral winter).

This analysis has shown that there are considerable biases in the climate model wind field. A modelled wave field is strongly dependent on the skill of the forcing winds, and thus surface wind biases introduce biases in derived modelled wave climate. Following the results of Hemer

et al. (2011a), we adjust the climate model surface winds for both climate and variability bias with the aim of improving the ability of the climate model to represent surface wind fields more adequately.

Figure 6.7 displays the annual mean bias between the bias-adjusted CCAM surface wind speed and the NCEP CFSR. The bias, relative to Figure 6.3, has been reduced considerably. Seasonal bias (Figure 6.9) indicates that bias is generally reduced throughout the annual cycle. However, during the northern winter (DJF and MAM), a notable positive bias (BA-CCAM overestimates wind speeds) is observed in the western north-equatorial Pacific, with a corresponding negative bias during northern summer (JJA and SON). This appears an artefact of the bias-adjustment procedure, which adjusts the full wind distribution consistently throughout the year. Thus, differences in cyclone distribution (during northern summer) are also applied during winter, effectively stretching the winter distribution.
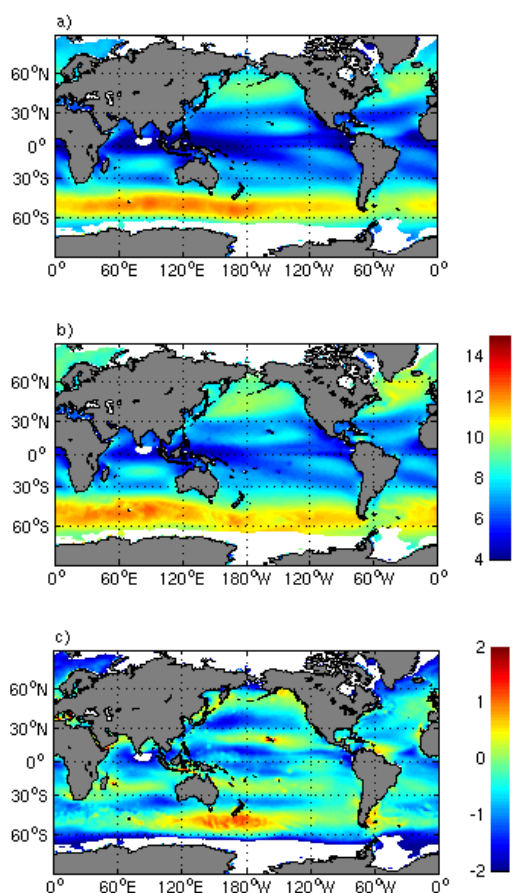
Figure 6.3. Mean surface wind speed (u-10), units m/s. a) from CCAM 60km ECHAM5; b) from NCEP CFS Reanalysis; and c) mean bias between CCAM 60km ECHAM5 and NCEP CFSR. Positive values indicates CCAM overestimates surface wind speed.
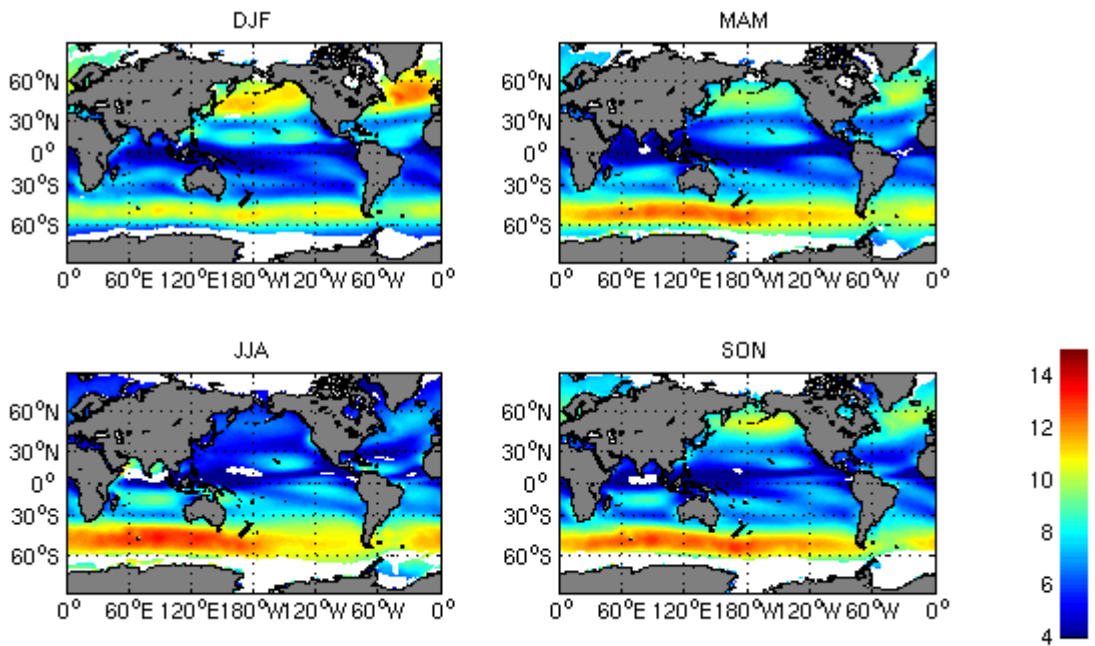
Figure 6.4. Seasonal mean surface wind speed (U10) from CCAM 60km ECHAM5 run. Units m/s.
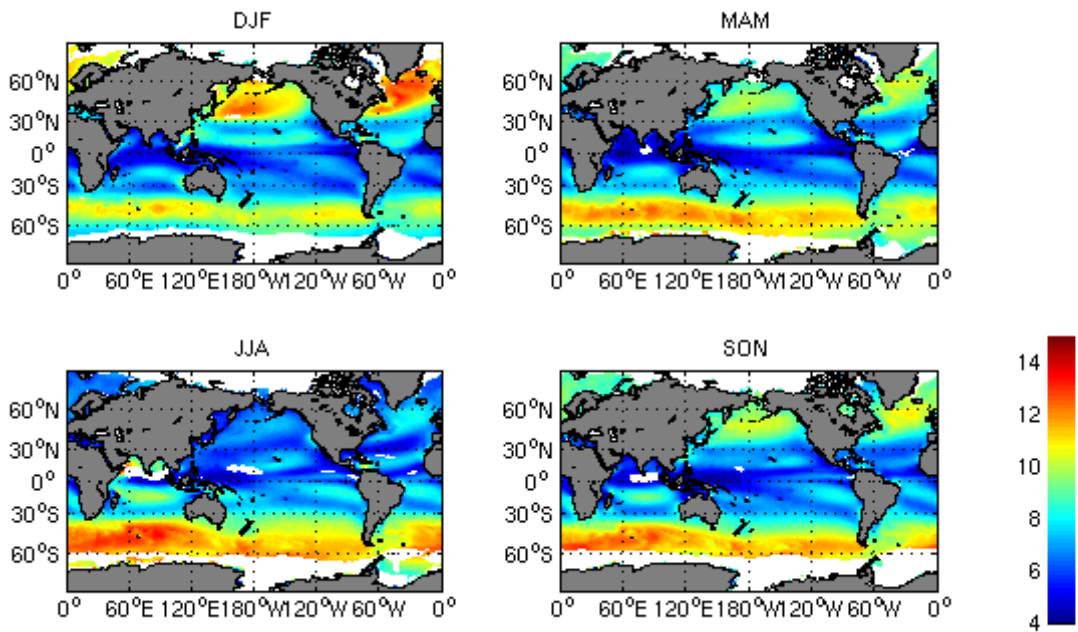
Figure 6.5. Seasonal mean surface wind speed (U10) from NCEP CFSR. Units m/s.
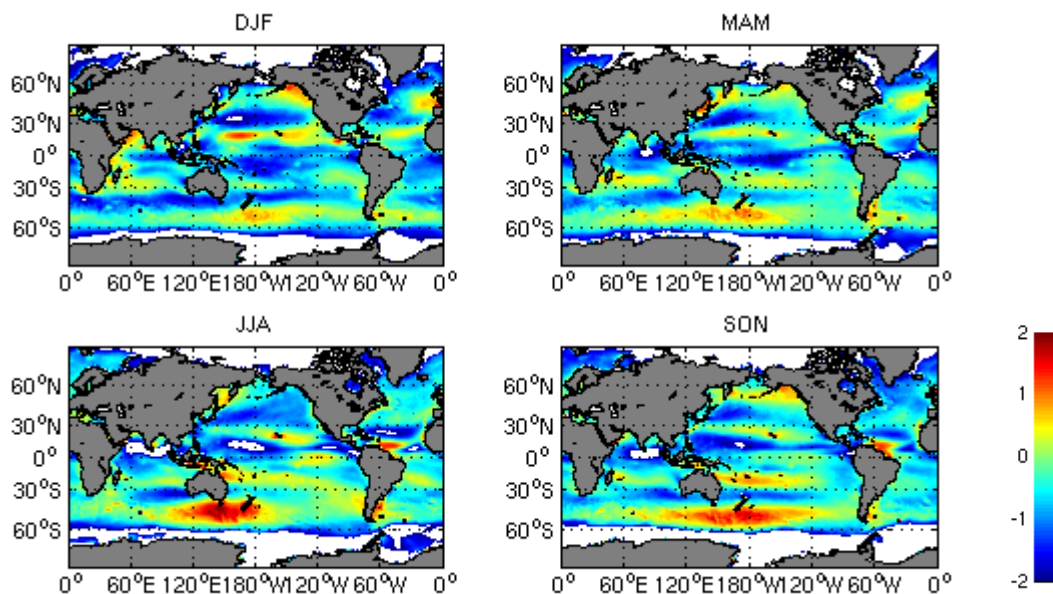
Figure 6.6. Seasonal mean bias of surface wind speed (U10) between CCAM 60km ECHAM5 run and NCEP CFSR. Units m/s. Positive bias indicates CCAM overestimates surface winds.
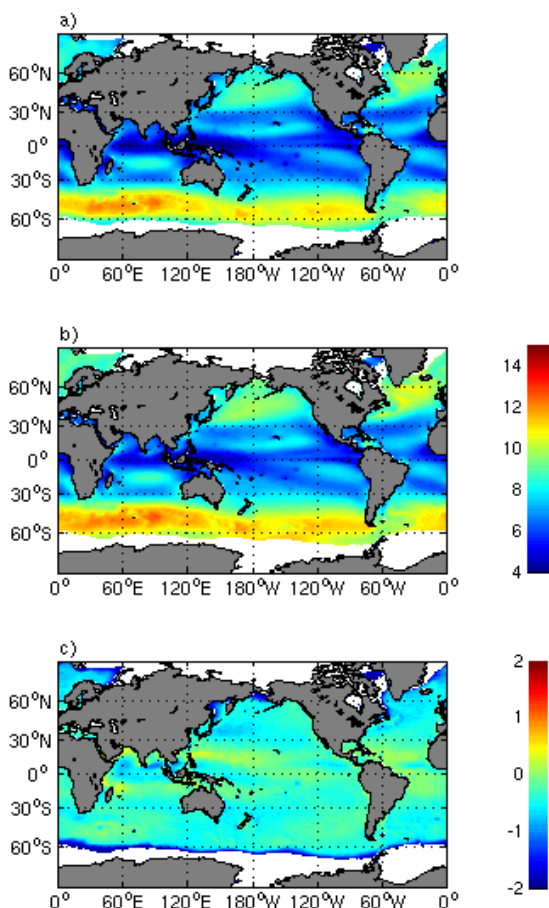
Figure 6.7. Mean surface wind speed (u-10), units m/s. a) from Bias-Adjusted CCAM 60km ECHAM5; b) from NCEP CFS Reanalysis; and c) mean bias between Bias-Adjusted CCAM 60km ECHAM5 and NCEP CFSR. Positive values indicates CCAM overestimates surface wind speed.
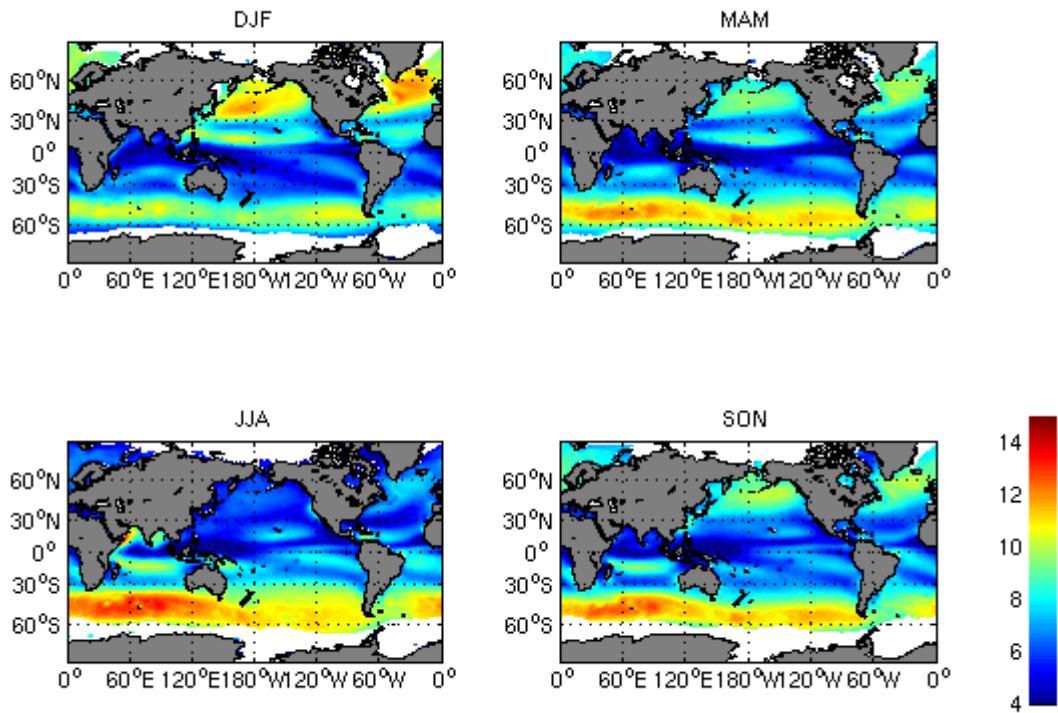
Figure 6.8. Seasonal mean surface wind speed (U10) from Bias-adjusted CCAM 60km ECHAM5 run. Units m/s.
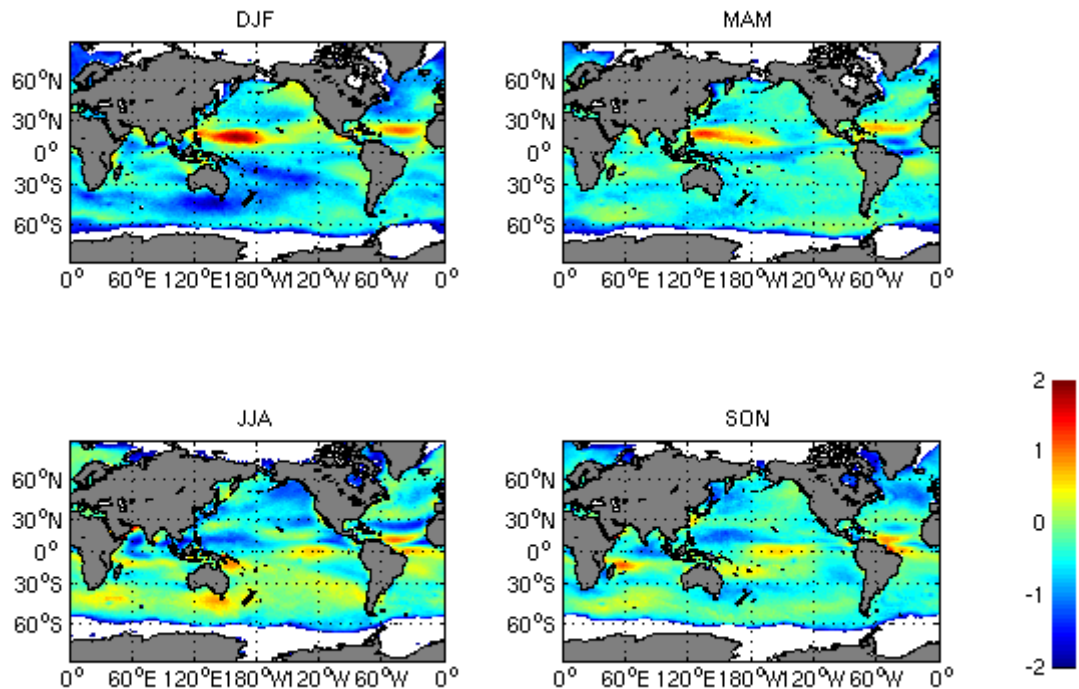
Figure 6.9. Seasonal mean bias of surface wind speed (U10) between Bias-Adjusted CCAM 60km ECHAM5 run and NCEP CFSR. Units m/s. Positive bias indicates BA-CCAM overestimates surface winds.

6.1.2 Evaluation of the Climate Change signal in the CCAM 60 km simulation

The climate change signal is evaluated for both the 60km CCAM downscaled CSIRO Mk3.5 and CCAM downscaled ECHAM5 simulations. Since one of the key causes of change in 10 m wind speed is circulation changes that can be associated with the mean sea level pressure pattern, both fields are examined. Note that the climate change signal of the sea surface temperatures from the host GCM is maintained in the CCAM simulation, although the actual temperatures are different, since they are bias corrected. However, since the CCAM simulations do not have any atmospheric forcing from the host GCM, the changes in atmospheric fields are totally determined by the response of CCAM to the sea surface temperature changes.

The changes noted between the 1980-1999 and 2080-2099 periods for the CCAM 60 km CSIRO Mk3.5 simulation for mean sea level pressure (Figure 6.10) and 10 m wind speed (Figure 6.11) are increases in pressure around 50ºS in DJF and MAM, with resulting increases in 10 m wind speeds around 60ºS in response to the increased pressure gradient. The pattern of changes in JJA and SON 10 m winds is not as clear in the Southern Ocean, with areas of increases and decreases related to regional pressure changes. There is some suggestion that the easterly trades in the northern Pacific increase around 10ºN, especially in MAM and JJA seasons. The cause of these changes is not obvious and needs further investigation. There is also some decrease in 10 m winds around Alaska.
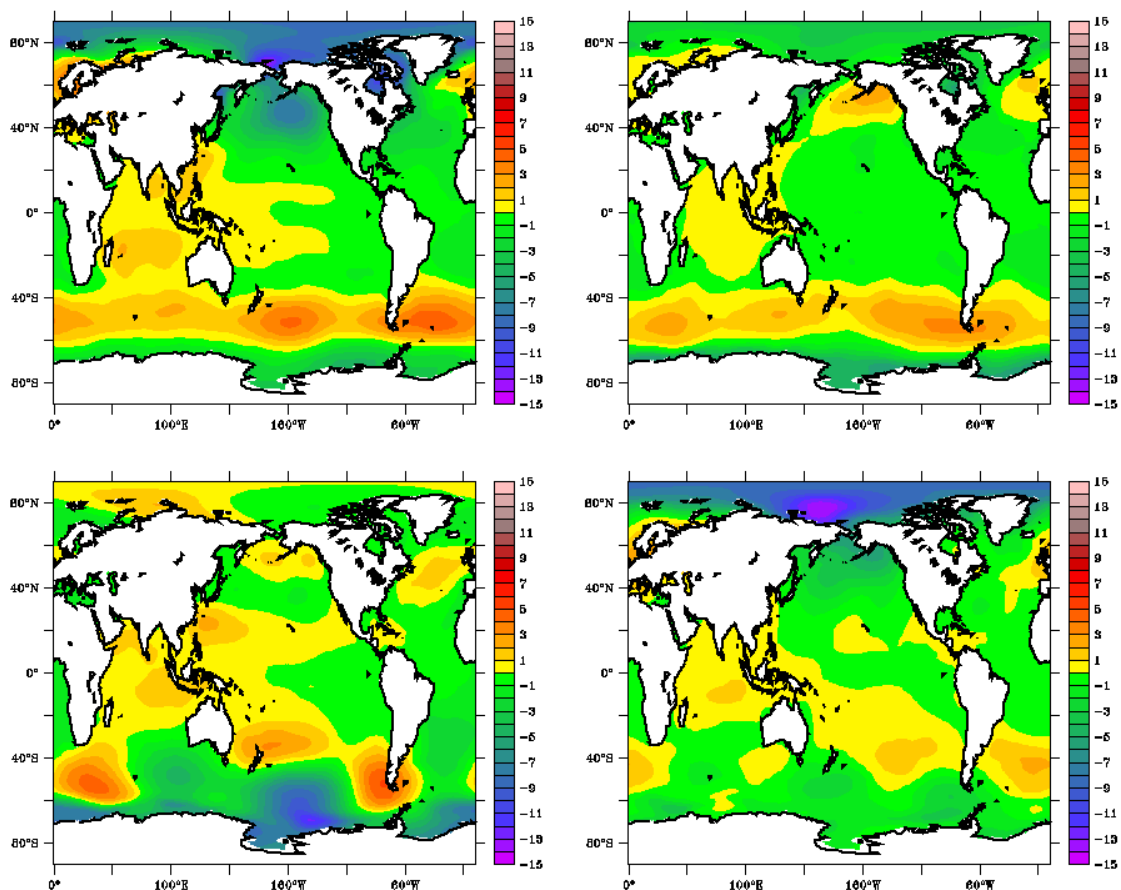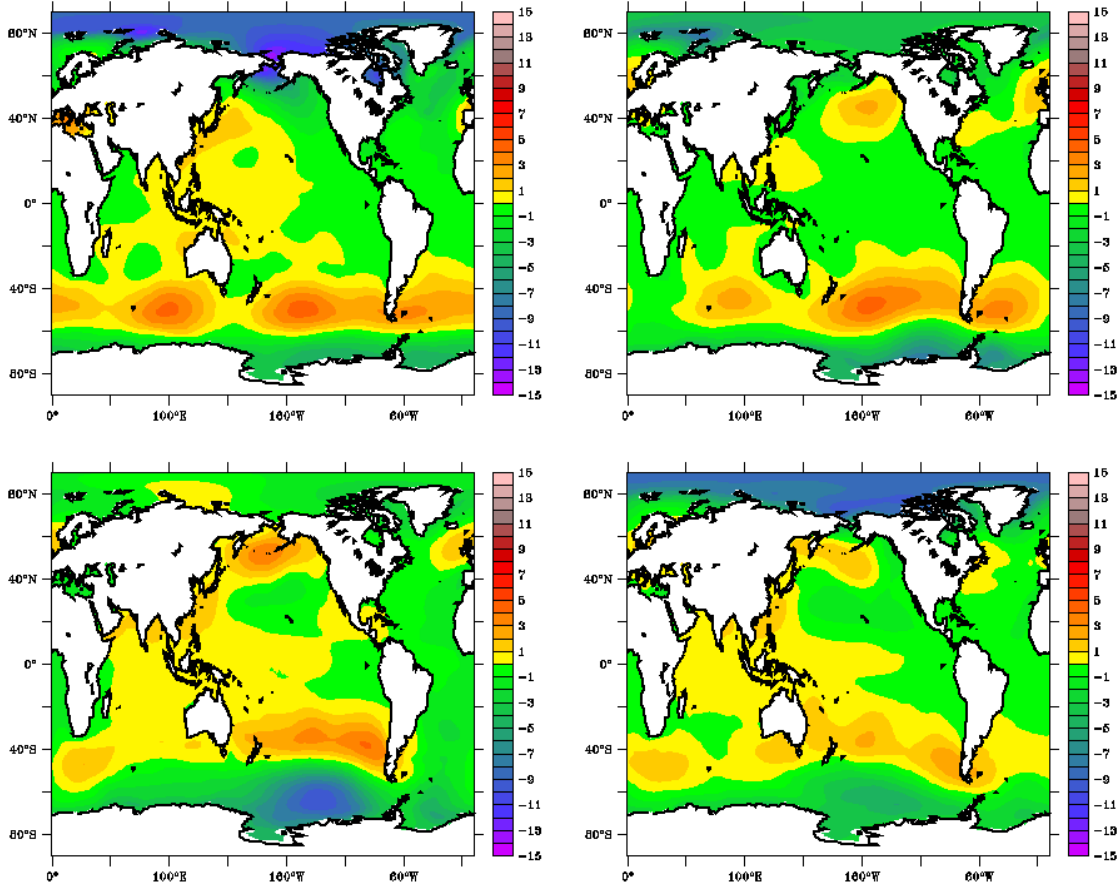

Figure 6.10: Change in mean sea level pressure 2080-2099 minus 1980-1999 period for CCAM 60 km CSIRO Mk3.5 simulation.
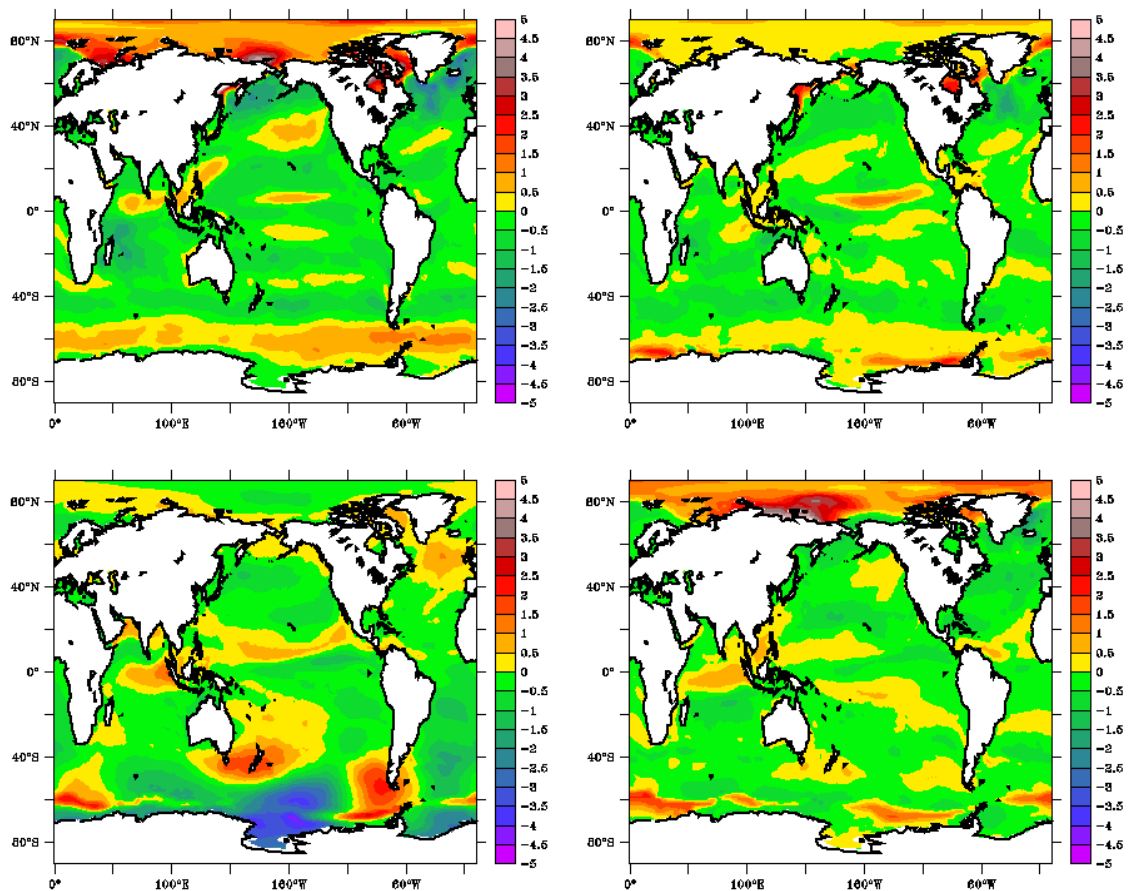
Figure 6.11: Change in 10 m wind speed 2080-2099 minus 1980-1999 period for CCAM 60 km CSIRO Mk3.5.

The changes in the CCAM 60 km ECHAM5 simulated mean sea level pressure (Figure 6.12) and 10 m wind speeds (Figure 6.13) show a similar pattern of Southern Ocean wind speed increase and pressure changes in DJF and MAM. However, in this simulation the increases in 10 m winds in the South Pacific are more spatially coherent and cover a larger area, extending from Australia to South America. There are also slightly greater increases in winds in the Southern Ocean in SON. The increases in northern Pacific trades noted in the previous simulation are not as evident in this simulation. In addition, the decreases in 10 m wind speed near Alaska are also not seen. Projected change in bias-adjusted wind fields are similar to the un-adjusted fields.

In summary, both simulations show increases in 10 m wind speeds in the Southern Ocean, especially in DJF and MAM seasons. Fairly large increases and decreases in winds are also evident in JJA in the South Pacific, but the pattern of change is not consistent between the two simulations. Elsewhere, the changes tend to be relatively small.

Figure 6.12: Change in mean sea level pressure 2080-2099 minus 1980-1999 period for CCAM 60 km ECHAM5 simulation.
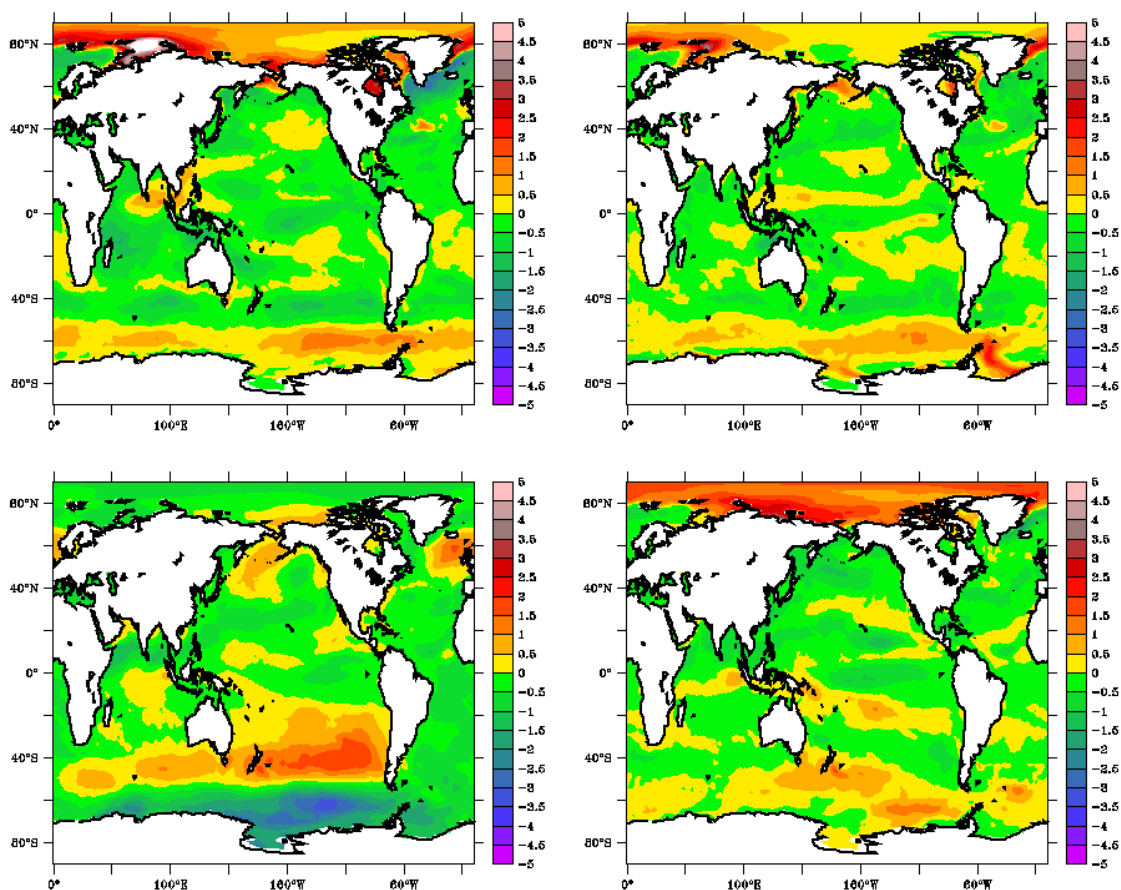
Figure 6.13: Change in 10 m wind speed 2080-2099 minus 1980-1999 period for CCAM 60 km ECHAM5 simulation.

6.2   Unadjusted CCAM forced wave models

The WaveWatch III spectral wave model has been implemented at 1° spatial resolution globally, and forced with 3-hourly surface winds taken from the CCAM C160 global model runs, which downscale a selection of CMIP3 GCMs. The wave spectrum is resolved by 24 frequency bins ranging from 0.04 to 0.3 Hz, and has a directional resolution of 15°. The model is run for 2 time-slices: 1979-2009 representing a present climate time-slice, and 2070-2099 representing a future period. At present, integrated wave properties Hs (significant wave height), Tz (mean wave period), and Dm (mean wave direction) are archived from the model runs only. This choice was made based on storage limitations. In future, additional data will be archived allowing distinction of sea and swell components of the wave spectrum at any point.

Appendix A resolves that ERA-Interim ably reproduces the observed significant wave heights, and provides some insight into representation of the model skill to represent the full directional wave climate. A key objective of the project is to assess the ability of a dynamical wave modelling approach to project potential changes in wave climate under future warmer climate scenarios. In this study, a dynamical wave modelling approach has been taken which follows the regional study outlined by Hemer et al. (2011a and 2011b).

In this section, we assess the skill of the wave model to describe the present wave climate (using ERA-Interim as a control), when forced directly with climate model derived surface winds. This model skill is determined by statistics derived from monthly mean significant wave heights, from the CCAM forced model (Hs_{clim}) and the control wave climate ($Hs_{control}$). We determine the total mean bias ($<Hs_{clim}>-<Hs_{control}>$) between these datasets (Figure 6.14a), and the total variability bias (the ratio between the variance of Hs_{clim} to the variance of Hs_{contol}; Figure 6.14b). We determine the mean bias in the annual cycle of significant wave height, and the annual cycle variability bias, to assess the skill of the climate model to represent the mean annual cycle of significant wave height.

This analysis determines the ability of the wave model to describe the present wave climate, when forced with surface winds derived from the downscaled CCAM climate model. The mean bias in wave height is relatively small across the Northern Pacific Ocean, with the climate model forced waves underestimating wave heights in the western sector by less than approx 0.2 m (Fig 6.14a). In the eastern equatorial, the climate model forced waves tend to overestimate wave heights by approximately 0.2 m. The overestimation of wave heights in the eastern sector of the equatorial and mid-latitude bands of the Pacific can be attributed to swell which has propagated from the high latitudes, where mean significant wave heights are overestimated - particularly in the southern extra-tropical storm belt. This observed bias in the high latitudes is consistent with the tendency for climate models to overestimate the zonal flows in the high latitudes indicated in Section 6.1. Figure 6.14b indicates variability of the southern ocean wave climate is also overestimated, which in turn affects the resultant swell regions. Figure 6.15 indicates the climate bias is relatively consistent in the eastern Pacific throughout the annual cycle, consistent with a strong positive bias in the swell generated in the extra-tropics propagating to the region. During the boreal winter in the north Pacific, wave heights are underestimated at latitudes of around 40°N, and overestimated further north at 50°N. During summer, the bias is relatively small. In the southern Pacific, the CCAM model also overestimates wave heights during the austral winter months. During the austral summer, the region of overestimated wave height is limited to the east where it is a signal of too large a swell component in the wave field.

The total variability bias is also large across the Pacific Basin (Figure 6.14b). A small region in the central Pacific has a variability bias less than 1, indicating that the variance is underestimated by the CCAM forced wave model, but the variance is overestimated, by almost an order of magnitude in places (particularly in the southern extra-tropical storm belt), in the remainder of the Pacific basin. The total variability bias encompasses two components - seasonal variability and the inter-annual variability. The variability bias of the seasonal signal (Figure 6.16) is particularly large in the equatorial band, suggesting that the variance in position of the intertropical convergence zone is not well represented. Variance is overestimated in the southern equatorial region, and underestimated in the northern equatorial band. The positive variability bias spans most of the southern Pacific. In the northern Pacific, the variability bias varies regionally and is not as large as observed in the southern Pacific (Figure 6.16). No clear coherent patterns are apparent in the inter-annual variability bias and this is considered beyond the scope of the current study.
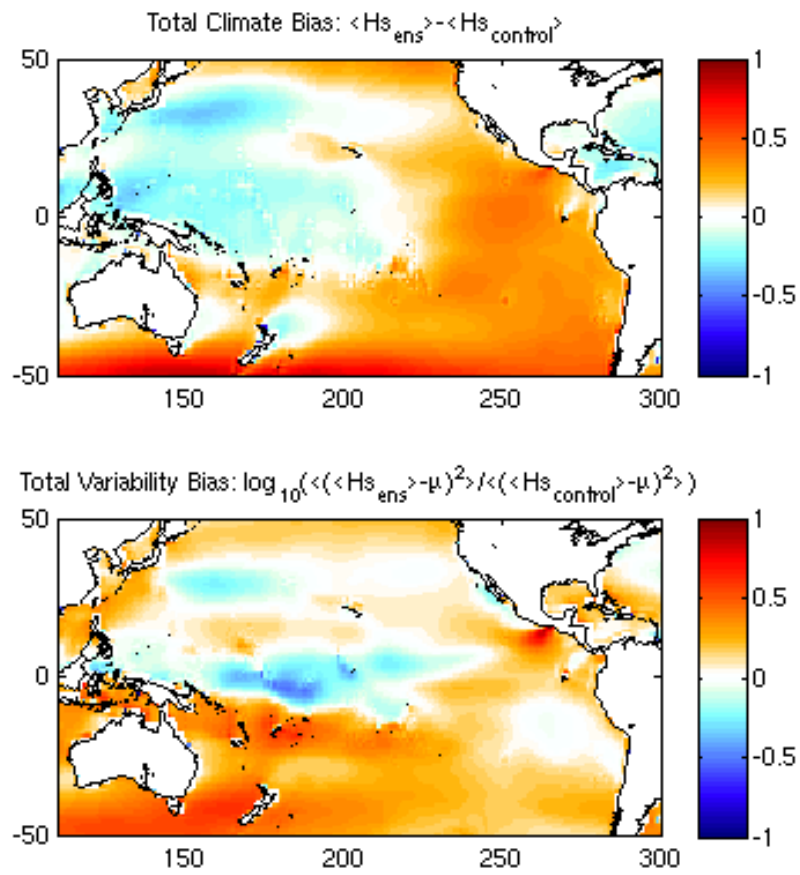
Figure 6.14: A) Total climate bias of significant wave height, between CCAM ensemble mean and ERA-Interim, units: metres, and B) total variability bias of monthly mean data (log10 scale), units: dimensionless.
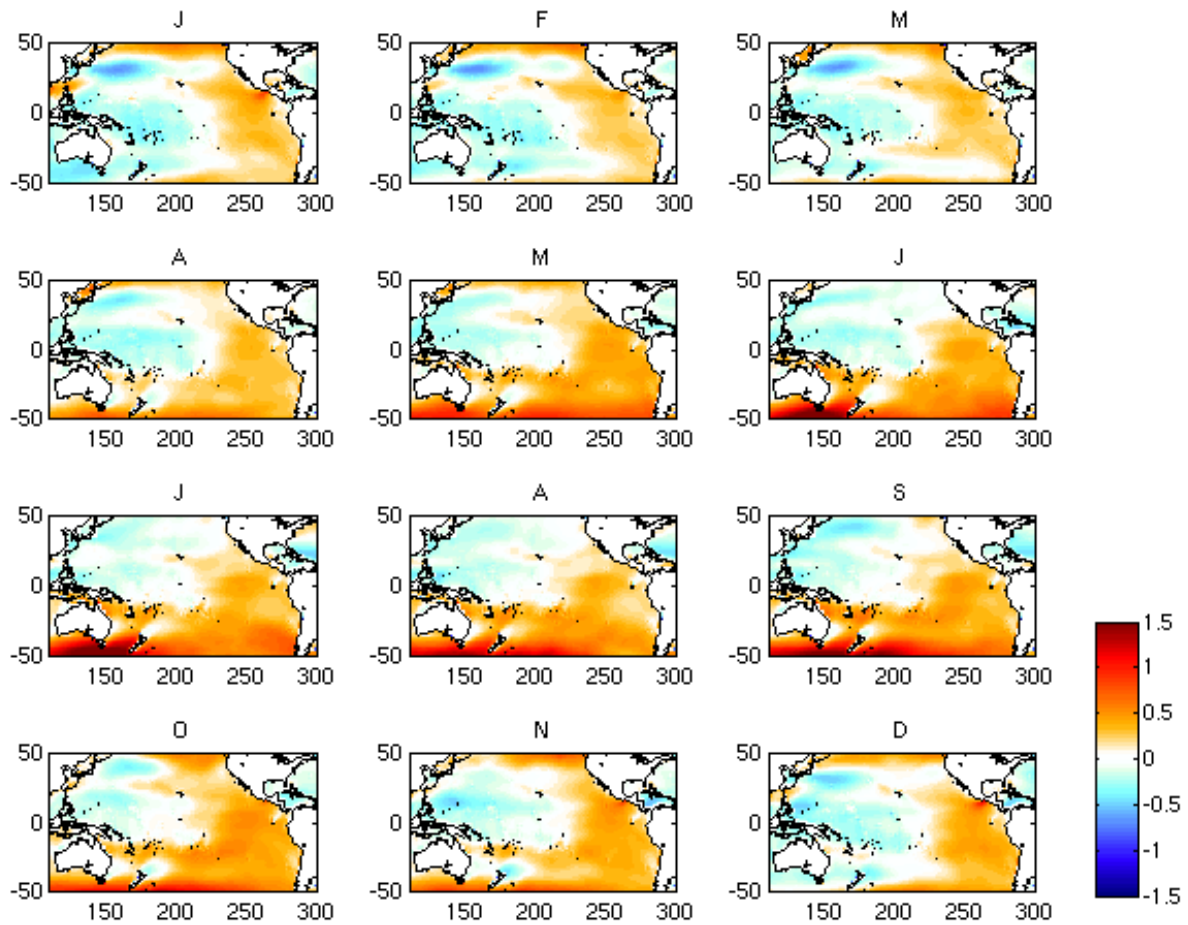
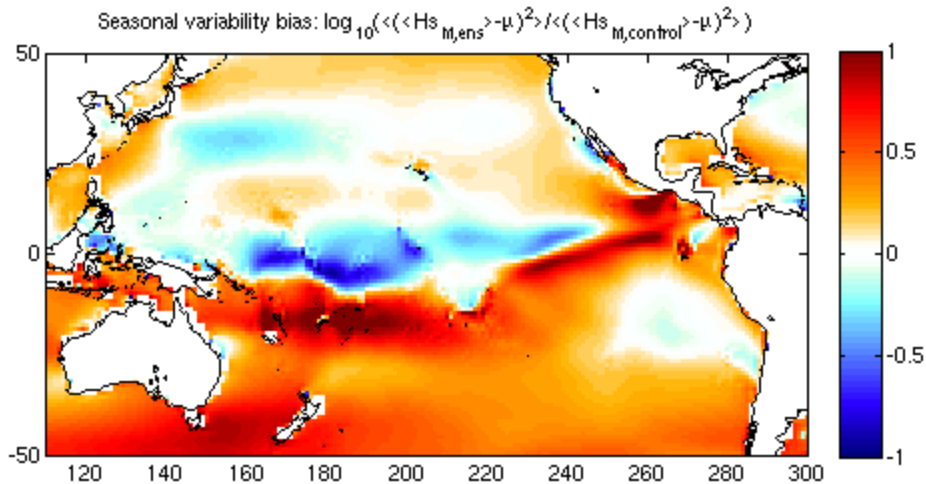Figure 6.15: Annual cycle of mean bias in significant wave height, between CCAM ensemble mean and ERA-Interim. Units: metres.

Figure 6.16: Significant wave height variability bias of the mean annual cycle (log10 scale). Ratio of seasonal variance of CCAM ensemble to seasonal variance of ERA-Interim. Units: Dimensionless.

6.2.1   Site Records

Wave roses from the CCAM forced wave model, for the same five locations as shown from the ERA-Interim data in Section 6.1.3, are given in Appendix B, Figures B1-5. The wave roses are an ensemble mean of both the CCAM downscaled Mk3.5 and CCAM downscaled ECHAM5 runs. Thus, the plotted wave roses are determined from a 42 year time-series (1989 to 2009 period, from two runs).

Within the directional extremes analysis (Figure 6.17), notable differences between the CCAM forced wave model climate and ERA-Interim include:

- Increased estimates of extreme wave height associated with north-westerly swell at the Hawaiian site – an increase from approx. 6m to 8m in 100-yr return period wave height from 320°N.

- Increased estimates of extreme wave height for south-easterly waves at the South Pacific site (100yr return interval wave height increase from approx 6m to 7m).

- Decreased estimates of extreme wave height associated with easterly trade wind generated waves at the western North Pacific site (100yr return interval wave height decrease from 8m to 6m from 90°E).

Hawaii

At the northern central Pacific location (Hawaii; Figure B1), the wave rose derived from the CCAM forced runs provide a relatively good representation of the wave climate described by ERA-Interim (Figure 5.13). There is strong seasonal variability, with northern Pacific swell dominating during the boreal winter, and north-easterly trade dominating during the boreal summer. During JJA, the CCAM derived wave field overestimates the ERA-Interim wave heights (dominated by wave heights 1.5-2m, are higher than the 1.5 m waves in the ERA derived climate), and south-easterly waves dominate the wave field (as opposed to easterly). Wave periods (not shown) are also relatively well represented. A slight overestimate of wave period of the north-westerly swell during the boreal winter is observed, with a larger component of waves with periods longer than 13s.

South-west Pacific (Fiji/Vanuatu)

The CCAM forced wave model provides a relatively good representation of the south-west Pacific wave climate (Figure B2) with respect to the ERA-Interim wave climate (Figure 5.14) with waves predominantly directed from the south-easterly quadrant, and austral winter swell from the south-south-west. The main difference between these two wave climates is the austral winter swell has a longer period (not shown; some waves with period >13s) and more energetic (some waves with Hs>4.5m).

Equatorial Pacific (Kiribati, Tuvalu)

The CCAM forced wave model provides an adequate representation of the equatorial Pacific wave climate (Figure B3) relative to ERA-Interim (Figure 5.15). Trade wind waves dominate throughout the year, dominated by the north-easterly trades during the austral summer and the

south-easterly trades during the austral winter. The height of the north-easterly waves during DJF are slightly smaller than estimated by ERA-Interim (very little waves of height > 3m), and the period of south-easterly waves (not shown) are longer than the ERA-Interim data (some waves with period >11s observed).

South Pacific (French Polynesia)

Considerable difference is observed between the CCAM derived wave climate (Figure B4) and the ERA-Interim wave climate (Figure 5.16) in the South Pacific region. Whereas the ERA-Interim wave field is dominated by southerly swell throughout the year, the CCAM wave climate has a much greater south-easterly component and is only dominated by southerly swell during the austral winter months (JJA). During the austral summer, very few southerly waves are observed in the CCAM record. The south-easterly waves have shorter period (dominated by 9-11s, as opposed to southerly waves dominated by 11-13s). These differences in wave field are considerable.

Western North Pacific

The CCAM derived wave climate in the western north Pacific (Figure B5) and the ERA Interim derived wave field (Figure 5.17) are very similar. Both wave fields are dominated by north-easterly waves which are slightly larger during the boreal winter, and are more easterly during the boreal summer.
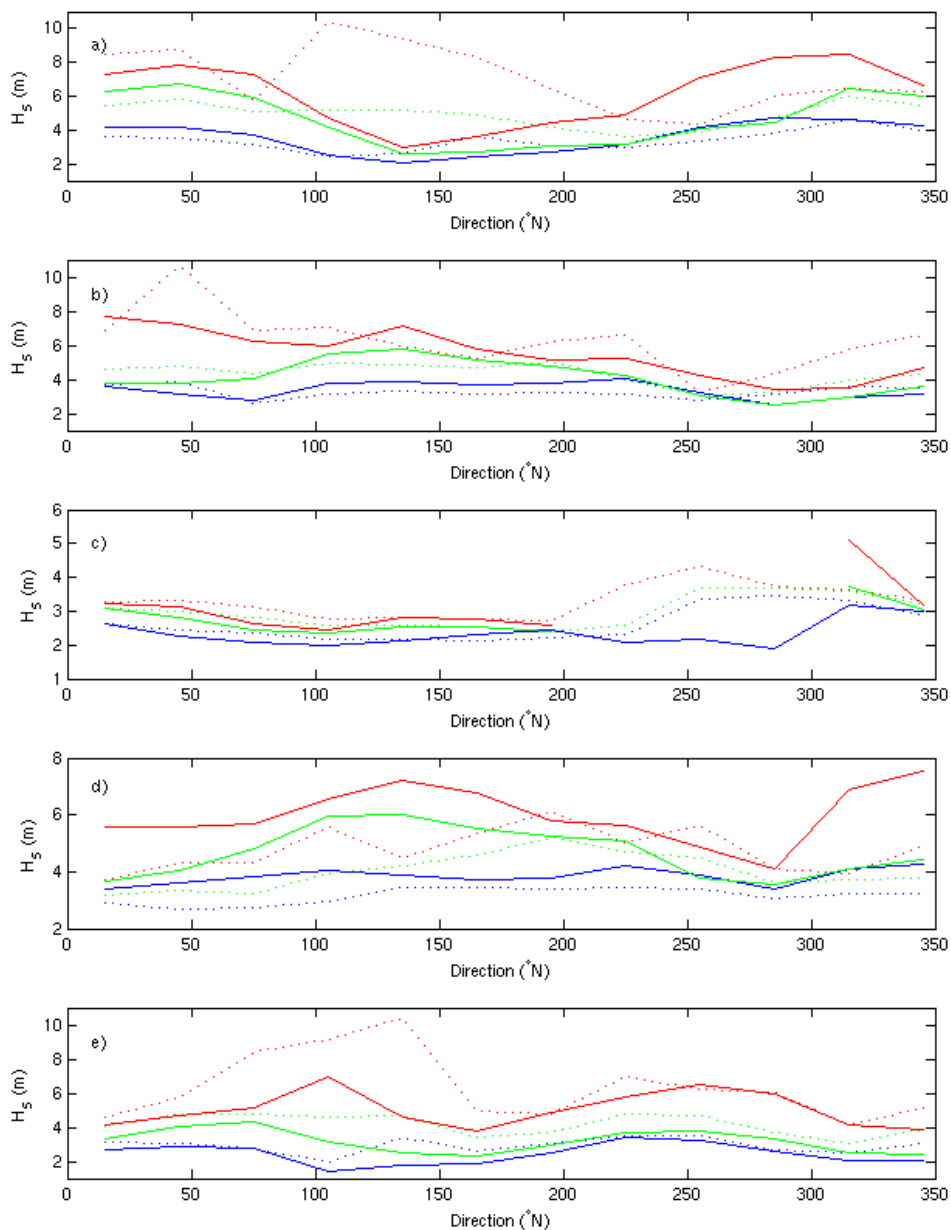
Figure 6.17: Return period significant wave heights by direction for 5 sites, from the CCAM derived 2-member ensemble wave field. a) Hawaii; b) South Pacific (Vanuatu-Fiji); c) Equatorial Pacific (Kiribati-Tuvalu); d) South Pacific (French Polynesia); e) Western North Pacific (Guam- Micronesia). The blue line represents the annual return significant wave height for each directional segment, the green line is the 10-yr return value, and the red line is the 100-yr return value. Dotted lines display respective values from ERA-Interim data (shown in Figure 5.18.

6.3   Bias-Adjusted CCAM forced wave models

When forced with bias-adjusted CCAM winds, the mean climate bias is seen to have much reduced spatial variability, with a consistently negative bias (BA-CCAM derived wave field underestimates wave field) of approximately 0.2m observed across the Pacific basin (Figure 6.18a). Positive biases are observed in only limited regions of the Coral, Philippine and East

China Seas. Little difference is observed between the total variability bias from the bias-adjusted wind forced run (Figure 6.18b) and the un-adjusted winds forced run (Figure 6.14b).

When forced with the bias-adjusted winds, seasonal variability of the mean bias is relatively constant (Figure 6.19b). Consistent with surface winds, we see a positive bias in the western North Pacific, particularly during northern winter months, and we attribute this to an artefact of the bias adjustment, adjusting distribution for maximum winds which occur in reality only during northern summer months, for all seasons.
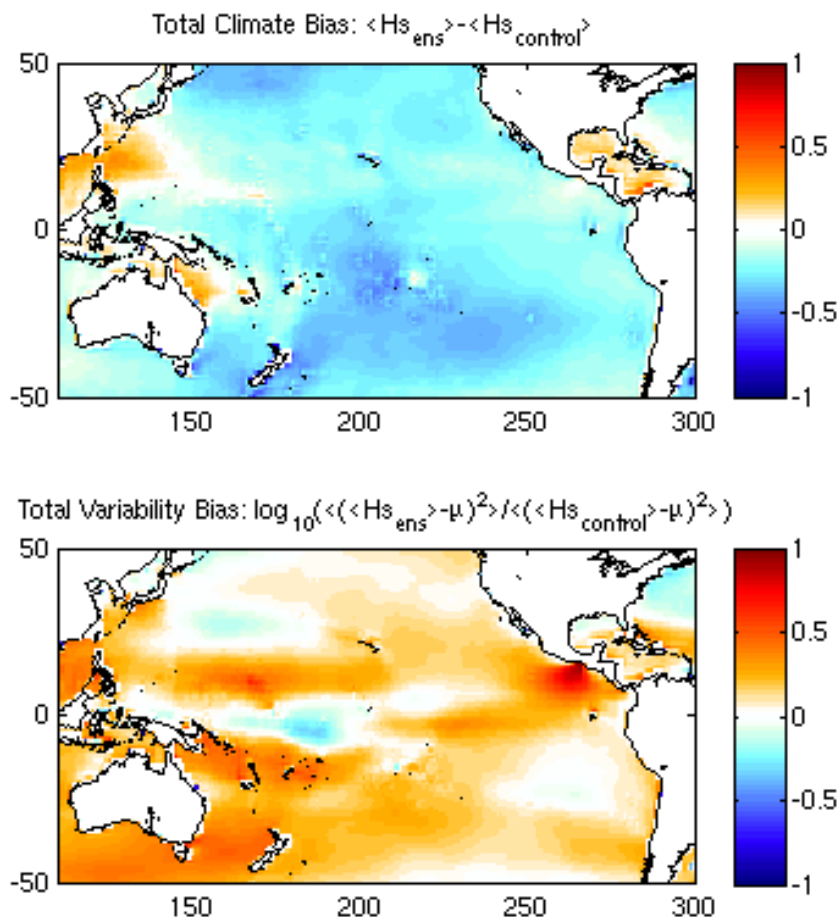
Figure 6.18: A) Total climate bias of significant wave height, between BA-CCAM ensemble mean and ERA-Interim, units: metres, and B) total variability bias of monthly mean data (log10 scale), units: dimensionless.
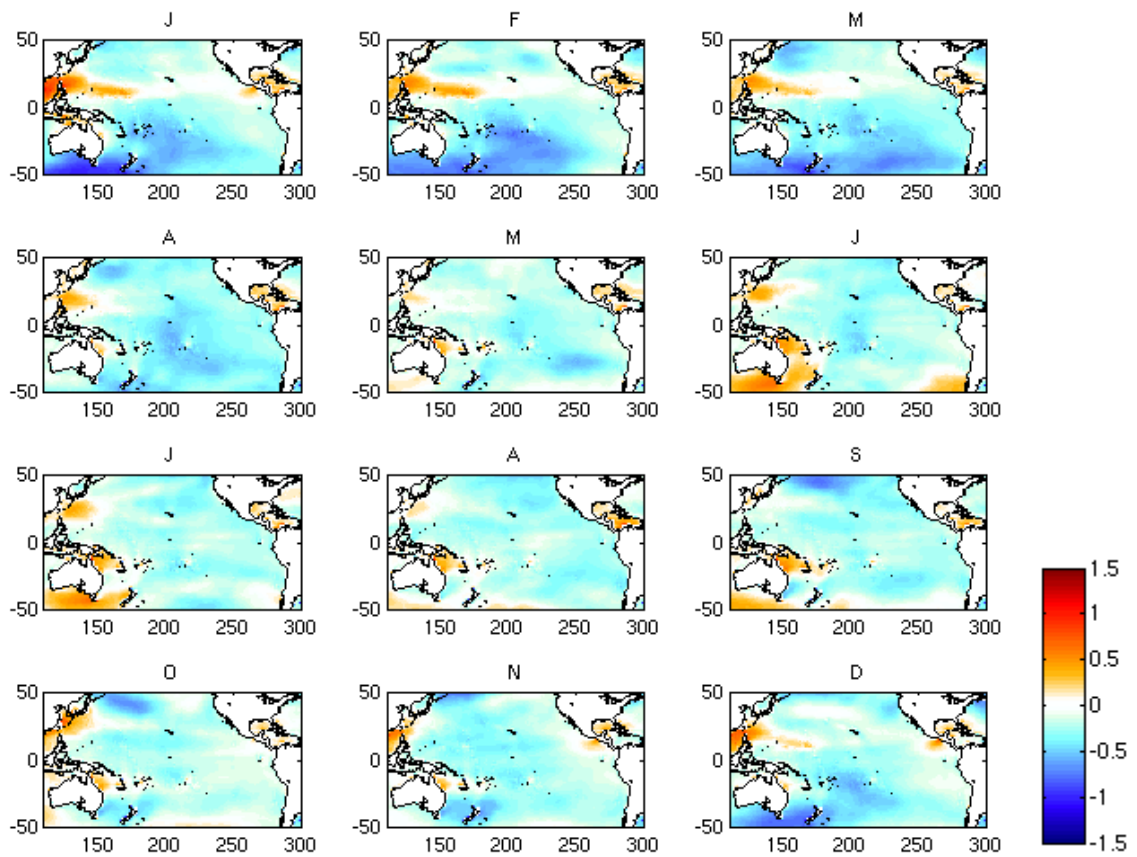
Figure 6.19: Annual cycle of mean bias in significant wave height, between CCAM ensemble mean and ERA-Interim. Units: metres.
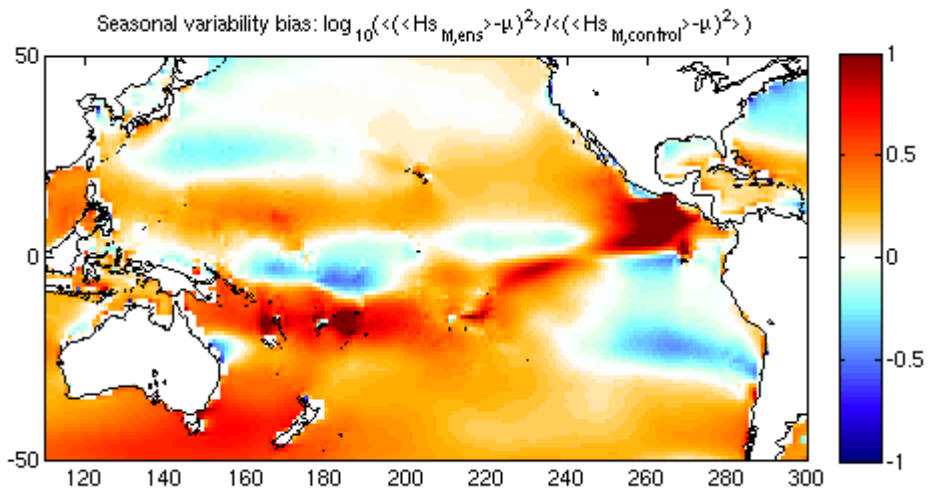
Figure 6.20: Significant wave height variability bias of the mean annual cycle (log10 scale). Ratio of seasonal variance of BA-CCAM ensemble to seasonal variance of ERA-Interim. Units: Dimensionless.

6.3.1   Site records

Hawaii

The influence of forcing the wave model with bias-adjusted winds on the wave field at the Hawaiian site is relatively small (Figure B6). The directional distribution of waves remains consistent with the ERA-Interim wave field (Figure 5.13). Typically the bias-adjusted wind forced fields have lower wave heights than those from the un-adjusted CCAM forced runs (Figure 6.18) which are more consistent with the ERA wave fields. However, during the northern winter, the height of northerly swell waves appear better represented from the un-adjusted model, as the height of waves is underestimated by the bias-adjusted model. Throughout other seasons, the bias-adjusted forced run wave field is more consistent with the ERA-Interim fields.

South-West Pacific

At the south-west Pacific site, the un-adjusted wind forced runs (Figure B7) tended to overestimate ERA-Interim wave heights (Figure 5.14). With the bias-adjusted forced runs, wave heights associated with the south-easterly trades are underestimated, and the influence of southerly swell appears under-represented.

Equatorial Pacific

The bias-adjusted forced run (Figure B8) has a tendency to limit distribution of waves contributing to the equatorial Pacific site. While the seasonal variability of wave direction is observed at the site (north-easterly waves during boreal winter, and south-easterly waves during the austral winter), the distribution of wave directions, and the height of waves, within each season tend to be underestimated.

South Pacific

The wave climate derived from the model forced with un-adjusted CCAM winds had a tendency to under-represent the influence of southern ocean swell at the South Pacific site (Figure B9). Forcing the wave model with bias-adjusted CCAM winds further accentuates this under-representation of southerly swell (Figure 6.31), such that wave heights are too low, and southerly swell observed only during austral winter months.

Western North Pacific

The wave field derived from the BA-CCAM runs in the Western North Pacific (Figure B10) shows improved representation of the wave field described by ERA-Interim in this region (Figure 5.17). Bias-adjustment of winds leads to increase in wave heights, but minimal change in directional distribution, when compared with wave field derived from un-adjusted CCAM forced runs (Figure 6.22).

Directional extremes analysis.

On assessment of directional extreme waves, notable influences of forcing the wave model with bias-adjusted winds are:

- Decrease in extreme northerly swell at the Hawaii site. The 100-yr return interval wave height for waves from 300°N decreases from approx. 9m for un-adjusted CCAM run to less than 5m from BA-CCAM run. The corresponding value from ERA-Interim data is 6.5m

- Decrease in extreme southerly swell at the South-West Pacific site. The 100-yr return interval wave height for waves from 180°N decreases from 6m from the un-adjusted CCAM run, to 4m from the BA-CCAM run.

- Small decrease in extreme north-easterly trade generated waves at the Equatorial Pacific site.

- Decrease in extreme southerly swell at the South Pacific site. The 100-yr return interval wave height for waves from 180°N decreases from 6m from the un-adjusted CCAM run, to 3.5m with the BA-CCAM run.

- Only slight change in extreme wave fields at North West Equatorial Pacific site are observed when bias-adjusted winds are used to force the wave model.

- Bias-adjustment of surface winds leads to decrease in extreme wave heights. No notable examples of increase in extreme wave height are observed.

Further studies are required to establish the cause of difference between climate model derived extreme wave conditions and those from ERA-Interim. It is not yet apparent whether differences in frequency or intensity of storm wave events are responsible.
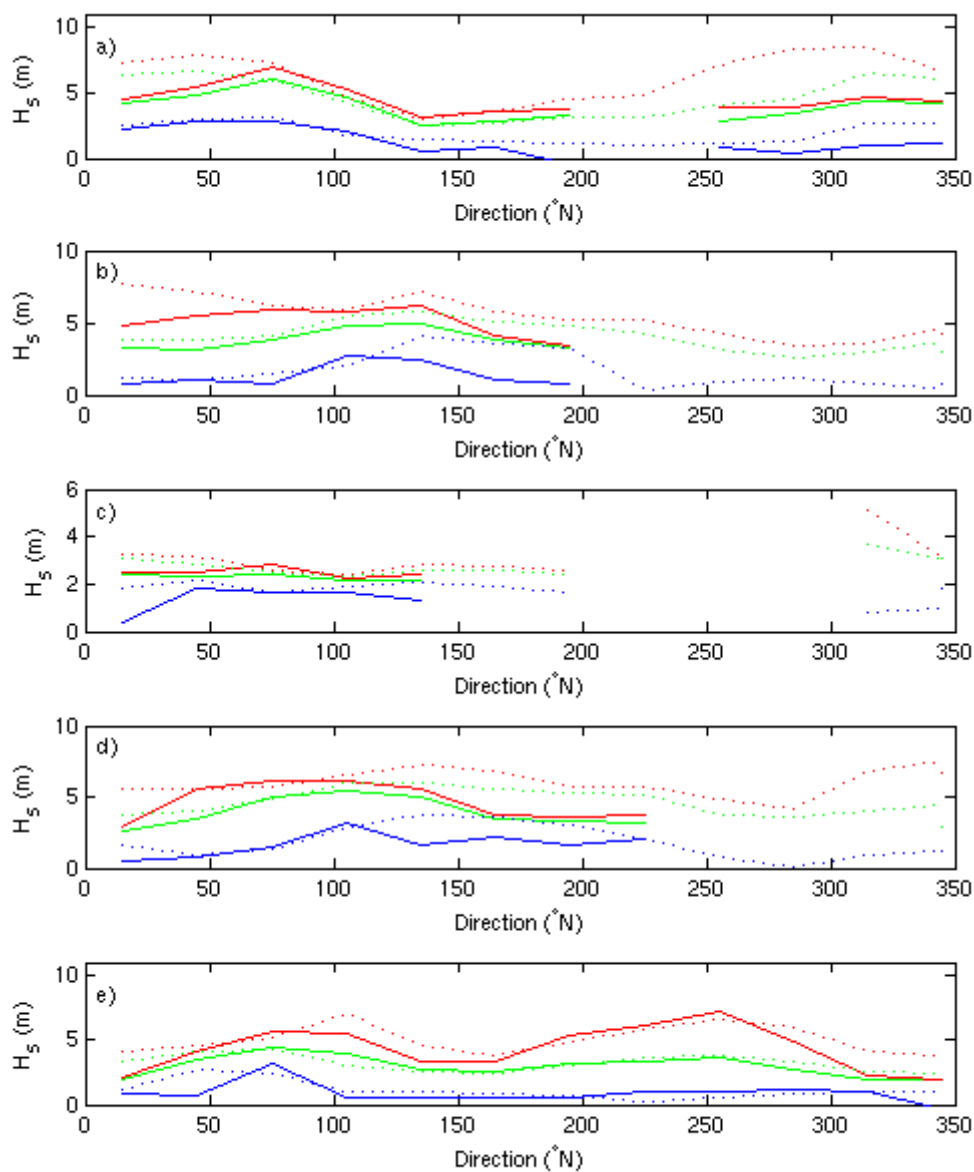
Figure 6.21: Return period significant wave heights by direction for 5 sites, from the BA-CCAM derived 2-member ensemble wave field. a) Hawaii; b) South Pacific (Vanuatu-Fiji); c) Equatorial Pacific (Kiribati-Tuvalu); d) South Pacific (French Polynesia); e) Western North Pacific (Guam- Micronesia). The blue line represents the annual return significant wave height for each directional segment, the green line is the 10-yr return value, and the red line is the 100-yr return value. Dotted lines display respective values from un-adjusted CCAM data (shown in Figure 5.18).

6.4 Preliminary evaluation of the Climate Change signal in the Pacific wave climate

6.4.1 Un-adjusted CCAM forced runs

The wave model was also forced using climate models winds from the future time-slice 2070-2099. These runs were implemented using the same configuration as for the 1979-2009 time-slice. A two member ensemble was carried out, with winds derived from the CCAM ECHAM5 and Mk3.5 runs. In this section, we present the differences in seasonal mean significant wave height (Figure 6.22), mean wave period (Figure 6.23), and mean wave direction (Figure 6.24), between the future 2070-2099 and the current 1979-2009 time-slices.

The projected changes in wave conditions reported below should be prefaced with a statement that they have high, unquantified uncertainty. A 2 member ensemble is insufficient to sample the range of uncertainty which occur with GCMs. Surface marine winds show little agreement between all available GCMs, and this translates to high uncertainty in the derived wave climate. Quantifying this uncertainty is a large task beyond the scope of the present study. Hemer et al. (2010a) have proposed internationally coordinated experiments to address this problem with wave climate projections, and presently the wave climate community is establishing a way forward to address these issues.

Notable changes in wave conditions are projected over the next century under the future high emission (SRES A2) climate scenario. Most notable is the increase in wave heights in the Southern Ocean during the austral winter months (JJA) with mean wave heights increasing by over 0.5m. These waves travel as swell towards the eastern equatorial Pacific, and increases in wave height are also projected in these regions. This is accompanied by an increase in mean wave period of up to 1 s at the equator. Changes in wave direction are also observed with a greater southerly component projected to occur. A projected increase of approximately 0.2m is projected throughout the PICT region. During the boreal winter (DJF), a decrease in mean wave heights of approximately 0.5m is projected in the north-west Pacific adjacent to the Japan coast. This projected change is accompanied by a decrease in wave period throughout the northwestern Pacific. The increase in wave period in the eastern Pacific is projected to occur throughout the year.
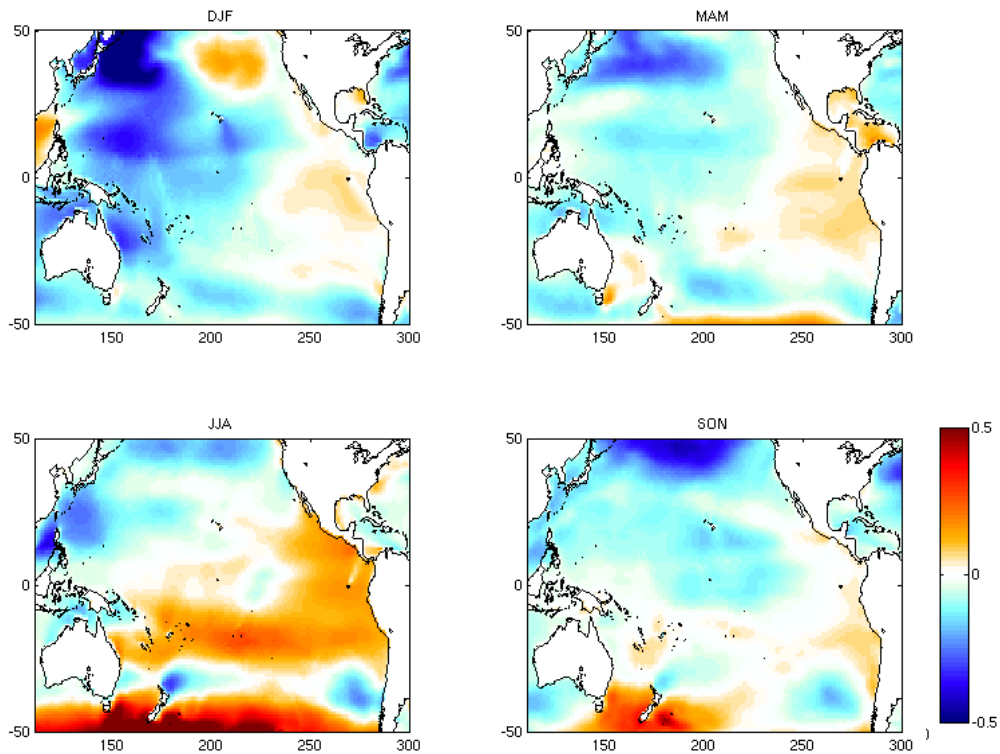
Figure 6.22: Change in mean significant wave height (m) 2070-2099 minus 1979-2009 period for 2-member CCAM forced ensemble.
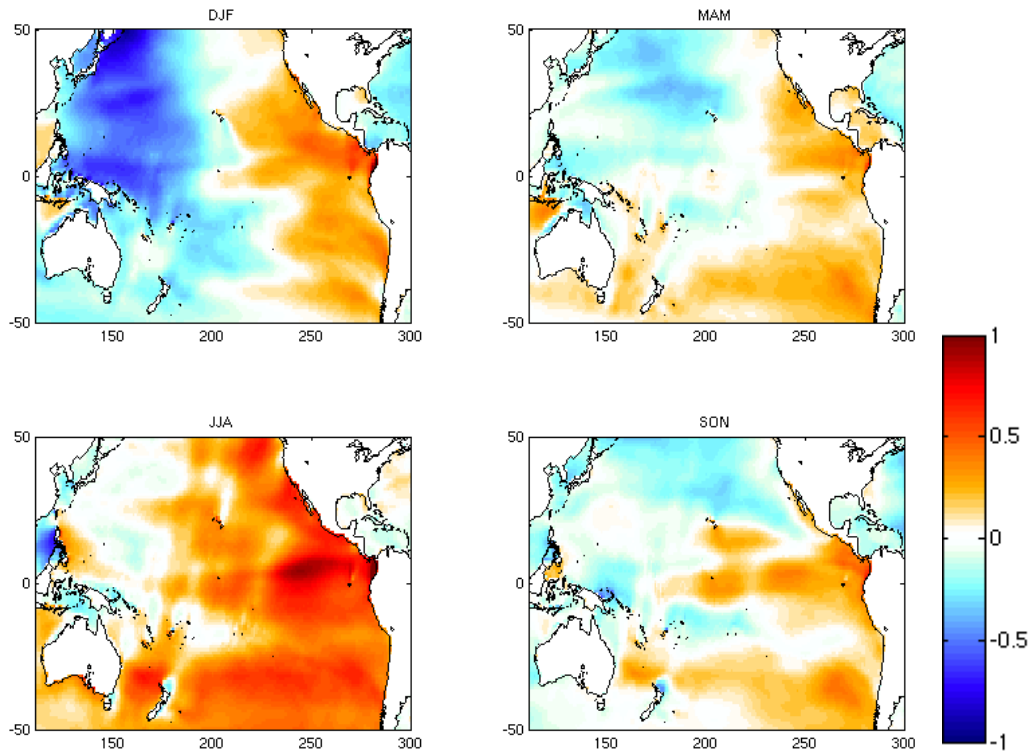

Figure 6.23: Change in mean wave period (s) 2070-2099 minus 1979-2009 period for 2-member CCAM forced ensemble.
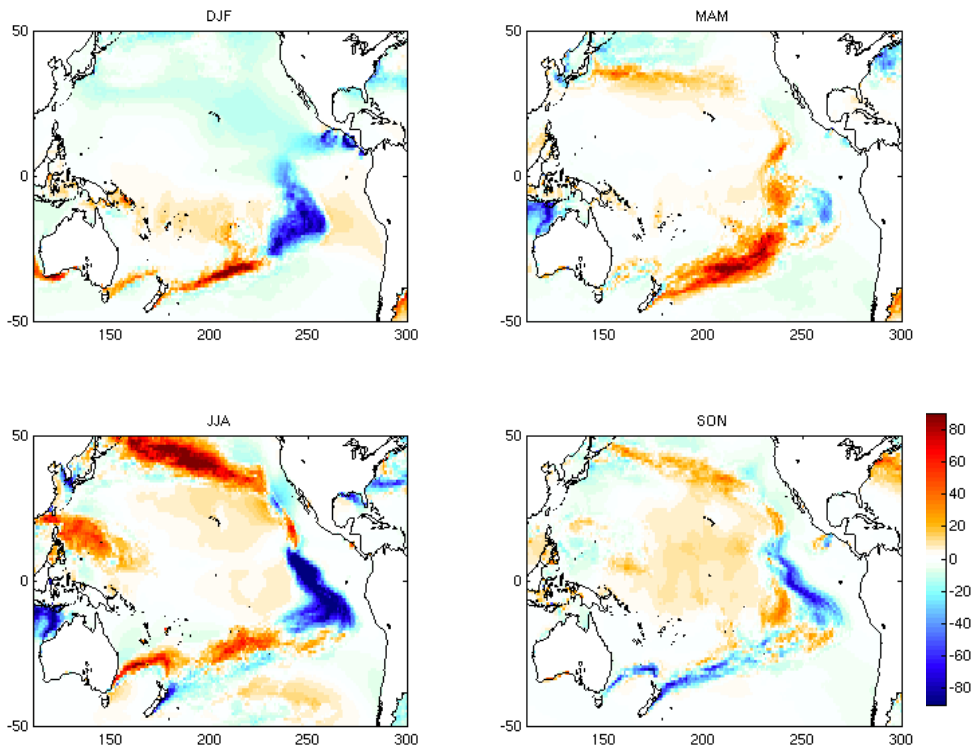
Figure 6.24: Change in mean wave direction (°) 2070-2099 minus 1979-2009 period for 2-member CCAM forced ensemble.

Site Records

We have determined wave roses from the 30-yr projected time-slice for the same 5 sites as presented in previous sections of the report, to assess projected changes in wave climate between the 1979-2009 wave roses (CCAM runs in Figures B11-15). The projected changes in wave conditions at these locations is slight. In summary, there is a tendency for projected wave climate to have smaller waves from all directions than the present wave climate. In those locations where southerly swell are observed (South and South-west Pacific), an increased number of large Southern ocean swell waves are projected to occur, but with no increase in mean wave height. Where south-easterly trade generated waves are observed, projected wave climate shows a slight decrease in wave heights. Northerly swell is also projected to decrease at all sites where observed. The magnitude of projected change at these locations is of similar magnitude to the amplitude of current inter-annual variations.
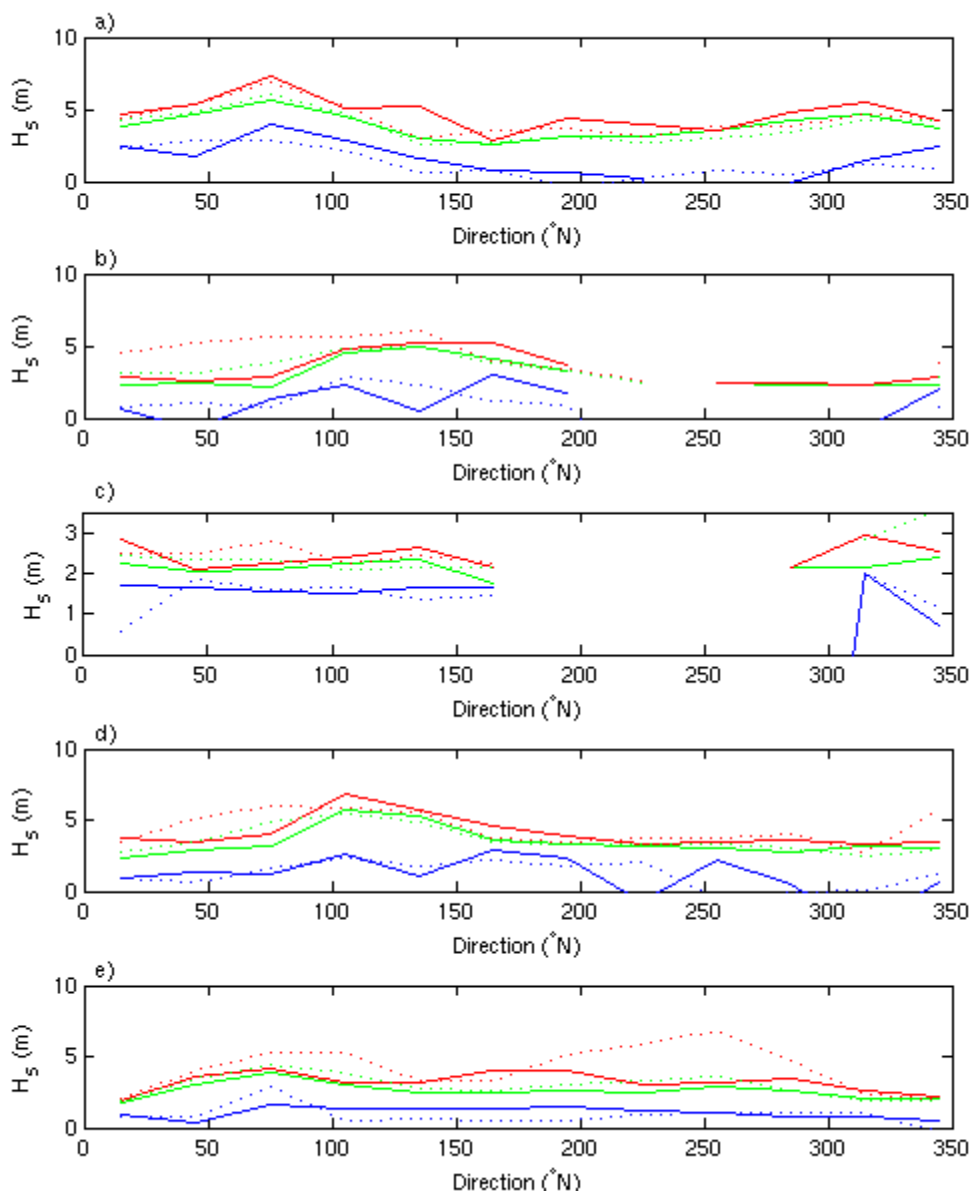
Figure 6.25: Projected 2070-2099 return period significant wave heights by direction for 5 sites, from the un-adjusted CCAM derived 2-member ensemble wave field. a) Hawaii; b) South Pacific (Vanuatu-Fiji); c) Equatorial Pacific (Kiribati-Tuvalu); d) South Pacific (French Polynesia); e) Western North Pacific (Guam- Micronesia). The blue line represents the annual return significant wave height for each directional segment, the green line is the 10-yr return value, and the red line is the 100-yr return value. Dotted lines show respective values from 1979-2009 CCAM time-slice.

6.4.2   Bias-adjusted CCAM forced runs

Figure 6.26 shows projected differences between 30-yr mean significant wave heights from current period (1979-2009) to future period (2070-2099) when the wave model is forced with bias-adjusted CCAM winds. Corresponding figures for mean wave period and mean wave direction are shown in Figures 6.27 and 6.28 respectively. Despite the reported variation in modelled wave climate based on un-adjusted or bias-adjusted CCAM wind forcing, the broad

qualitative structure of projected changes in wave climate are consistent between both run-sets, that is regions with positive (negative) change correspond between datasets. Regions with absolute change greater than 5% (correspondingly positive or negative) in both datasets include: most of the western Pacific during the boreal winter; the Pacific sector of the Southern Ocean and the equatorial south Pacific during austral autumn and winter months; the tropical north-west Pacific and northern extratropics during boreal spring and summer. These small projected changes in wave conditions in the region of PICTs over the 21st Century are qualitatively consistent with prior statistical (Wang and Swail, 2006) and dynamical (Mori et al., 2010) projection studies. All studies tend to project decreases in the western Pacific, and increases in the eastern Pacific, with increases in the Southern Ocean being a dominant feature driving the eastern Pacific increase (through swell propagation).

Significant changes in wave period are projected for large portions of the Pacific, which are robust across both runs. These include increased wave period across most of the eastern Pacific during austral summer, autumn and winter seasons, and decreased wave period in the western Pacific during the boreal winter and spring. While features are broadly consistent when looking at projected changes in wave direction, we observe an eastward shift in position when forced with bias-adjusted winds. Significant changes in wave direction of up to 10-20° rotation in mean wave direction are projected in the Solomon Island region during the austral spring and summer months, which could be expected to lead to a morphological island response.
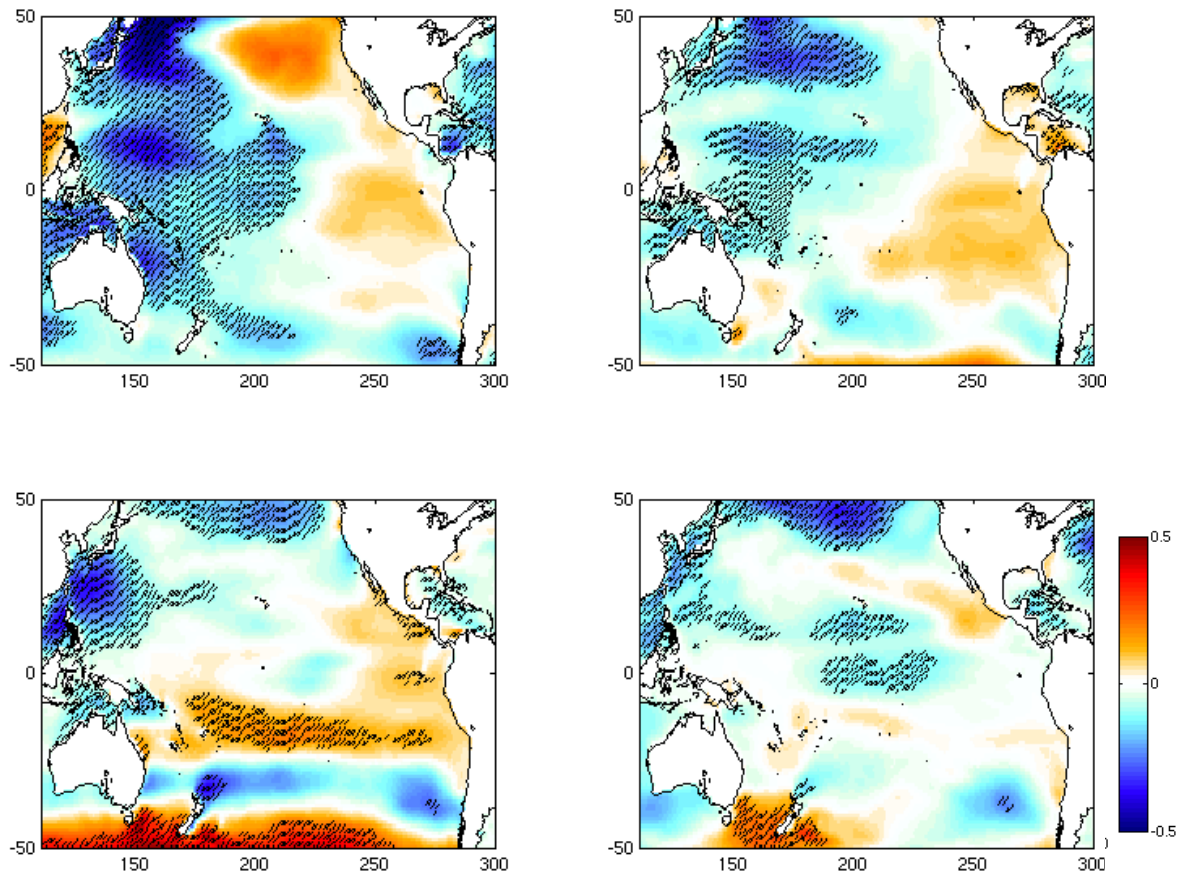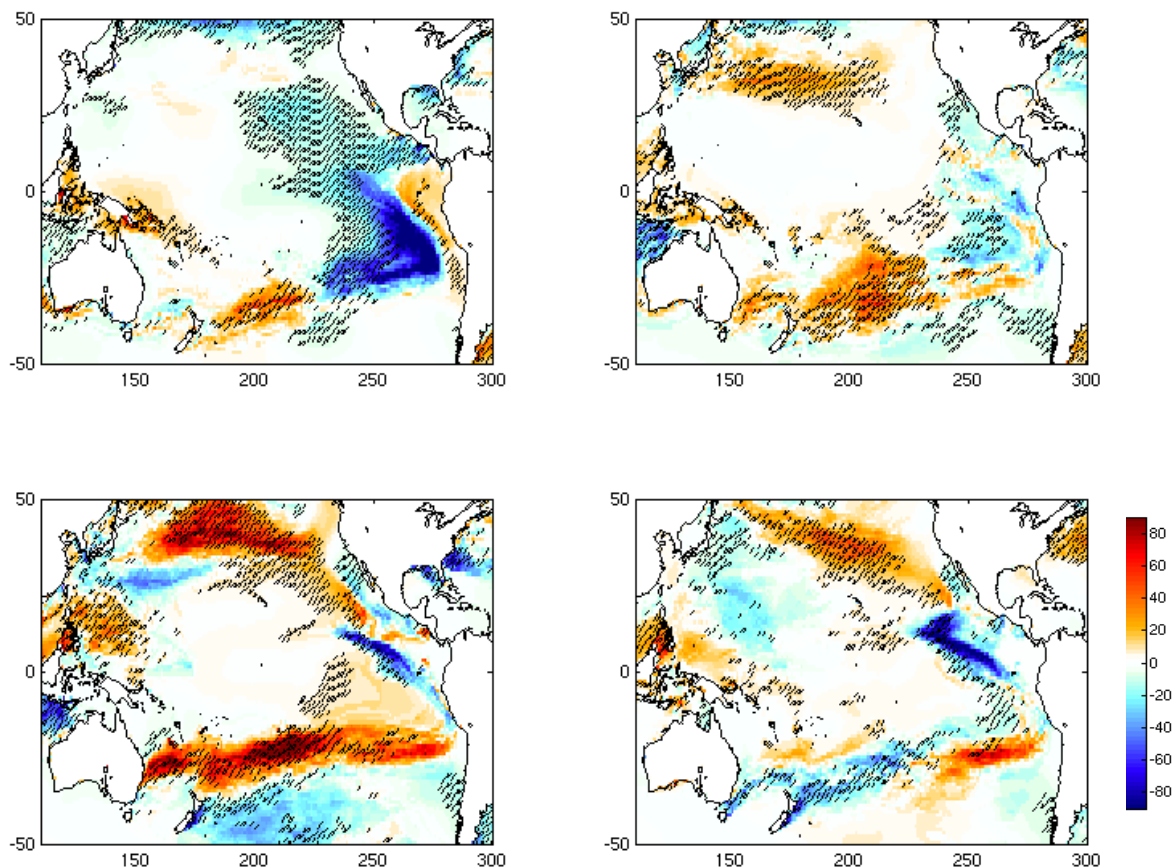
Figure 6.26: Change in mean significant wave height (m) 2070-2099 minus 1979-2009 period for 2-member BACCAM forced ensemble. Hashed areas indicate regions where change is consistently greater than 5% in both un-adjusted and bias-adjusted runsets.
DJF: top-left; MAM: top-right; JJA: bottom-left; SON: bottom-right.
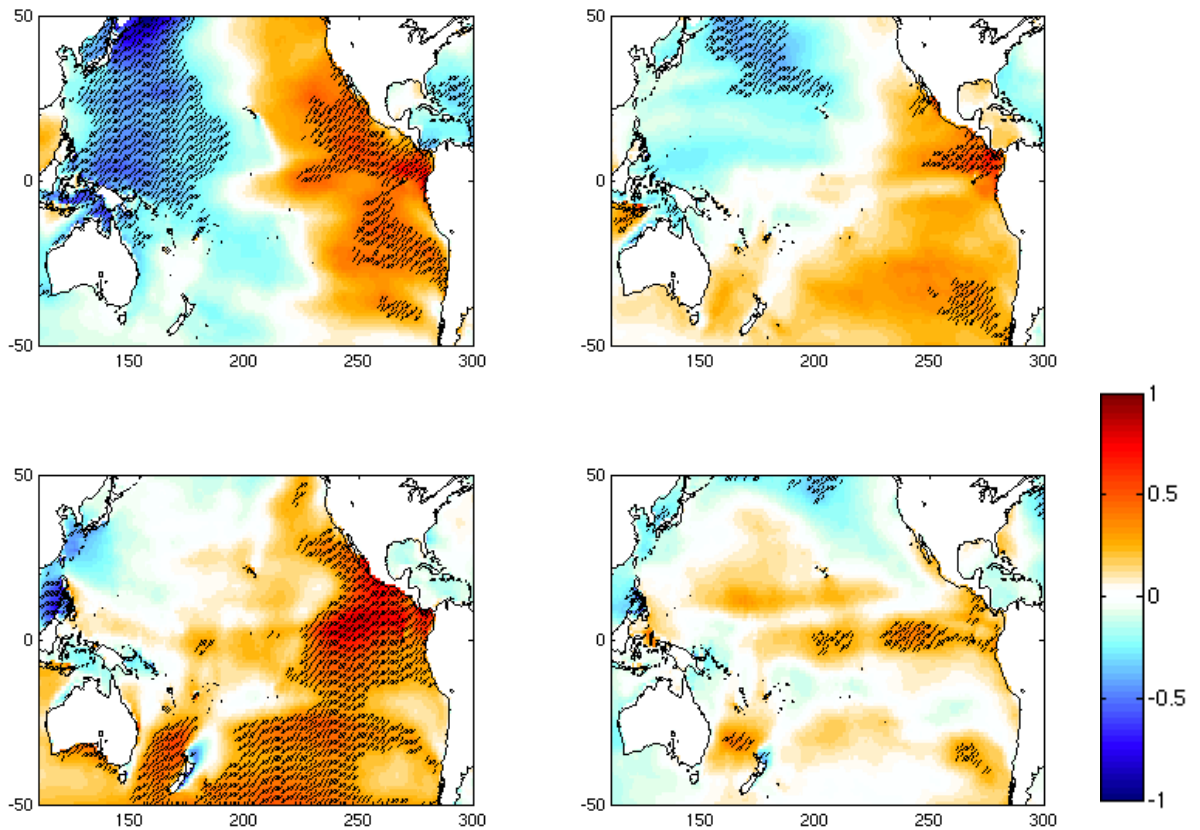
Figure 6.27: Change in mean wave period (s) 2070-2099 minus 1979-2009 period for 2-member BA-CCAM forced ensemble. Hashed areas indicate regions where change is Consistently greater than 0.25 s in both un-adjusted and bias-adjusted runsets. DJF: top-left; MAM: top-right; JJA: bottom-left; SON: bottom-right.

Significant changes in wave direction are also projected during the austral autumn and winter seasons at the southern and eastern most PICTs.

Figure 6.28: Change in mean wave direction (°) 2070-2099 minus 1979-2009 period for 2-member BACCAM forced ensemble. Hashed areas indicate regions where change is consistently greater Than 5° in both un-adjusted and bias-adjusted runsets.
DJF: top-left; MAM: top-right; JJA: bottom-left; SON: bottom-right.

Site records

Figures B16-20 display projected 2070-2099 wave-roses at the 5 sites previously outlined. Relative to the 1979-2009 wave-roses, we observe projected changes are relatively small (within range of inter-annual variability) and consistent with those observed from the un-adjusted CCAM forced runset. Figures 6.30 and 6.31 show annual mean wave roses at each site, for un-adjusted and bias-adjusted run-sets respectively. These display the small changes in annual mean wave climate projected at each site in each run set.

Figure 6.29: Projected 2070-2099 return period significant wave heights by direction for 5 sites, from the BACCAM derived 2-member ensemble wave field. a) Hawaii; b) South Pacific (Vanuatu-Fiji); c) Equatorial Pacific (Kiribati-Tuvalu); d) South Pacific (Fre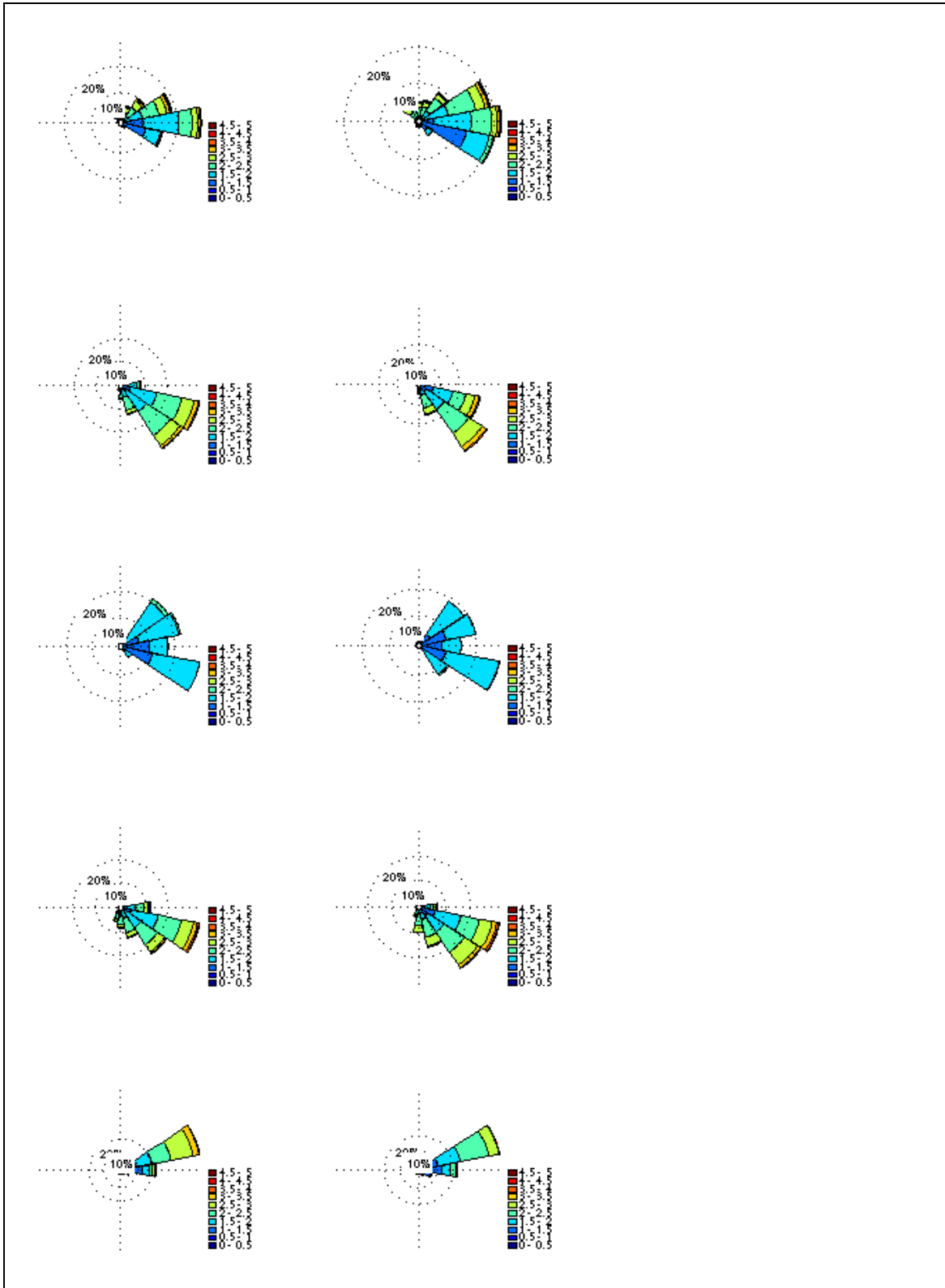nch Polynesia); e) Western North Pacific (Guam- Micronesia). The blue line represents the annual return significant wave height for each directional segment, the green line is the 10-yr return value, and the red line is the 100-yr return value. Dotted lines show respective values from 1979-2009 time-slice.
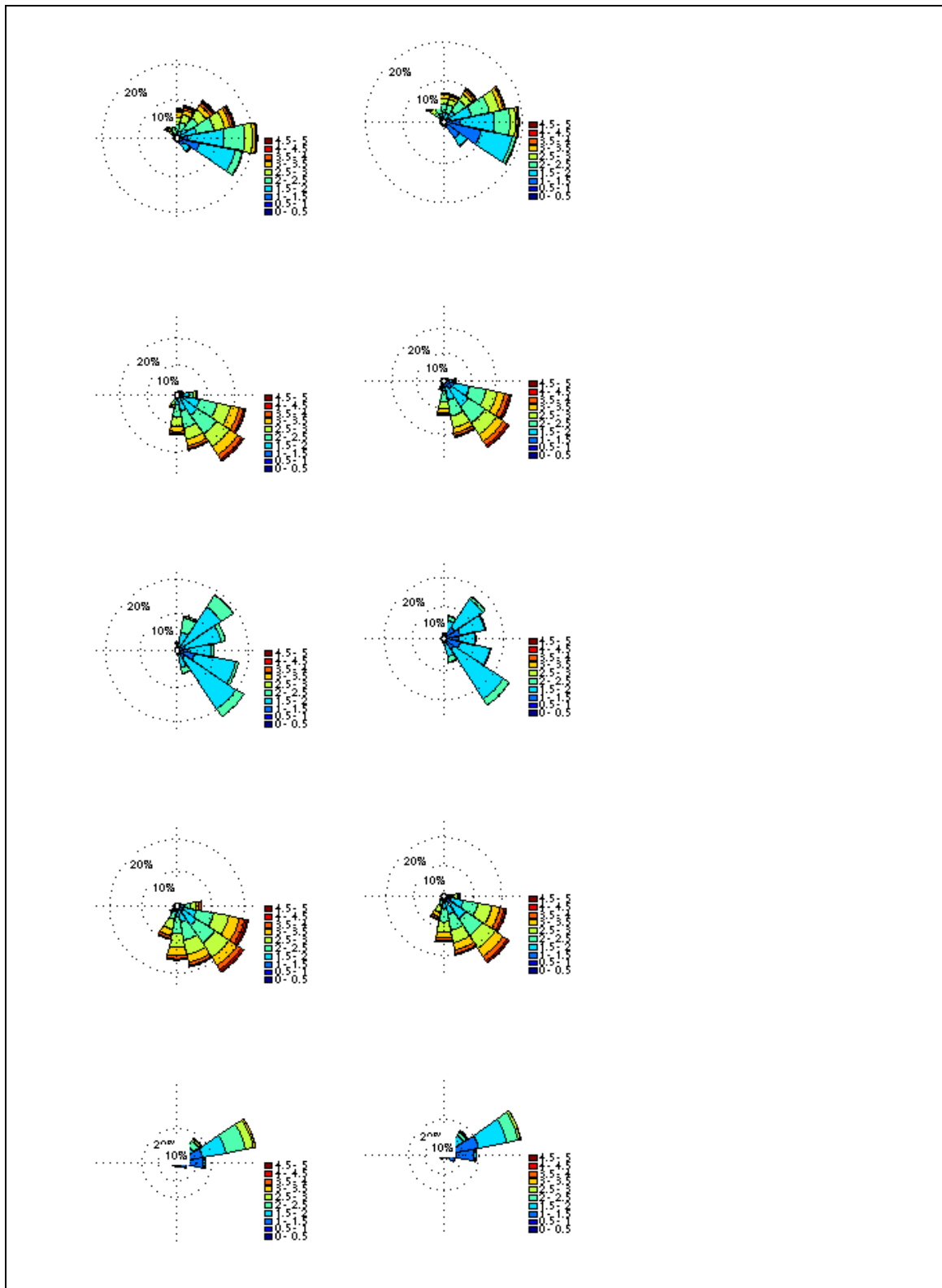
Figure 6.30. CCAM forced changes in annual wave-roses. Left Column, 1979-2009 time-slice, right column, 2070-2099 time-slice. Row 1) Hawaii; Row 2) South Pacific (Vanuatu-Fiji); Row 3) Equatorial Pacific (Kiribati-Tuvalu); Row 4) South Pacific (French Polynesia); Row 5) Western North Pacific (Guam- Micronesia).

Figure 6.31. BA-CCAM forced changes in annual wave-roses. Left Column, 1979-2009 time-slice, right column, 2070-2099 time-slice. Row 1) Hawaii; Row 2) South Pacific (Vanuatu-Fiji); Row 3) Equatorial Pacific (Kiribati-Tuvalu); Row 4) South Pacific (French Polynesia); Row 5) Western North Pacific (Guam- Micronesia).

7.   RECOMMENDATIONS

The in situ observational wave record in the region of PICTs is limited to a relatively short term, study in the late 1980s and early 1990s. These data provide valuable understanding of seasonal variability of wave properties in the region, however have limited application for understanding climatological variability in wave climate. A long-term wave observation programme would provide information for ongoing coastal hazard assessments aiming to understand island shoreline response to climatological variability and change. Considerable capability in wave measurements was developed in the region during the previous study. Whether this capability remains in the region is unknown, however building on this prior program and the archived datasets would be invaluable. This would involve ongoing operation of wave measuring buoys (or other wave measuring devices – e.g., HF radar), similar to the Australian Government Agency for International Development (AusAID) South Pacific Sea Level Monitoring Program, hosted by the Australian Government Bureau of Meteorology, at locations of previous deployments.

Available wave model products archive only select integrated wave parameters (significant wave height, mean wave period and mean wave direction). These archives are insufficient to describe the multi-modal characteristics of the Pacific wave climate. We propose a high-quality multi-decadal hindcast be carried out, which represents the Pacific wave climate, and archives high temporal resolution (e.g., hourly) characteristics of multiple sea states (height, period and direction of local wind sea, and primary and secondary modes of swell), and spectral data at appropriate locations.

The proposed hindcast must span all of the Pacific Ocean (ultimately global), and computing and storage limitations restrict this hindcast to relatively coarse resolution (~0.5-1°). For the PICT region, nested high resolution wave models should be applied to provide high spatial resolution information in coastal and nearshore regions to support coastal hazard assessments.

Regional capability to carry out high resolution, national or island scale wave studies should be developed. The proposed hindcast should aim to provide boundary conditions for these nested studies, which may be used by regional organisations to develop in-house modelling capability. Collaboration with SOPAC-SPC is underway to support this recommendation.

When forced directly with climate model winds, the wave climate in some regions is not well represented by the wave model. This leads to low confidence in the projected changes in wave climate. To overcome deficiencies in the climate model winds, adjustment of climate and variability bias of the surface winds is made, following the method outlined by Hemer et al. (2011a). When forced with bias adjusted climate model winds, minor improvement in the representation of the mean wave climate is achieved, but representation of the extreme wave climate decreases in performance. Mean wave field projections are predominantly consistent between the two run-sets (model forced with un-adjusted winds, and model forced with bias-adjusted winds). This result indicates a robust response of the projected wave field, despite bias-adjustment of forcing wind fields for these given climate model fields. Projected changes between current wave climate conditions and the future 2070-2099 time-slice are relatively small. Projected changes for mid-century (2030-2050) time-slice in the region of PICTs will be small, and within the range of current inter-annual variability (and current model error). The usefulness of wave climate models to help improve understanding of the past and the future, is

currently limited by the model skill. The skill of the next generation of climate models to reproduce wave climate variability must be assessed, in addition to ongoing development of improved wind bias adjustment schemes to support wave climate projection studies. Ultimately, climate model improvement to provide robust surface wind fields is required to support wave projection, and consequent coastal impacts of climate change studies.

A range of wave climate projections is observed within the four-member ensemble. Although this ensemble is too small to adequately quantify the range of values within the projected conditions, it does suggest large uncertainty exists within the wave climate projections once multiple levels of uncertainty are considered. Sources of uncertainty include emission scenarios (un-tested in this study), model uncertainty (different global climate model forcing which is tested here), downscaling approaches (here a single regional climate model is used) and wave modelling approaches (a dynamical approach is taken for this study – a statistical approach may further increase uncertainty). The sources of uncertainty must be understood when projecting climate variables. However, with respect to wave climate projections, a quantitative assessment of each of these multiple levels of uncertainty is a considerable task for a single research group. Consequently, isolated studies generating projections of wave climate should contribute to an international community ensemble of wave projections, following method outlined by Hemer et al (2010a), to allow quantification of the multiple levels of wave projection uncertainty.

REFERENCES

ABC News, 2011. Huge waves swamp Fiji hotel rooms. http://abcaustralia.com/news/2011-05-20/huge-waves-swamp-fiji-hotel-rooms/2722600. [Accessed 27-July-2011].

Aucan, J., 2006. Directional Wave Climatology for the Hawaiian Islands from Buoy Data and the Influence of ENSO on Extreme Wave Events from Model Hindcast. 9th International Workshop on Wave Hindcasting and Forecasting. JCOMM Technical Report No. 34 / WMO-TD. No. 1368.

Barstow, S.F. and Haug, O., 1994a. The Wave Climate of the Cook Islands, SOPAC Tech. report no. 200.

Barstow, S.F. and Haug, O., 1994b. The Wave Climate of the Kingdom of Tonga, SOPAC Tech. report no. 201.

Barstow, S.F. and Haug, O., 1994c. The Wave Climate of Vanuatu, SOPAC Tech. report no. 202.

Barstow, S.F. and Haug, O., 1994d. The Wave Climate of Tuvalu, SOPAC Tech. report no. 203.

Barstow, S.F. and Haug, O., 1994e: The Wave Climate of Western Samoa, SOPAC Tech. report no. 204.

Barstow, S.F. and Haug, O., 1994f. The Wave Climate of Fiji, SOPAC Tech. report no. 205.

Barstow, S.F. and Haug, O., 1994g. The Wave Climate of the South Pacific, SOPAC Tech. report no. 206.

Barstow, S.F. and Falnes, J., 1996. The Wave Climate of the South Pacific, SOPAC Misc. report no. 234.

Barstow, S.P. and M. Patiale, 1992. An Appraisal of the Visual Wave Observations at Funafuti, 1984-92. SOPAC Technical Report 147.

Bidlot, J. R., S. Abdalla and P. A. E. M. Janssen, 2005: A revised formulation for ocean wave dissipation in CY25R1. Tech. Rep. Memorandum R60.9/JB/0516, Research Department, ECMWF, Reading, U. K.

Caires S, Sterl A. 2005. A new non-parametric method to correct model data: application to significant wave height from the ERA-40 reanalysis. *Journal of Atmospheric and Oceanic Technology* **22**(4): 443–459.

Graber, H.C., V.J. Cardone, R.E. Jensen, D.N. Slinn,S.C. Hagen, A.T. Cox, M.D. Powell, and C. Grassl. 2006. Coastal forecasts and storm surge predictions for tropical cyclones. A timely partnership program. *Oceanography* 19(1):130–141.

Grech, A., and Coles, R.G. (2010) *An ecosystem-scale predictive model of coastal seagrass distribution.* Aquatic Conservation: marine and freshwater ecosystems , 20 (4). pp. 437-444. ISSN 1099-0755

Guilyardi, E., A. Wittenberg, A. Federov, M. Collins, C. Wang, A. Capotondi, G. van Oldenborgh, and T. Stockdale, 2009. Understanding El Niño in ocean-atmosphere general circulation models: Progress and challenges. *BAMS*, 90, 325-340.

Hall, S.J., 1994. Physical Disturbance and Marine Benthic Communities: Life in Unconsolidated Sediments. Oceanography and Marine Biology: An Annual Review 32, 179–239.

Hemer, M.A., J.A. Church and J.R. Hunter (2010) Variability and trends in the wave climate of the Southern Hemisphere. *Int. J. Climatol.*, 30, 475-491. DOI: 10.1002/joc.1900

Hemer, M.A., X.L. Wang, J.A. Church and V.R. Swail (2010a) Coordinated global ocean wave projections. *Bull. Amer. Meteor. Soc.*, 91(4), 451-454. DOI: 10.1175/2009BAMS2951.1

Hemer, M.A., K.L. McInnes and R. Ranasinghe (2011a) Climate and variability bias adjustment of climate model derived winds for an east Australian dynamical wave model. *Ocean Dynamics*

Hemer, M.A., K.L. McInnes and R. Ranasinghe (2011b) Exploring uncertainty in regional east Australian wave climate projections. *International Journal of Climatology.*

Holthuijsen LH. 2007. *Waves in Oceanic and Coastal Waters*. Cambridge University Press: Cambridge, 387.KOMAR, P.D. (1971) The mechanics of sand transport on beaches. *J. Geophys. Res.,* 76, 713-721.

Katzfey, J.J., J. McGregor, K. Nguyen and M. Thatcher, 2009. Dynamical downscaling techniques: Impacts on regional climate change signals. *Proceedings of the 18th World IMACS / MODSIM Congress, Cairns, Australia 13017 July 2009*. 3942-3947.

Komen, G.J., Cavaleri, L., Donelan, M., Hasselmann, K., Hasselmann, S. and Janssen, P.A.E.M. 1994. *Dynamics and modelling of ocean waves.* Cambridge University Press, Cambridge, UK, 532 pp.

Kruger, J.C., 2009. Preliminary analysis of the 10 December 2008 extreme wave event for Takuu atoll, PNG, using ECMWF ERA-interim data, kindly provided by ECMWF in collaboration with WMO, and other public access remote sensing data. SOPAC. Pers Comm.

Lowe, Ryan J., James L. Falter, Stephen G. Monismith, Marlin J. Atkinson, 2009: Wave-Driven Circulation of a Coastal Reef–Lagoon System. *J. Phys. Oceanogr.*, **39**, 873–893. doi: 10.1175/2008JPO3958.1

Luo, J.-J. *et al*. Interaction between El Niño and Extreme Indian Ocean Dipole. J. Clim. doi:10.1175/2009JCLI3104.1 (2010).

REFERENCES

Marra, J.J., E. Shea, U. Kari and E. Wong, 2008. Pacific Region Integrated Climatology information products. *Proceedings of the International Conference on Southern Hemisphere Meteorology and Oceanography.* NOAA:
http://www.pacificstormsclimatology.org/index.php?page=events-wnp

McGehee, D.D. and S. Boc. 1997. Results of Monitoring Study of Agat Harbor, Guam. US Army Corps of Engineers, TR CHL-97-22. 165p.

McGregor, J. L., and Dix, M. R., 2008. An updated description of the conformal-cubic atmospheric model. High Resolution Simulation of the Atmosphere and Ocean, Hamilton, K. and Ohfuchi, W., Eds., Springer, 51-76

Meehl, G.A., C. Covey, T. Delworth, M. Latif, B. McAvaney, J.F.B. Mitchell, R.J. Stouffer, and K.E. Taylor, 2007. The WCRP CMIP3 Multimodel Dataset: A New Era in Climate Change Research. *Bull. Amer. Meteor. Soc.*, 88, 1383-1394.

Mori, N., T. Yasuda, H. Mase, T. Tom and Y. Oku, 2010. Projection of extreme wave climate change under the global warming, *Hydrological Research Letters* Vol.4, pp.15-19. (doi:10.3178/hrl.4.15)

Nicholls, RJ, Wong PP, Burkett VR, Codignotto JO, Hay JE, McLean RF, Ragoonaden S and Woodroffe CD, 2007. Coastal systems and low-lying areas. Climate Change 2007: Impacts, Adaptation and Vulnerability. Contribution of Working Group II to the Fourth Assessment Report of the Intergovernmental Panel on Climate Change, M.L. Parry, O.F. Canziani, J.P. Palutikof, P.J. van der Linden and C.E. Hanson, Eds., Cambridge University Press, Cambridge, UK, 315-356.

NOAA CPC, 2011. NOAA Climate Prediction Centre. Available at:
http://www.cpc.ncep.noaa.gov/products/precip/CWlink/daily_ao_index/teleconnections.shtml
[Accessed: 27-July-2011].

Rooney, J.and Fletcher, C.H., 2005. Shoreline Change and Pacific Climatic Oscillations in Kihei, Maui, Hawai'i. Journal of Coastal Research, 21(3), 535-547.

Sasaki, W., S.I. Iwasaki, T. Matsuura ad S. Iizuka, 2005. Recent increase in summertime extreme wave heights in the western North Pacific. *Geophysical Research Letters,* 32, L15607, doi: 10.1029/2005GL023722.

Slott, J.M., A.B. Murray, A.D. Ashton and T.J. Cowley, 2006. Coastline responses to changing storm patterns. *Geophysical Research Letters*, 33, L18404, doi: L10.1029/2006GL027445.

Snodgrass, F.E., Groves, G.W., Hasselmann, K.F., Miller, G.R., Munk W.H., and Powers, W.H., 1966. Propagation of Ocean Swell across the Pacific. *Philosophical Transactions of the Royal Society of London. Series A, Mathematical and Physical Sciences*, 259(1103) (May 5,), pp. 431-497.

Sterl A, Caires S. 2005. Climatology, variability and extrema of ocean waves: the web-based KNMI/ERA-40 wave atlas. *International Journal of Climatology* **25**(7): 963–977.

Storlazzi, C.D., M.E. Fieldm J.D. Dykes, P.L. Jokiel E. Brown, 2001. Wave control on reef morphology and coral distribution: Molokai, Hawaii. 2001 Waves workshop. Available at: http://walrus.wr.usgs.gov/staff/cstorlazzi/WaveReefs_WAVES2001.pdf

Tolman, 2009: User manual and system documentation of WAVEWATCH III™ version 3.14. NOAA / NWS / NCEP / MMAB Technical Note **276**, 194 pp + Appendices

Uppala, S.M., Kallberg, P.W., Simmons, A.J., Andrae, U.; Costa Bechtold, V. da, Fiorino, M., Gibson, J.K., Haseler, J., Hernandez, A., Kelly, G.A., Li, X., Onogi, K., Saarinen, S., Sokka, N., Allan, R.P., Andersson, E., Arpe, K., Balmaseda, M.A., Beljaars, A.C.M., Berg, L. van d., Bidlot, J., Bormann, N., Caires, S., Chevallier, F., Dethof, A., Dragosavac, M., Fisher, M., Fuentes, M., Hagemann, S., Holm, E.; Hoskins, B.J., Isaksen, L., Janssen, P.A.E.M., Jenne, R., McNally, A.P., Mahfouf, J-F., Morcrette, J-J., Rayner, N.A., Saunders, R.W., Simon, P., Sterl, A.; Trenberth, K.E., Untch, A., Vasiljevic, D., Viterbo, P. Woollen, J., 2005. The ERA-40 re-analysis. In: Quarterly Journal of the Royal Meteorological Society 131, 2961-3012. http://dx.doi.org/10.1256/qj.04.176

Vitousek, S.and Fletcher, C.H., 2008. Maximum annually recurring wave heights in Hawaii. *Pacific Science,* 62 (4), 541-553.

Wang, X.L., and V.R. Swail, 2006. Climate change signal and uncertainty in projections of ocean wave heights. *Clim. Dyn*., 26, 109–126.

Young, I.R., Zieger, S. And Babanin, A.V., 2011, Global trends in wind speed and wave height, Science, 332, 451-455, doi:10.1126/science.1197219

Zieger, S., Vinoth, J. and Young, I.R., 2009, Joint calibration of multi-platform altimeter measurements of wind speed and wave height over the past 20 years, J. Atmos. & Ocean. Tech., 26, 12, 2549-2564, doi: 10.1175/2009JTECHA1303.1.

ACKNOWLEDGEMENTS

APPENDIX A – VERIFICATION OF ERA-INTERIM WAVE FIELD

Two observational datasets are available to the study: The buoy dataset, which is limited in space and time; and the altimeter dataset, which is limited in providing monthly statistics of significant wave height only. These datasets are supplemented by the ERA-Interim reanalysis dataset, which includes a more complete range of wave variables (Hs, Tz and Dm), and are uniform in both space (global at 1.5° resolution) and time (6-hourly from 1989 to 2009). The reanalysis is a model product however, and hence some validation of these data in their representation of the Pacific regional wave climate is required.

A.1 Assessment of ERA-Interim against buoy data

Twelve buoys were selected across the Pacific region to assess the performance of ERA-Interim data. These buoys are detailed in Table A1. The focus of this study is on monthly statistics (hsm – monthly mean significant wave height; tzm – monthly mean wave period; dmm - mean wave direction; $hsm90$ - Monthly 90th percentile of significant wave height; $tzm90$ – monthly mean wave period of waves larger than $hsm90$; $dmm90$ – monthly mean wave direction of waves larger than hsm90; $hsm99$ - Monthly 99th percentile of significant wave height; $tzm99$ – monthly mean wave period of waves larger than hsm99; $dmm99$ – monthly mean wave direction of waves larger than $hsm99$). These statistics are determined from buoy data and ERA-interim data, for co-aligned periods. These monthly statistics from the combined buoy records (all 12 buoys for Hs, 6 buoys for Tz and 4 buoys for direction) were then compared with the ERA-interim data. Table A2 summarises comparisons for monthly Hs, Tm and Dm statistics. Of interest also is the monthly anomalies, after the seasonal cycle has been removed for each of these variables. Table A3 summarises comparisons of monthly Hs, Tm and Dm statistics, after the mean annual cycle has been removed. To derive these values, the buoy derived mean annual cycle is removed from the monthly buoy data, and similarly for the reanalysis data.

Comparing the monthly mean buoy and ERA-Interim data identifies several issues. Wave heights compare well across all buoy sites. ERA-interim data underestimates monthly mean wave heights slightly (slope 0.847), and the root-mean-square error between buoy and reanalysis of 0.237 m. The underestimation of wave heights by the reanalysis increases with the larger percentiles. The mean bias between buoy and reanalysis Hsm99 is 0.411 m, and the Root-Mean-Square-Error (RMSE) is 0.78 m. The higher percentiles also indicate greater scatter, with scatter index values (RMSE normalised by the mean wave height) of 0.1 m for the monthly mean wave heights, and 0.19 m for the 99th percentile monthly wave heights. Figure A1, displaying the mean annual cycle, indicates that this is consistent across all buoys.

Mean wave periods are overestimated by the reanalysis by approximately 2.4 s, regardless of whether mean or high percentiles are considered. Despite this, we see high correlation between buoy and reanalysis wave periods. Table A3 suggests that the relatively large bias is consistent in time, which indicates that considerable value remains in the reanalysis derived wave periods. Figure A2, displaying the mean annual cycle, indicates that this is consistent across all buoys.

Only limited wave direction data is available for comparison (182 months across four buoy sites – on average less than 4 years of records per buoy). In addition to the limited length of

Table A1. Details of buoys selected for validation of ERA-Interim records.

Buoy No.	Longitude (°E)	Latitude (°N)	Start Date	End Date	Water Depth
NDBC Buoys					
52200	144.789	13.354	Sep-2004	Dec-2009	200
51028	206.087	0.00	Oct-1997	Mar-2009	4747
51001	197.721	23.445	Feb-1981	Dec-2009	3430
51004	207.618	17.525	Nov-1984	Oct-2009	5082
46006	222.536	40.754	Apr-1977	Dec-2009	4151
46066	205.039	52.737	May-2000	Dec-2009	4541
SOPAC Buoys					
Rarotonga, Cook Islands	200.277	-21.266	May-1987	July-1992	154
Eua, Tonga	184.585	-21.8383	June-1992	Sep-1992	-
Tongatapu, Tonga	184.741	-21.2338	May-1985	July-1992	154
Funafuti, Tuvalu	179.215	-8.525	May-1990	April-1992	585
Efate, Vanuatu	168.55	-17.875	Nov-1990	Feb-1992	285
Upolu, W. Samoa	187.7692	-13.99	Sep-1989	July-1992	104

data, our analysis is hampered in that only peak wave direction is archived in the buoy records (the direction of waves with peak energy in the wave spectrum) and only mean wave period is archived in the reanalysis. While the overall mean values compare relatively well (bias of 18.34°, 15.28° and -2.3° (buoy data has larger directions, measured clockwise from due North) *Dm*, *Dmm90* and *Dmm99* respectively), the RMSE between monthly buoy and reanalysis data (for mean and high percentiles) is large. This is accompanied by large scatter between records, and low correlation. We attribute these large differences to the situation that different direction variables are being compared, and these poor comparison statistics are not a fair measure of the quality of the reanalysis derived wave directions. The observation that the overall mean values compare relatively well suggests the reanalysis reproduces wave directions at least as well as the skill of the wave model to produce wave period.

Buoys 51001, 51004, 46006 have relatively long records (approximately 28, 25 and 32 years respectively). A trend analysis, regressing the monthly values for each variable against time was carried out to determine trend in these records. The records were shortened to begin in 1989, limiting data to 20 years for each record, so that trends between buoy and reanalysis could be compared. Table A4 shows trends in monthly wave height statistics from these buoys. Red text indicates significant trend. No significant differences between buoy and reanalysis derived trends is observed. This provides confidence in the reanalysis record, that no apparent trends are observed in the dataset (like those reported by Hemer (2010) in the ERA-40 reanalysis).

Table A2. Scatter plot statistics from comparison between monthly mean buoy and ERA-interim data, combining records from all buoys. Note directional comparisons are comparing mean wave direction from the reanalysis and peak wave direction from the buoys.

Variable	n	Buoy Mean	Era Mean	RMSE	R	Slope	SI
Hsm (m)	1038	2.373	2.344	0.237	0.954	0.847	0.10
Hsm90 (m)		3.238	3.065	0.405	0.958	0.847	0.13
Hsm99 (m)		4.18	3.769	0.780	0.945	0.797	0.19
Tzm (s)	863	6.740	9.244	2.533	0.911	1.035	0.38
Tzm90 (s)		7.685	10.030	2.472	0.861	0.936	0.32
Tzm99 (s)		8.295	10.343	2.392	0.788	0.828	0.29
Dmm (°N)	182	110.30	91.96	91.45	0.386	0.285	0.68
Dm90 (°N)		140.72	125.44	89.42	0.610	0.550	0.64
Dm99 (°N)		148.10	150.40	100.2	0.535	0.530	0.83

Table A3. Scatter plot statistics from comparison between monthly mean buoy and ERA-interim data, after mean annual cycle is removed, combining records from all buoys. Note directional comparisons are comparing mean wave direction from the reanalysis and peak wave direction from the buoys. Note SI is not defined, as mean values are near to zero.

Variable	N	BIAS	RMSE	R	Slope
Hsm (m)	1038	-0.003	0.168	0.794	0.632
Hsm90 (m)		-0.005	0.275	0.788	0.847
Hsm99 (m)		-0.015	0.520	0.771	0.610
Tzm (s)	863	-0.007	0.279	0.688	0.763
Tzm90 (s)		-0.007	0.472	0.662	0.838
Tzm99 (s)		-0.007	1.001	0.658	0.752
Dmm (°N)	182	-17.1	85.15	0.335	0.252
Dm90 (°N)		1.86	99.21	0.574	0.393
Dm99 (°N)		19.5	138.93	0.240	0.219
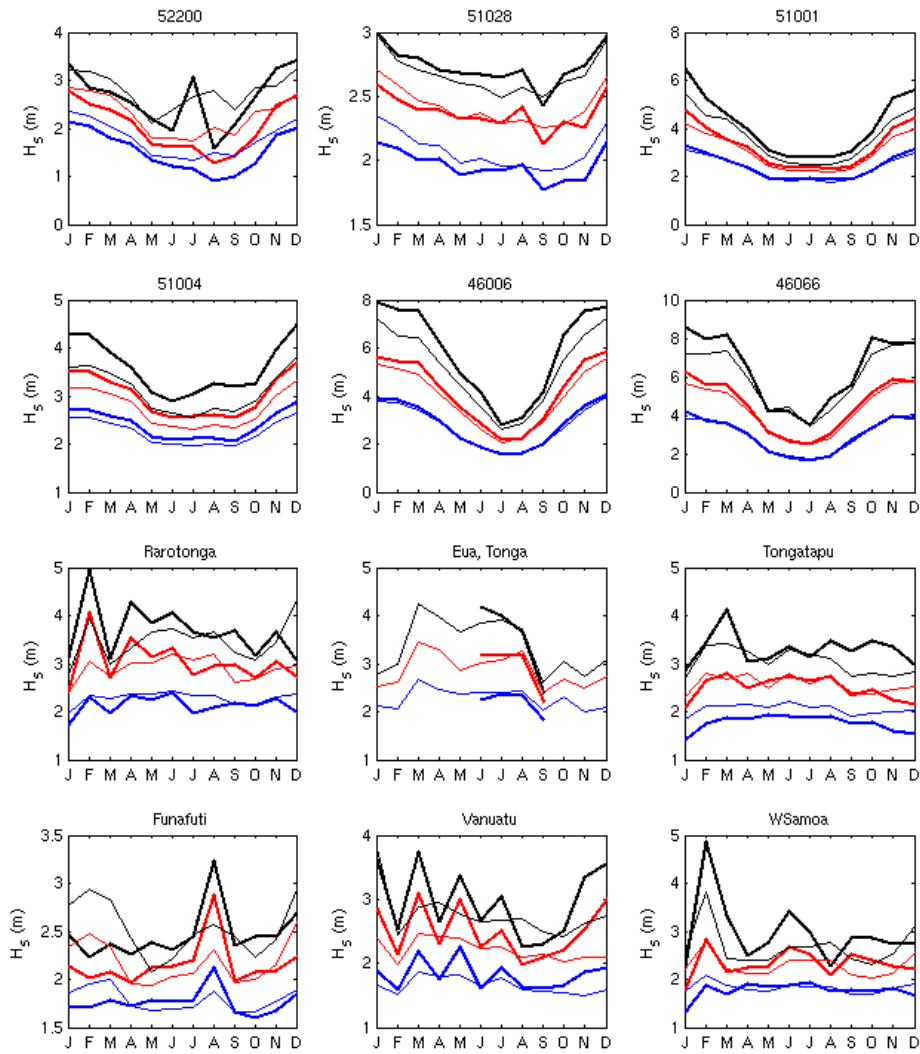
Figure A1: Comparison of ERA-Interim and Buoy mean annual cycle, for each of 12 buoys (buoy ID given in title). Thick line- Buoy record; thin line – ERA-Interim record. Blue – mean annual cycle of monthly mean Hs; red – mean annual cycle of monthly 90th percentiles of Hs; black is mean annual cycle of monthly 99th percentiles of Hs.
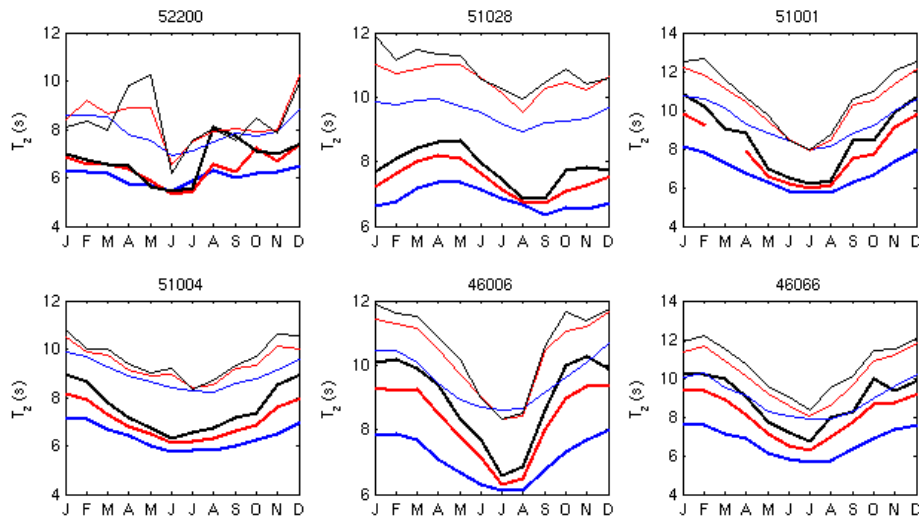
Figure A2: Comparison of ERA-Interim and Buoy mean annual cycle, for each of 12 buoys (buoy ID given in title). Thick line- Buoy record; thin line – ERA-Interim record. Blue – mean annual cycle of monthly mean Tz; red – mean annual cycle of Tz for Hs larger than *Hsm90*; black is mean annual cycle of Tz for Hs larger than *Hsm99*.

Table A4. Trends in monthly significant wave height statistics in monthly buoy and ERA-Interim statistics.

Buoy	Dataset	Mean (m/yr)	90th (m/yr)	99th (m/yr)
51001	Buoy	-0.0066 +/- 0.0059	-0.0053 +/- 0.010	-0.002 +/- 0.016
	ERA-Interim	0.0010 +/- 0.0041	0.0028 +/- 0.0072	0.0061 +/- 0.012
51004	Buoy	-0.0035 +/- 0.0052	-0.0087 +/- 0.0078	-0.018 +/- 0.013
	ERA-Interim	0.0053 +/- 0.0041	0.0056 +/- 0.0065	0.0066 +/- 0.0086
46006	Buoy	0.0084 +/- 0.0115	0.0111 +/- 0.018	0.024 +/- 0.034
	ERA-Interim	0.0071 +/- 0.0096	0.0141 +/- 0.016	0.0242 +/- 0.026

A.2 Assessment of ERA-Interim against altimeter record

ERA-Interim (EI) monthly Hs statistics (Hsm, Hsm90, Hsm99) were interpolated from the 1.5° grid on which the ERA-Interim data are available to the 2° grid on which the altimeter data are available, using a bilinear method. The monthly Hs statistics from ERA-Interim and the Altimeter dataset were compared spatially and temporally, over the period 1989-2009 (when data are available from both records). We define the Pacific Ocean basin as spanning the region 50°S to 50°N, 110°E to 300°E. We further isolate 3 further regions, the south Pacific (SPO) spanning 50°S to 20°S, the equatorial Pacific (EPO) spanning 20°S to 20°N, and the northern

Pacific (NPO) spanning 20°N to 50°N. Figure A3 shows the 21-yr (1989-2009) mean Hs from the altimeter and ERA-interim data, and the difference. Notable features of these figures are the slight underestimation of Hsm by ERA-interim over most of the Pacific basin by approximately 0.1 m, the larger underestimation of Hsm by ERA-interim in areas sheltered from the predominant westerly wave climate (e.g., eastern Australia, eastern New Zealand, Japan, and also Hawaii), and the overestimate of wave heights in swell dominated regions (e.g., the eastern equatorial Pacific). The overestimate in the eastern equatorial Pacific (and other swell dominated regions) is primarily due to the well documented lack of swell dissipation in the wave model source terms used in this model. The general underestimate of wave heights throughout the rest of the domain is most likely due to the combined influence of ERA-interim winds underestimating real wind fields, and the resolution of ERA-interim not sufficiently resolving storm centres, such that the intensity of storm systems is underestimated. Such an underestimate of the storm centres would limit the size of waves generated and able to propagate throughout the Pacific basin as swell. To assess how well storm wave systems are represented by the ERA-interim data, we also compare Hsm90 and Hsm99 between datasets (Figure A3). However this analysis suffers as the altimeter data, with low frequency repeat cycles, may also miss storm wave events. Increased underestimation of Hsm90 by ERA-interim extends over a larger region than for Hsm. The overestimation in the swell dominated eastern equatorial Pacific is also reduced. The Hsm90 tends to reflect the lack of intensity in the ERA-interim data. The Hsm99 results however, show that ERA-interim values are larger than altimeter derived values in the Southern Ocean (on the edge of the domain). The long repeat cycles of the altimeter are missing observations of peaks of the storm wave events, and hence underestimate the true storm wave values. The differences between altimeter and ERA-interim are of order 10%, indicating relative consistency in the two datasets, across all percentile levels.

The mean annual cycle of the Pacific wave climate is dominated by the seasonal storms in the extra-tropical storm belts (Figure 5.1). In the northern winter months (Dec-Mar), storms in the northern Pacific generate large storm waves with the largest waves (mean of approximately 4.5m) centred at approximately 180°E, 45°N. In the northern summer months, these large waves are not seen in the North Pacific. Large waves generated in the southern extra-tropical storm belt display greater consistency, with large waves observed in the Southern Pacific throughout the year. However, the northward extent of large waves is farthest during the northern summer months. The contour of 3-m waves shifts across a meridional range of approximately 10°, from approximately 40°S in January to approximately 30°S in June. Comparison of the mean annual cycle between datasets (Figure A4) shows that during the northern winter months (Dec-Mar), Era-Interim wave heights underestimate altimeter values (negative bias) in the northern storm belt, and overestimate (positive bias) altimeter wave heights in the equatorial Pacific south of the equator. During the northern summer months (Jun-Aug), these biases are reduced, but a negative bias is seen in the southern ocean storm belt. These characteristics are similarly observed when comparing Hsm90 between the two datasets.

Analysis of the anomalies indicates that anomalies compare well between altimeter and ERA-Interim derived values. The RMS error for mean Hs (Hsm) is 0.034 m, and 0.135 m for the storm waves (Hsm99), when determined across the full Pacific basin. Mean values of each statistic are 2.36 m and 3.97 m respectively. The variance of the anomalies is largest in the North Pacific, despite the South Pacific having the larger waves. This is consistent with the observation of constant influence of the Southern Ocean generated waves as observed in the

annual cycle. The equatorial Pacific displays the smallest variance of the three sub-regions, both absolute and relative to the mean magnitude.

In summary, ERA-Interim wave heights compare well with altimeter derived values. We see evidence that storm wave events may be underestimated by approximately 10%, however the variability (both seasonal and inter-annual) is well represented relative to the altimeter dataset. It is this variability which is most critical in determining what are the drivers of wave climate in the Pacific region. These analyses provide confidence in the wave height statistics derived from ERA-Interim. The few available buoy data provide some insight into the skill of the reanalysis to reproduce wave periods and directions, but more data are required for validation to be confident in these variables.

Finally, monthly regional mean wave heights have been determined for the full Pacific basin (110°E - 300°E, 50°S – 50°N), and three subregions: the northern Pacific (north of 20°N); the southern Pacific (south of 20°S) and the equatorial Pacific (between 20°S and 20°N). The regional mean annual cycle time-series is then removed from this time-series to obtain a time-series of anomalies after the annual cycle is removed (e.g., Figure A5 displays this for Hsm Pacific mean). Good agreement between Altimeter and ERA-interim derived anomalies is observed – Table A5 presents the root-mean-square error for each set of monthly statistics (Hsm, Hsm90 and Hsm99) across the Pacific, and the three sub-regions independently.
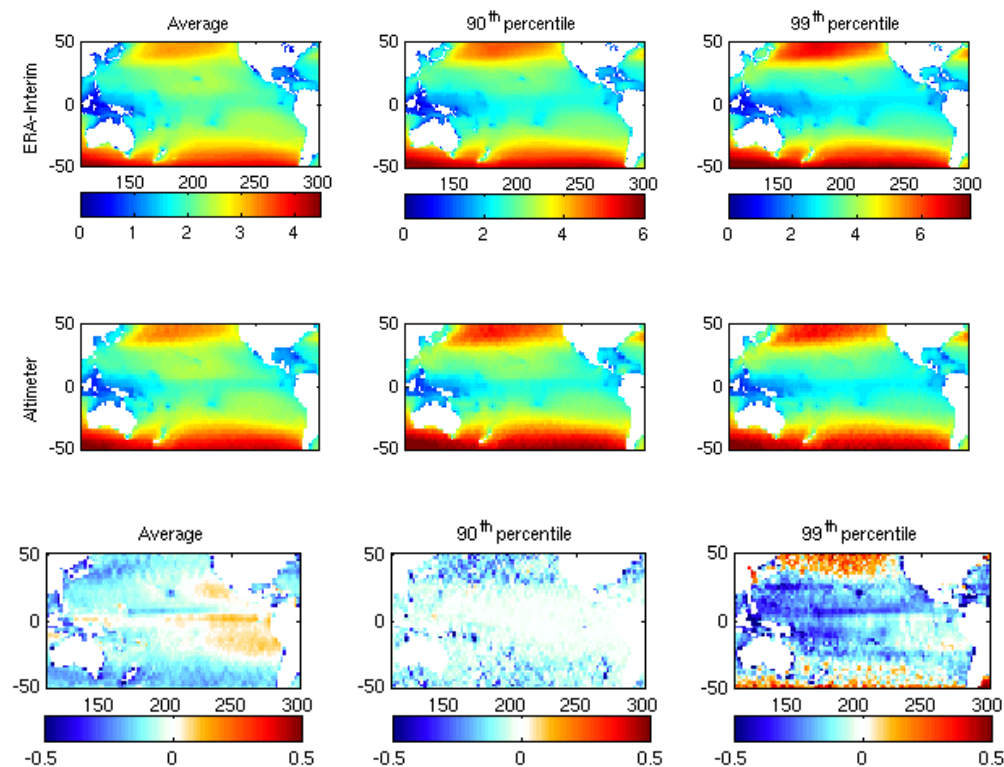
Figure A3: Top Row: Mean Hsm (left), Hsm90 (middle) and Hsm99 (right)
respectively from ERA-Interim, over period 1992-2008. Units: metres.
Middle Row: Repeated from Altimeter record, over period 1992-2008.
Bottom Row: Mean bias of Hsm (left), Hsm90 (middle) and Hsm99 (right) between
ERA-Interim and Altimeter data. Positive values indicate that ERA values are
larger than Altimeter values.
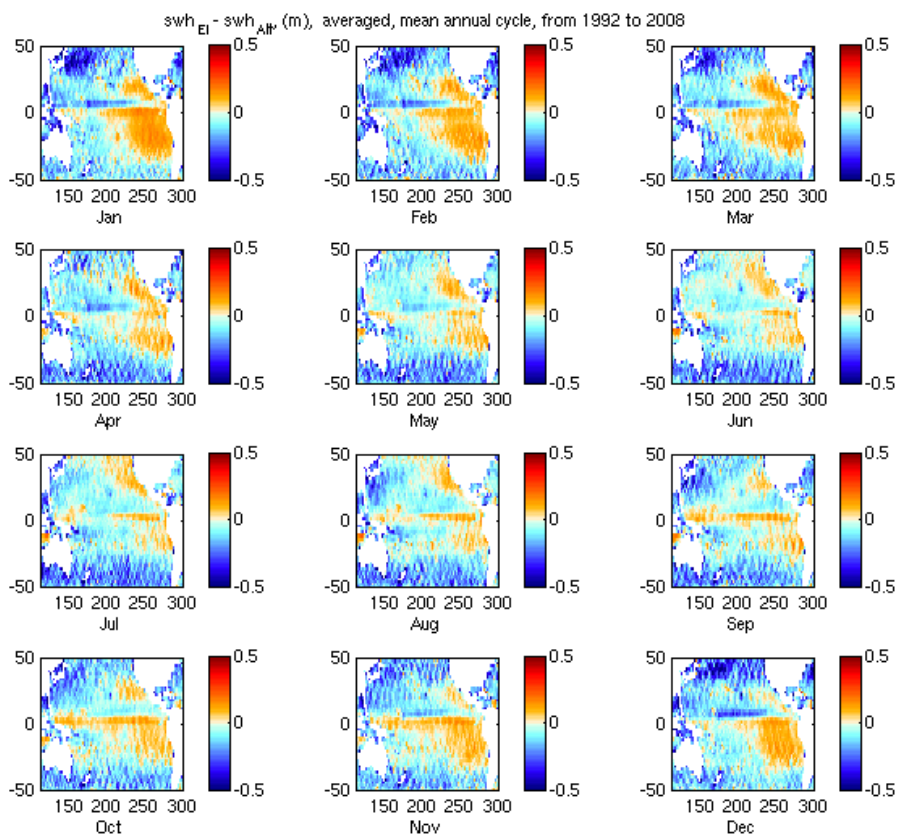
Figure A4: Bias in mean annual cycle of Hsm (m). Positive values indicate ERA-interim overestimates altimeter derived values.
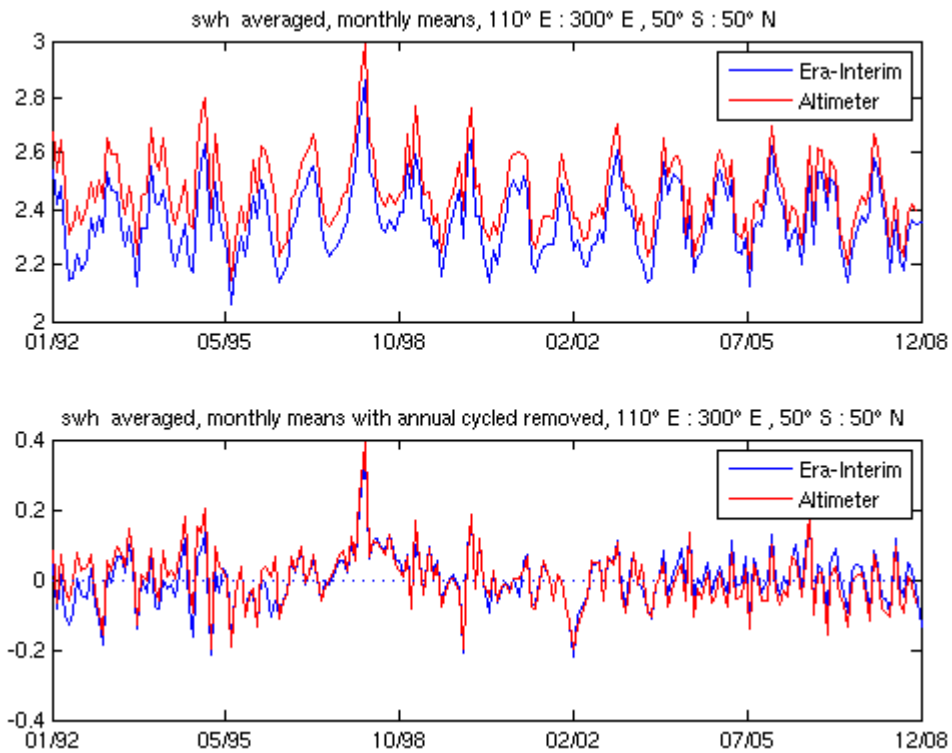
Figure A5: Top: Pacific basin regional mean Hsm time-series (metres). Bottom: Pacific basin regional mean Hsm, with mean annual cycle removed (anomaly).

Table A5. Comparison of intera-nnual variability between ERA-Interim and altimeter records. Table shows ERA-interim derived regional mean and variance of anomaly, and the root-mean-square error between the ERA-interim and Altimeter derived anomalies (regional monthly means with mean annual cycle removed).

	Statistic	Hsm	Hsm90	Hsm99
Pacific:	Mean (m)	2.360	3.155	3.969
	Variance of anomaly (m^2)	0.006	0.011	0.022
	RMS of anomaly (EI – Alt) (m)	0.034	0.057	0.135
NPacific:	Mean (m)	2.278	3.224	4.323
	Variance of anomaly (m^2)	0.014	0.035	0.085
	RMS of anomaly (EI – Alt) (m)	0.048	0.088	0.200
SPacific:	Mean (m)	3.017	4.112	5.23
	Variance of anomaly (m^2)	0.015	0.030	0.061
	RMS of anomaly (EI – Alt) (m)	0.043	0.073	0.207
EqPacific	Mean (m)	1.891	2.346	2.724
	Variance of anomaly (m^2)	0.005	0.008	0.0139
	RMS of anomaly (EI – Alt) (m)	0.032	0.049	0.079

APPENDIX B – WAVE ROSES FROM CCAM FORCED WAVE MODEL, FOR REPRESENTATIVE SITES

Un-adjusted CCAM forced runs (1979-2009).
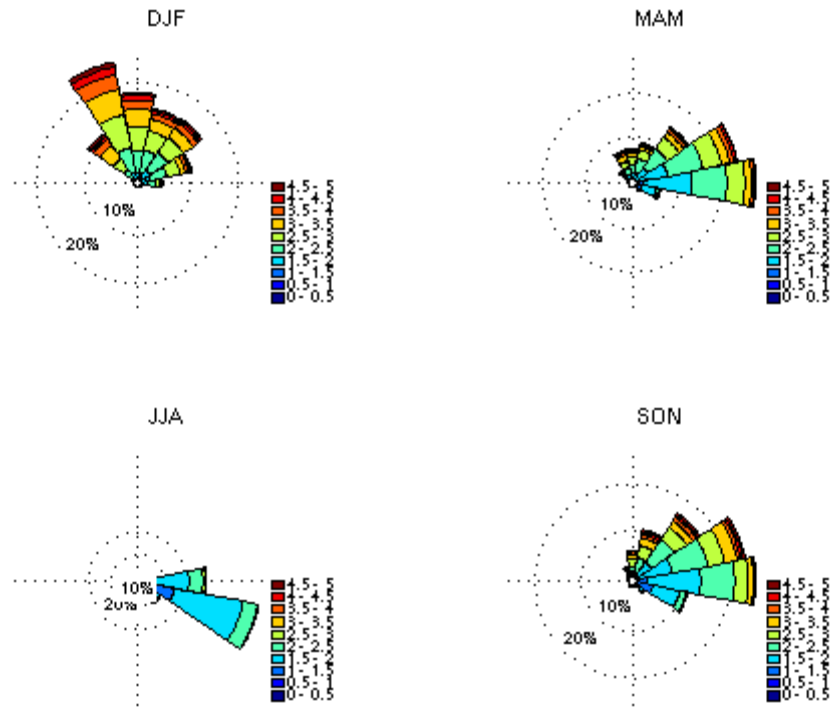
Figure B1: Wave rose for Hawaii showing significant wave height distribution by mean wave direction. Determined from 2-member ensemble of CCAM forced wave model runs.
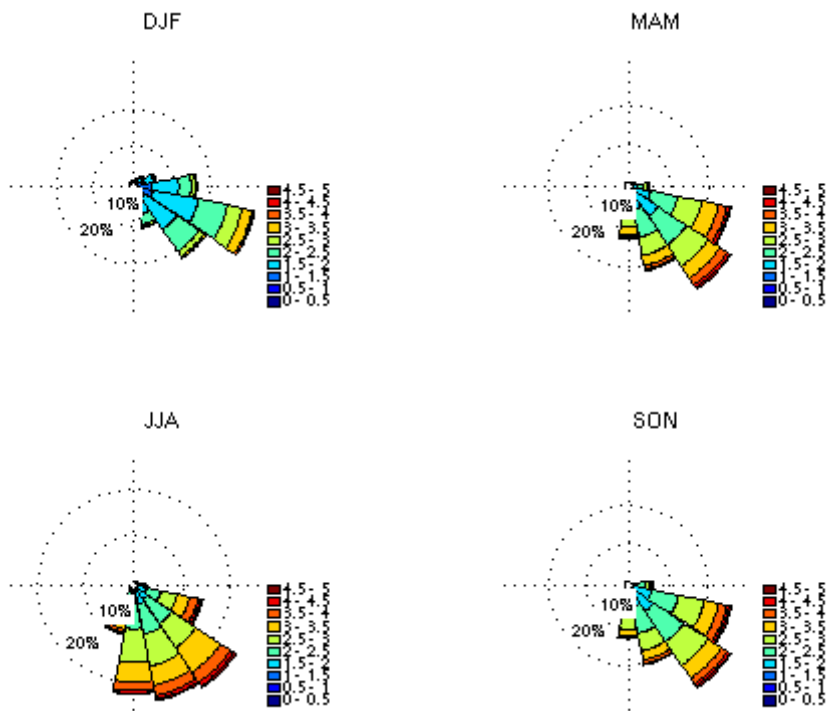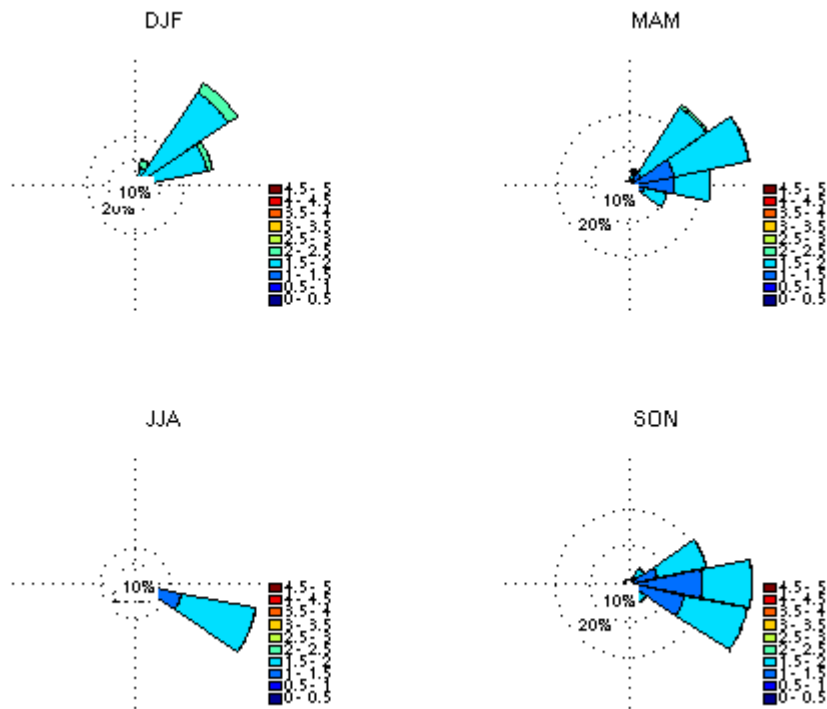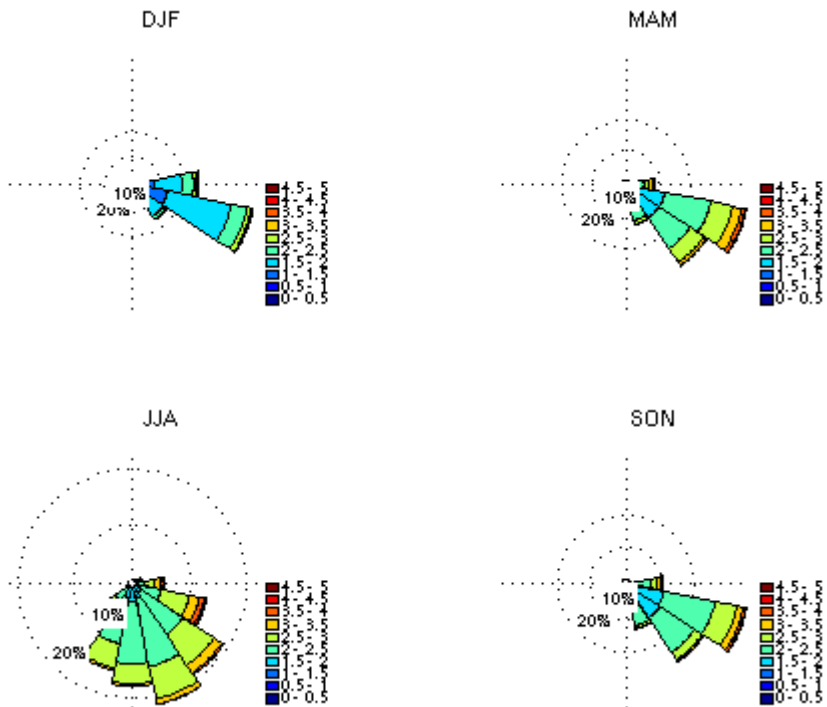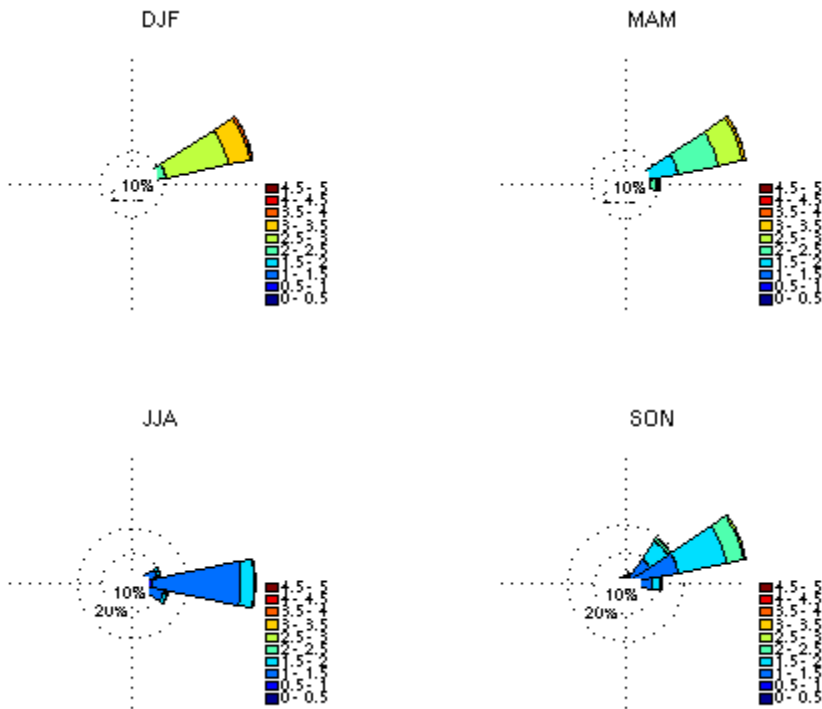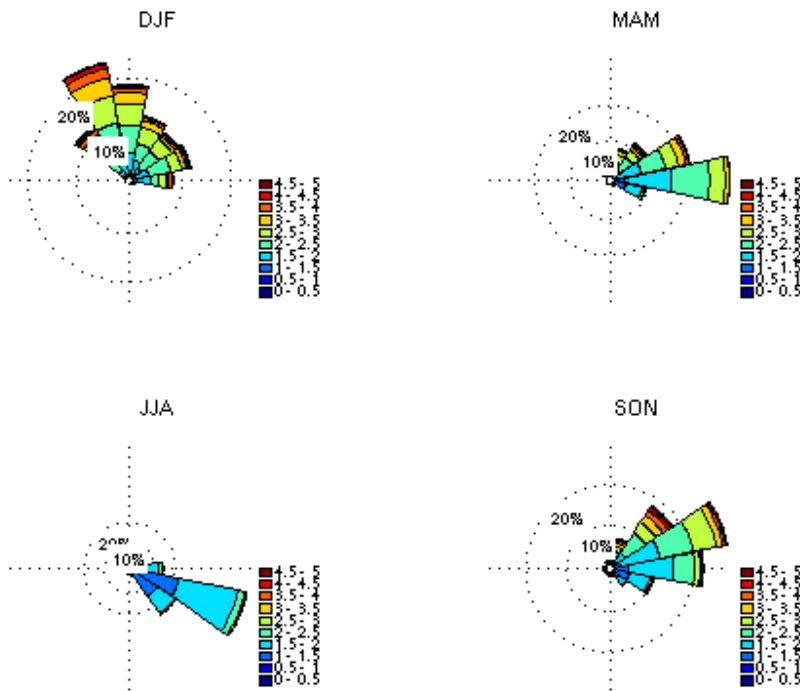
Figure B2: Wave rose for South-west Pacific showing significant wave height distribution by
mean wave direction. Determined from 2-member ensemble of CCAM forced wave model
runs.
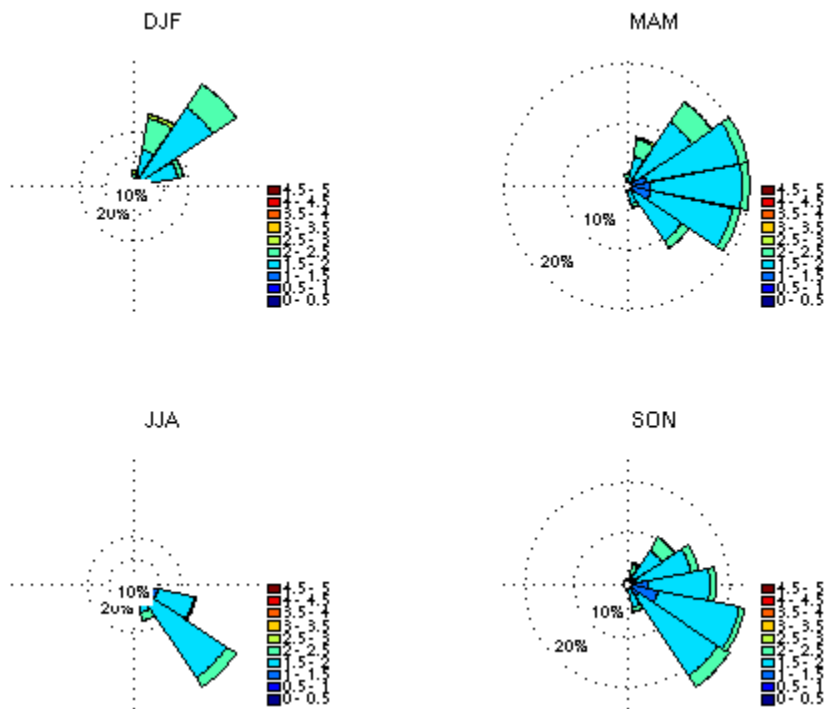
Figure B3: Wave rose for Equatorial Pacific showing significant wave height distribution by
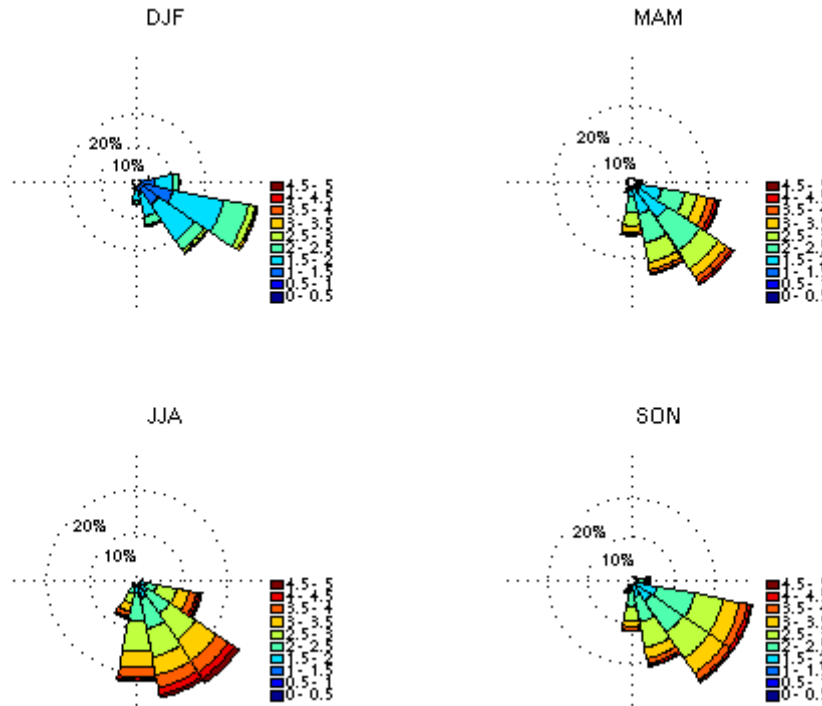mean wave direction. Determined from 2-member ensemble of CCAM forced wave model
runs.

Figure B4: Wave rose for South Pacific showing significant wave height distribution by mean wave direction. Determined from 2-member ensemble of CCAM forced wave model runs.
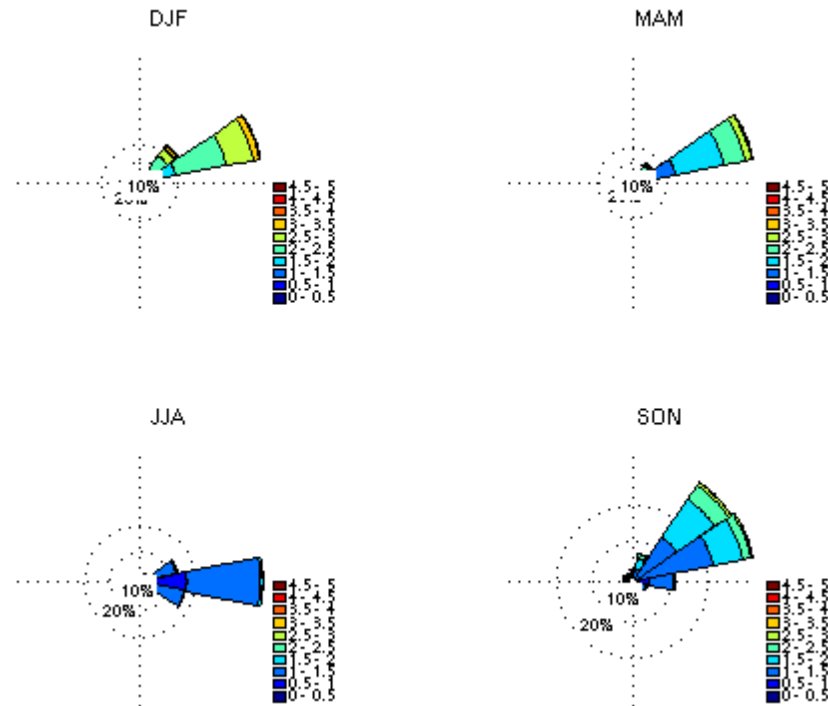
Figure B5: Wave rose for Western North Pacific showing significant wave height distribution by mean wave direction. Determined from 2-member ensemble of CCAM forced wave model runs.
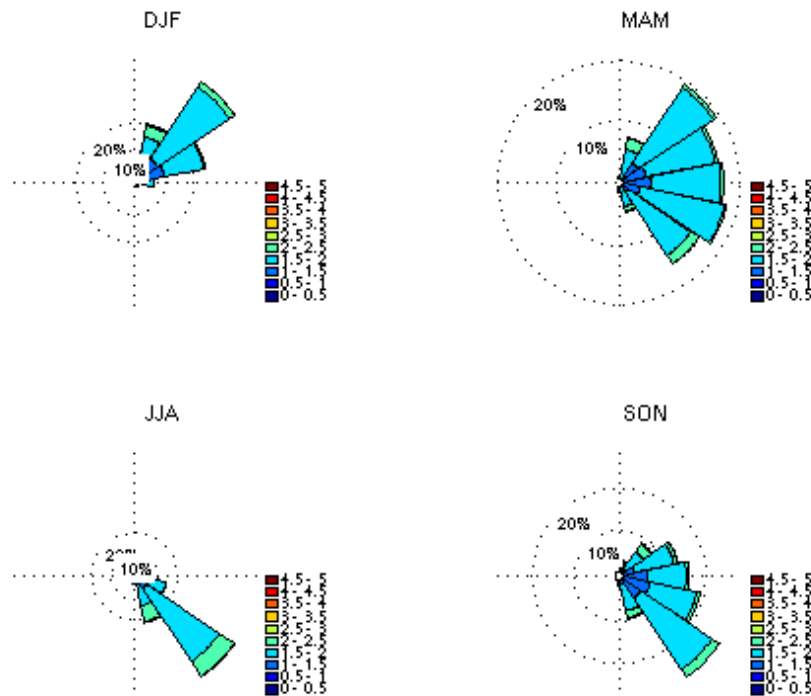
Bias-adjusted CCAM forced runs (1979-2009).
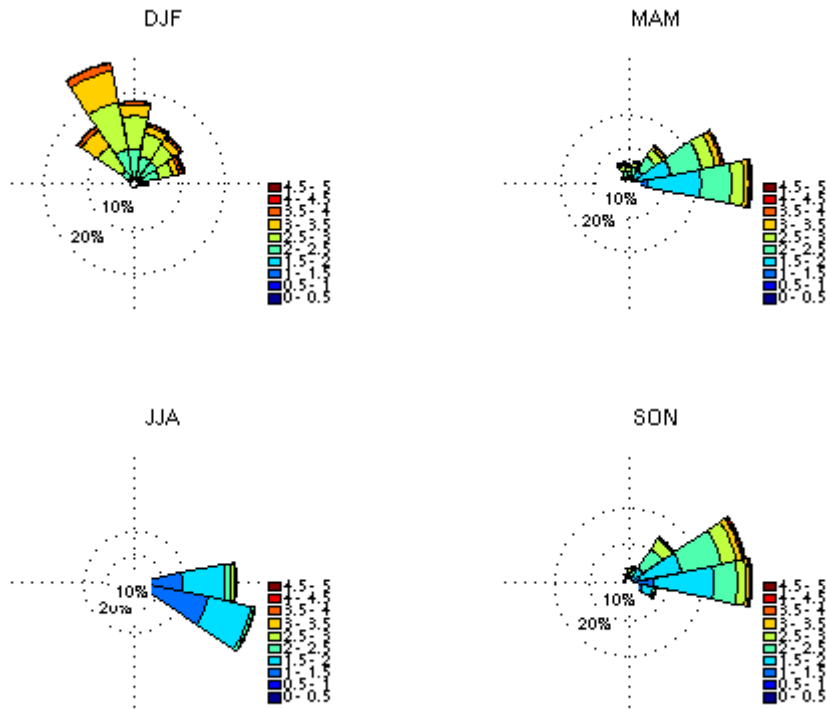
Figure B6: Wave rose for Hawaii showing significant wave height distribution by mean wave direction. Determined from 2-member ensemble of BA-CCAM forced wave model runs.
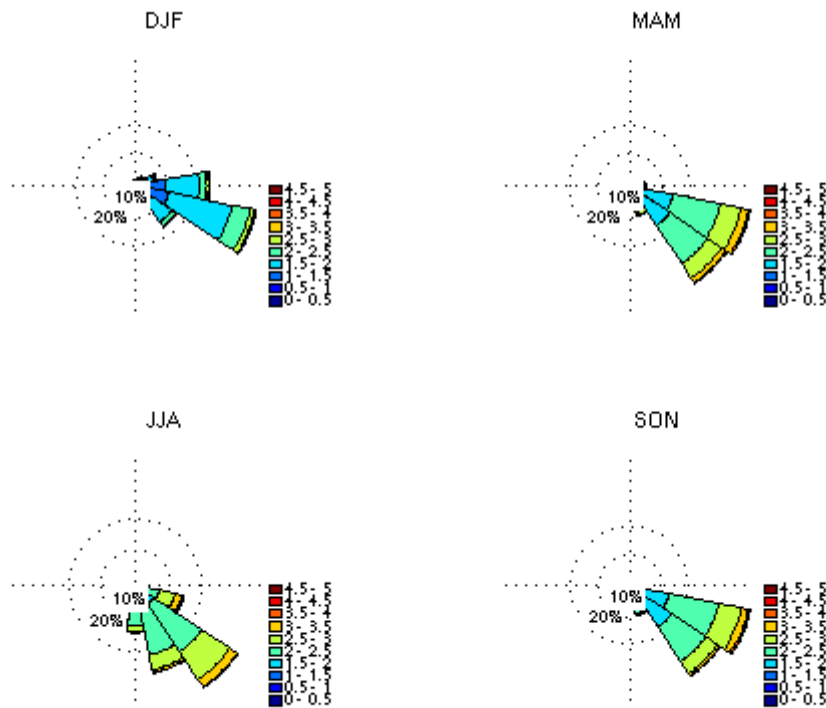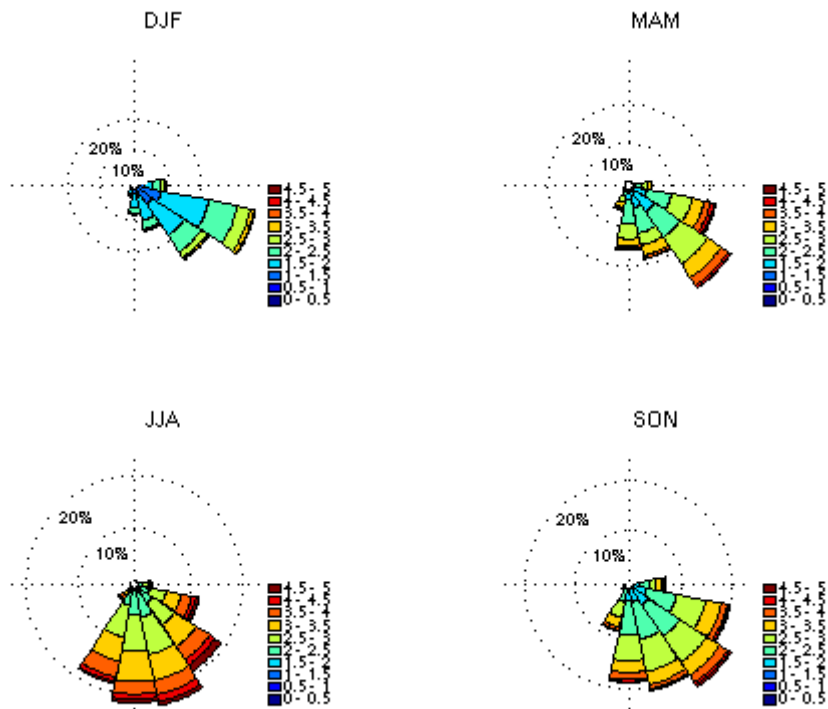

Figure B7: Wave rose for South-west Pacific showing significant wave height distribution by mean wave direction. Determined from 2-member ensemble of BA-CCAM forced wave model runs.

Figure B8: Wave rose for Equatorial Pacific showing significant wave height distribution by mean wave direction. Determined from 2-member ensemble of BA-CCAM forced wave model runs.

Figure B9: Wave rose for South Pacific showing significant wave height distribution by mean wave direction. Determined from 2-member ensemble of BA-CCAM forced wave model runs.
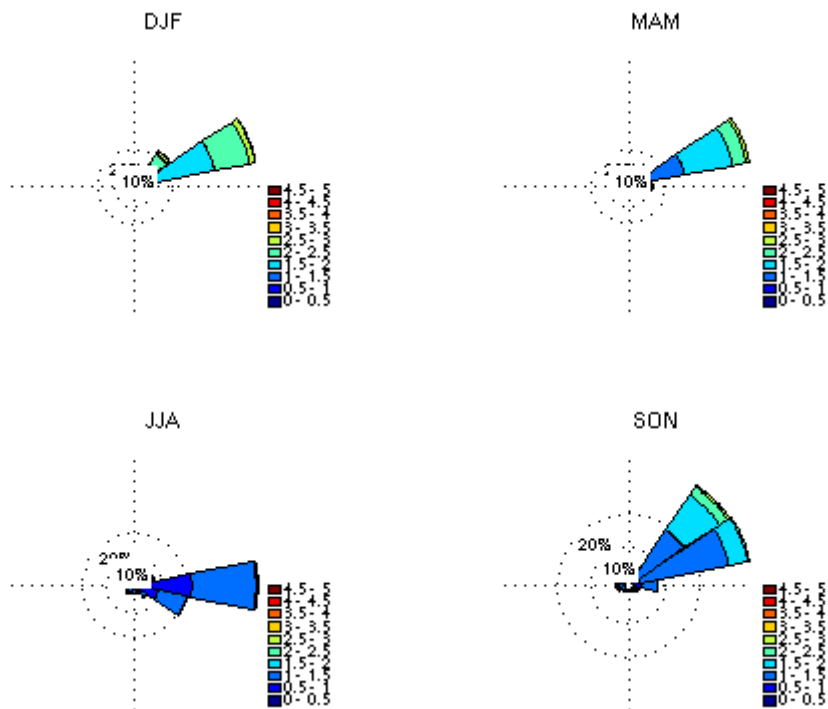
Figure B10: Wave rose for Western North Pacific showing significant wave height
distribution by mean wave direction. Determined from 2-member ensemble of BA-CCAM
forced wave model runs.

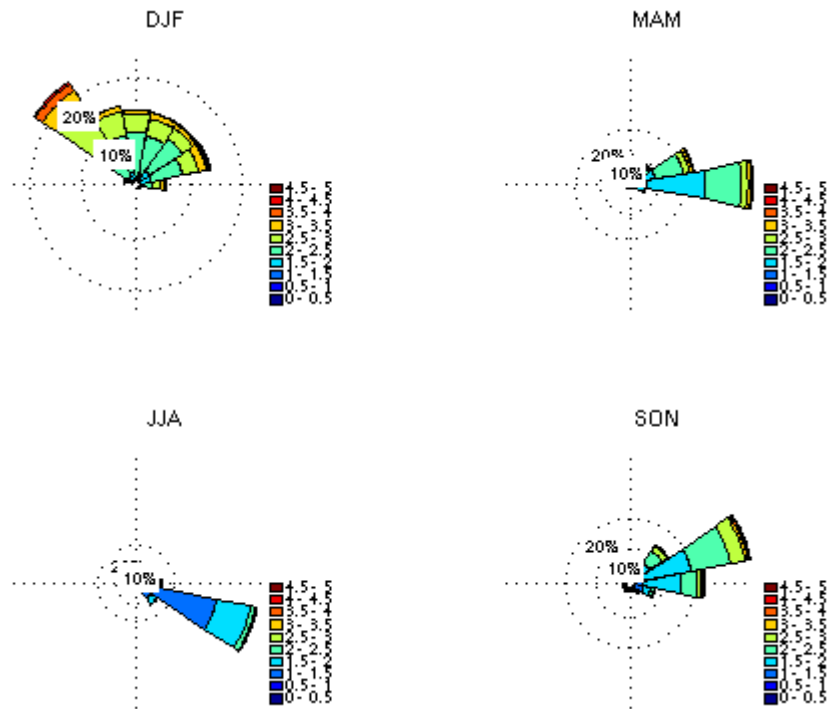## Un-adjusted CCAM forced runs (2070-2099).

Figure B11: Projected 2070-2099 time-slice Wave rose for Hawaii showing significant wave
height distribution by mean wave direction. Determined from 2-member ensemble of CCAM
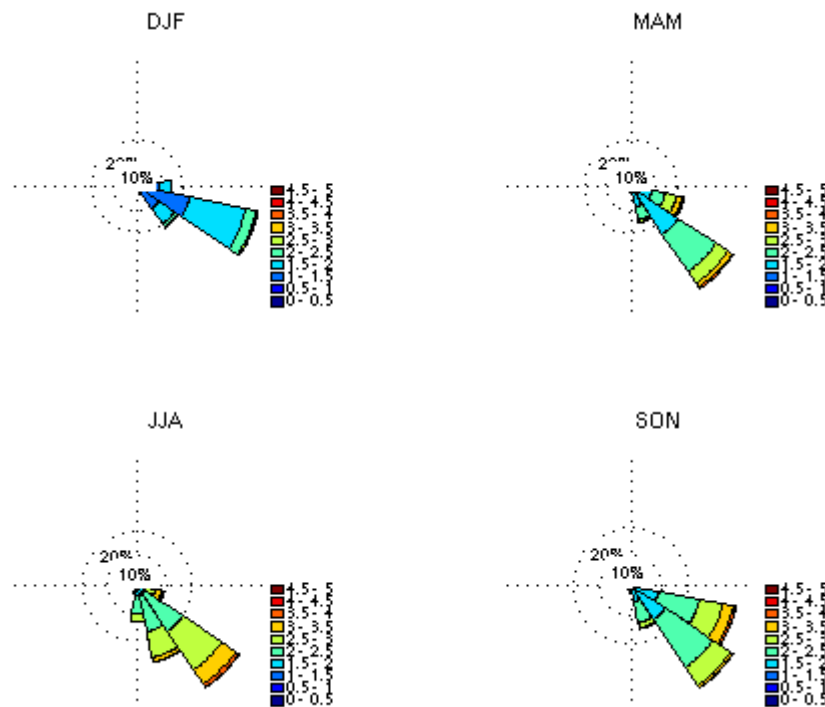forced wave model runs.

Figure B12: Projected 2070-2099 time-slice wave rose for South-west Pacific showing
significant wave height distribution by mean wave direction. Determined from 2-member
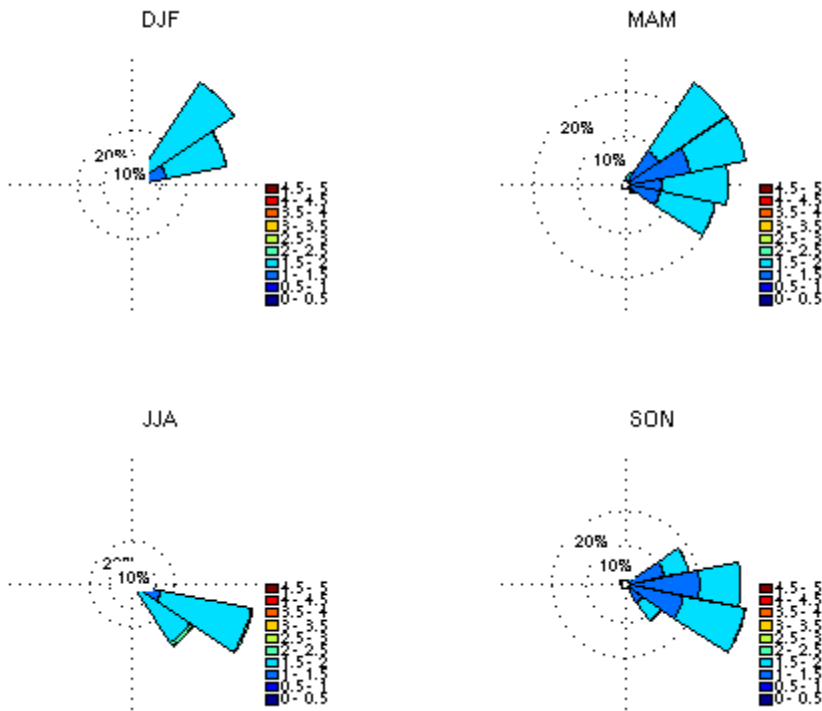ensemble of CCAM forced wave model runs.

Figure B13: Projected 2070-2099 time-slice wave rose for Equatorial Pacific showing
significant wave height distribution by mean wave direction. Determined from 2-member
ensemble of CCAM forced wave model runs.

Figure B14: Wave rose for South Pacific showing significant wave height distribution by mean wave direction. Determined from 2-member ensemble of CCAM forced wave model runs.

Figure B15: Wave rose for Western North Pacific showing significant wave height distribution by mean wave direction. Determined from 2-member ensemble of CCAM forced wave model runs.
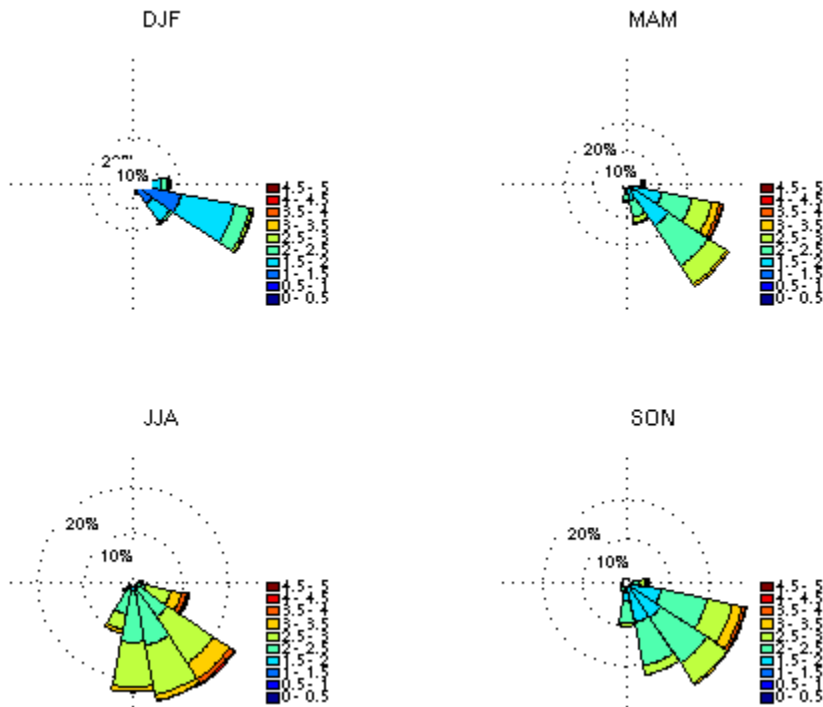
Bias-adjusted CCAM forced runs (2070-2099).

Figure B16: Projected 2070-2099 time-slice Wave rose for Hawaii showing significant wave height distribution by mean wave direction. Determined from 2-member ensemble of BA-CCAM forced wave model runs.

Figure B17: Projected 2070-2099 time-slice wave rose for South-west Pacific showing significant wave height distribution by mean wave direction. Determined from 2-member ensemble of BA-CCAM forced wave model runs.

Figure B18: Projected 2070-2099 time-slice wave rose for Equatorial Pacific showing
significant wave height distribution by mean wave direction. Determined from 2-member
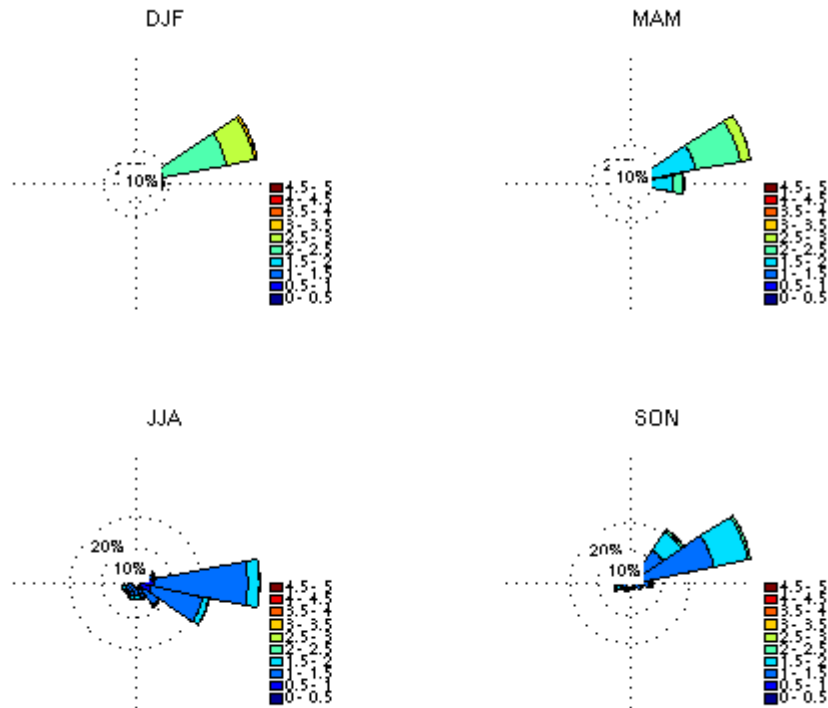ensemble of BA-CCAM forced wave model runs.

Figure B19: Projected 2070-2099 time-slice wave rose for South Pacific showing significant
wave height distribution by mean wave direction. Determined from 2-member ensemble of
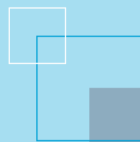BA-CCAM forced wave model runs.

Figure B20: Projected 2070-2099 time-slice wave rose for Western North Pacific showing
significant wave height distribution by mean wave direction. Determined from 2-member
ensemble of BA-CCAM forced wave model runs.